[redacted]

Report No. BMI-1852

Special Distribution

AEC Contract W-7405-eng-92

(Task No. 24) RECENT DEVELOPMENTS IN REACTOR MATERIALS TECHNOLOGY

by

Eugene M. Simons
Stanley W. Porembka
Donald L. Keller

November 1, 1968

[redacted]

BATTELLE MEMORIAL INSTITUTE
Columbus Laboratories
505 King Avenue
Columbus, Ohio 43201

DISTRIBUTION
To [redacted]

[redacted]

Reports previously issued in this series are as follows:

BMI-1800 – May 1, 1967
BMI-1811 – August 1, 1967
BMI-1821 – November 1, 1967
BMI-1827 – February 1, 1968
BMI-1838 – May 1, 1968
BMI-1846 – August 1, 1968

DISCLAIMER

No. of Copies	*Distribution*
1	AEC Albuquerque Operations Office
1	AEC Canoga Park Area Office
1	AEC Chicago Patent Group
1	AEC Division of International Affairs, Brussels
1	AEC Library, Washington
1	AEC New Brunswick Area Office (NBAO)
1	AEC New York Operations Office
1	AEC Patent Office
2	Aerojet General Corporation (AEC)
2	Aerojet-General Corporation (NASA)
2	Aerojet General Corporation, Sacramento (AEC)
1	Aerojet General Corporation, San Ramon (NASA)
1	Aerospace Corporation, San Bernardino (AF)
1	Air Force Strategic Air Command
1	Air Force Technical Applications Center
1	Ames Laboratory (AEC)
1	Argonne National Laboratory (AEC)
1	Army Aberdeen Proving Ground
2	Army White Sands Missile Range
1	Atomic Power Development Associates, Inc. (AEC)
2	Atomics International (AEC)
1	AVCO Corporation (NASA)
14	Battelle-Northwest (AEC)
1	Bellcomm, Incoporated (NASA)
4	Bettis Atomic Power Laboratory (AEC)
1	Brookhaven National Laboratory (AEC)
1	Bureau of Mines, Albany (INT) (AEC)
2	Combustion Engineering, Inc. (NRD) (AEC)
2	Douglas Aircraft Corporation, MSSD (AF)
1	Dow Chemical Company, Rocky Flats (AEC)
3	Du Pont Company, Aiken (AEC)
1	Du Pont Company, Wilmington (AEC)
1	EG&G, Inc., Goleta (AEC)
1	EG&G, Inc., Las Vegas (AEC)
1	EG&G, Inc., San Ramon (AEC)
2	General Dynamics/Fort Worth (AF)
1	General Dynamics/Electric Boat Division (AEC)
3	General Electric Company, Cincinnati (AEC)
1	General Electric Company (AEG) (NASA)
1	General Electric Company (MSD) (AEC)
3	General Electric Company, San Jose (AEC)
1	Goodyear Atomic Corporation (AEC)
1	Gulf General Atomic Incorporated (AEC)
1	IIT Research Institute (AEC)
1	Institute for Defense Analyses (ARPA)
1	Isotopes, Inc., Middle River (AEC)
1	Jet Propulsion Laboratory (NASA)
1	Johns Hopkins University (Navy)
3	Knolls Atomic Power Laboratory (AEC)
1	Lawrence Radiation Laboratory, Berkeley (AEC)
2	Lawrence Radiation Laboratory, Livermore (AEC)
1	Lockheed-Georgia Company (NASA)
3	Los Alamos Scientific Laboratory (AEC)
1	Materials Advisory Board (ARPA)
1	Mound Laboratory (AEC)
1	MSA Research Corporation (AEC)
1	NASA Langley Research Center
4	NASA Lewis Research Center
1	NASA Marshall Space Flight Center
2	NASA, Washington
2	National Lead Company of Ohio (AEC)
4	National Reactor Testing Station (INC) (AEC)
1	Navy Air Systems Command
1	Navy Facilities Engineering Command
1	Navy Office of the Chief of Naval Operations
1	Navy Ordnance Laboratory
1	Navy Ordnance Systems Command
1	Navy Radiological Defense Laboratory
1	Navy Research Laboratory
1	Navy Ship Systems Command Headquarters
1	Nuclear Materials and Equipment Corporation (AEC)
5	Oak Ridge National Laboratory (AEC)

No. of Copies	*Distribution*
1	Pratt and Whitney Aircraft Division (NASA)
1	Public Health Service (HEW)
1	Radio Corporation of America, Cranbury (AEC)
1	Rand Corporation (AF)
1	Reactive Metals, Inc., Ashtabula (AEC)
1	Republic Aviation Division (NASA)
4	Sandia Corporation, Albuquerque (AEC)
1	Sandia Corporation, Livermore (AEC)
1	Shock Hydrodynamics, Inc. (DASA)
1	Tracerlab, Richmond (AF)
1	TRW Systems (AEC)
1	TRW Systems (NASA)
2	Union Carbide Corporation (ORGDP) (AEC)
1	Union Carbide Corporation (Paducah Plant) (AEC)
1	Union Carbide Corporation (Y-12 Plant) (AEC)
1	Westinghouse Electric Corporation, Lima (NASA)
1	Westinghouse Electric Corporation, WAL(AEC)
10	AEC Division of Technical Information Extension

TABLE OF CONTENTS

TABLE OF CONTENTS
(Continued)

RECENT DEVELOPMENTS IN REACTOR MATERIALS TECHNOLOGY

PREFACE

This classified quarterly review is prepared by Battelle Memorial Institute at the request of the Division of Technical Information of the U. S. Atomic Energy Commission. It attempts to make available, as quickly as possible, the highlights of new developments and significant findings from current work related to materials for nuclear-reactor systems.

It is hoped that persons who wish to keep abreast of technical advances in a general way will find these reports sufficiently comprehensive and informative for their needs. In addition, those who require more detailed information can use the reports as a starting point and select pertinent references from the lists which appear at the ends of the sections.

I. FUEL AND FERTILE MATERIALS

1. Uranium and Uranium Alloys

Unalloyed Uranium

The Yugoslavians[1a] studied the thermodynamics of uranium grain growth. The free energy of activation was found to increase linearly with temperature in the interval 450 to 600°C, with the temperature coefficient being 17.3 cal/(mole)(°K) and a mean value for the given interval of 107,750 cal/mole. The free energy of grain growth, the entropy of the system, and the enthalpy of the system were $+3.5 \times 10^{-1}$ cal/mole, -3.2×10^{-4} cal/(mole)(°K), and $+9.3 \times 10^{-2}$ cal/mole, respectively.

Basic information on the deformation mechanisms in alpha-phase uranium is provided by a series of articles in the Journal of Nuclear Materials.[2-5] M. H. Yoo[2] calculated the effective shear moduli dislocation-line energies, dislocation widths, and Peierls-Nabarro stresses and substantiated that (010)[100] is the primary slip system at room temperature and (001)[100] is the secondary slip mode. These calculations also correctly predict the prevalence of (001)[100] slip over (010)[100] slip above the range 325 to 350°C. The easy-glide parameter for dislocation mobility of various slip systems calculated by the Czechoslovakians[3] from anisotropic elasticity data agrees with Yoo's results. This parameter was used as the criterion for the principal slip system. Figure I-1 shows this parameter for edge dislocation in alpha uranium where the upper curve denotes the operative system. The French[4] also found the same slip systems to be operative by tension testing of single crystals of alpha uranium. The Czechoslovakians[5] also examined the possible dissociation of dislocations on the primary slip systems.

Alpha-Phase Uranium Alloys

In a study at the University of Florida,[6] alloys with additions of aluminum (203 to 750 ppm), carbon (795 ppm), iron (135 to 287 ppm), and silicon (122 to 399 ppm) resulted in the following conclusions on structural changes associated with deformation at high temperatures.

1. Uranium resembles other metals in most of its high-temperature deformation characteristics.
2. Grain growth accompanies deformation.
3. New grains maintain a size which is larger at higher temperatures and slower deformation rates.
4. New grain formation is promoted by alloying which lowers the recovery temperature of alpha uranium.
5. Silicon additions maintain a fine grain size in the alpha uranium during tensile straining and thermal cycling.

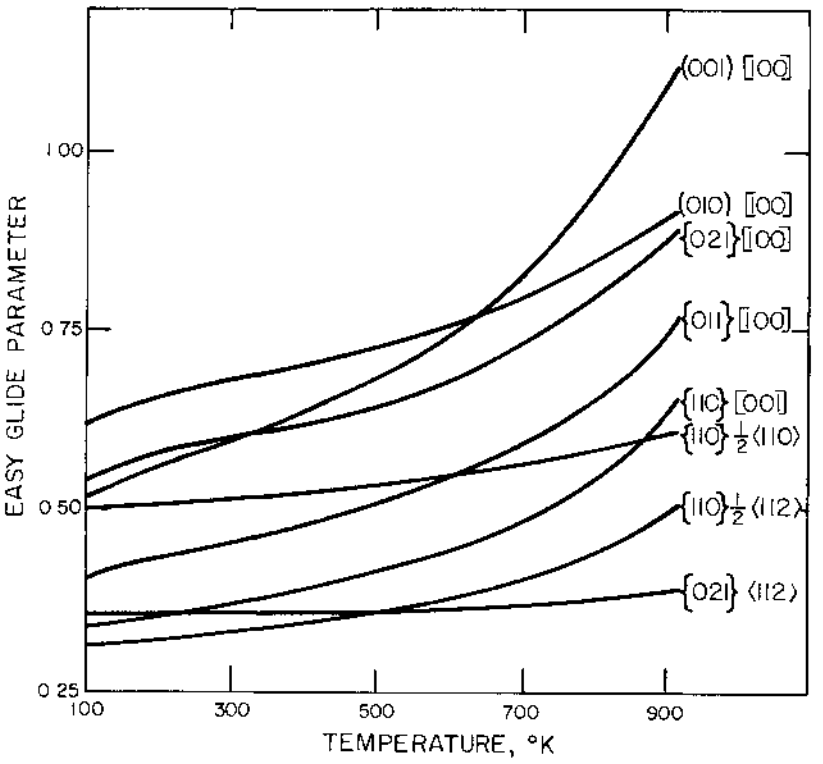

Fig. I-1. Temperature dependences of the easy-glide parameter for edge dislocations.[3]

The recrystallization kinetics of "adjusted" uranium (700 ppm aluminum and 250 ppm iron) were studied by the British.[7] Figure I-2 shows the recrystallization time at 600, 625, and 650°C. Precipitation of new phases in an adjusted alloy with 710 ppm aluminum, 1000 ppm carbon, 250 ppm iron, and 50 ppm silicon was also examined.[8] It was concluded that iron and aluminum in adjusted uranium is retained in solution on quenching from the alpha phase and on heating in the alpha region, and only the phase UAl_2 precipitates. The time dependence of the precipitation process is consistent with precipitation occurring at subgrain boundaries and on individual dislocations within subgrains. A change in the precipitation rate occurs below about 500°C.

The French[9] investigated the effect of boron on the recrystallization of alpha-phase uranium with 0.2 to 0.4 at.% molybdenum. Small additions (100 ppm) of boron led to pronounced refinement of the alpha grain size even for slow cooling rates. The UB_2 precipitates acting as heterogeneous nuclei caused this refinement. The boron also refined the grain structure of dilute U-Si, U-Cr, U-Mo-Al, U-Mo-Si, and U-Mo-Sn alloys as long as the boride particles were finely dispersed.

The Polish[10] determined the effect of 0.5 to 3 wt.% molybdenum on the tensile properties of uranium. It was found that alloying with 1.1 wt.% molybdenum increased the tensile strength of uranium from 36.1 to 94 kg/mm^2 (51,000 to 133,000 psi) at 20°C and from 5.1 to 20.5 kg/mm^2 (7,200 to 29,000 psi) at 600°C. Further increases in molybdenum content did not have any significant effect on the strength of uranium.

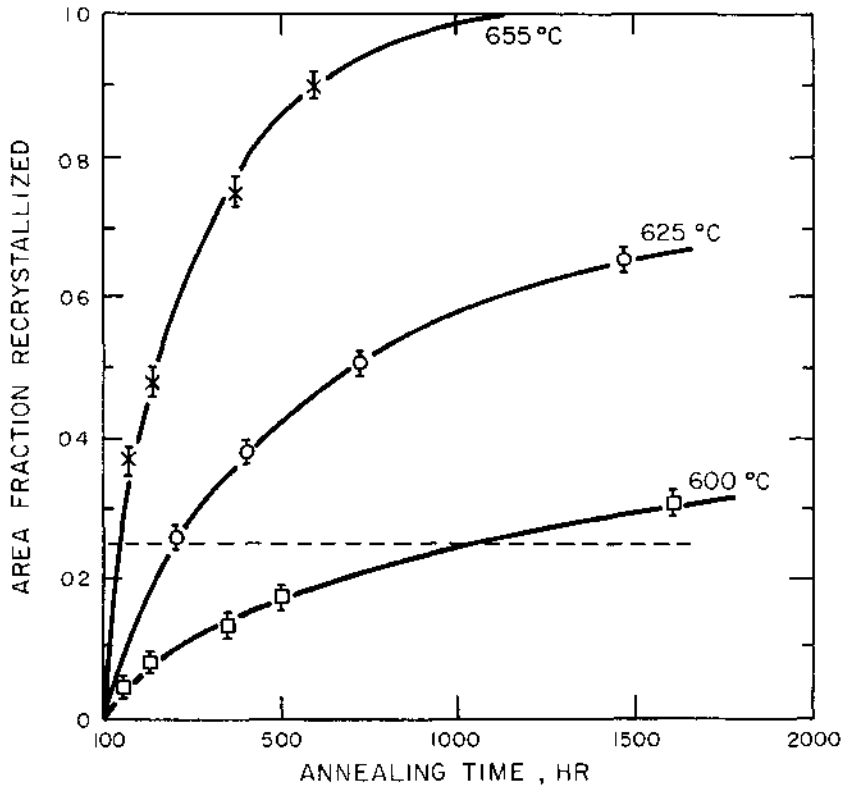

Fig. I-2 Effect of annealing on recrystallization of "adjusted" uranium.[7]

Petzow et al.[11] have presented phase equilibria data in the U-UMn_2-UFe_2 and UAl_2-UMn_2-UFe_2 systems. Complete solubility exists between the intermetallic phase U_6Fe and U_6Mn, as well as between UFe_2 and UMn_2. Therefore, the two-phase zones α-uranium + $U_6(Mn, Fe)$ and $U_6(Mn, Fe)$ + $U(Mn, Fe)_2$ dominate almost the entire system at room temperature.

Delta-Phase Alloys

The Canadians[12] studied the delta-peritectoidal reaction in U-Si alloys and concluded that:

1. Carbon concentrations of up to 2000 ppm lower the peritectoid temperature and form a region of three-phase equilibrium between uranium, U_3Si_2, and U_3Si.

2. The three-phase region has an upper limit of 860°C and a lower limit of 790°C in an alloy containing 2000 ppm carbon.

3. The higher the carbon, up to 2000 ppm, the lower the optimum temperature for transformation to U_3Si.

4. Increasing the carbon concentration and thus lowering the optimum transformation temperature does not significantly affect the rate of transformation.

(R. D. Koester and M. S. Farkas)

2. Plutonium

Plutonium Metal and Alloys

Experiments at Rocky Flats have resulted in the successful growth of large crystals of a Pu-3.3 at.% Ga alloy using a modified Bridgman technique.[13] Large polygonized grains (to 6 mm) were grown by slowly transforming an epsilon phase that was created by slow freezing of the melt. Long anneals of over 200 hr resulted in some highly perfect grains.

Ternary U-15Pu-10Zr and U-15Pu-15Zr* alloys are being prepared at Los Alamos[14] by induction melting in both conventional crucibles and in "cold" crucibles. Homogeneous alloys have been prepared at 1400°C in less than 10 min by mechanical stirring of a melt consisting of plutonium and a prealloyed U-Zr binary. The reaction of crucible materials and coatings with the ternary U-15Pu-12.7Zr alloy at 1400°C for short times is being studied. The most promising crucible coating appears to be a colloidal suspension of Y_2O_3 sprayed onto the crucible surfaces. In the "cold" crucible method, the ternary alloy is prepared by melting and stirring inside a water-cooled metallic crucible. A frozen alloy skin next to the crucible prevents impurity pickup from the crucible.

The Pu-Zr equilibrium diagram up to 10 at.% zirconium developed by Battelle–Northwest (Fig. I-3) differs from previously published diagrams.[15] The existence of a zeta intermediate solid-solution phase (2.5 to 2.7 at.% zirconium) was confirmed. Phase-stability studies indicate that the retained delta phase transforms to beta phase, the rate of transformation decreasing with increasing zirconium content. The retained beta phase is unstable and gradually transforms to alpha phase. The data indicate that the beta-retained Pu-Zr alloy would have limited use as an engineering material due to its instability.

Measurement of the solubilities of various metallic elements in liquid plutonium over the temperature range 700 to 1000°C is continuing at Los Alamos.[16] The data, some of which are summarized in Table I-1, fit empirical equations of the form $\log_{10} N_i = A - (B/T)$, where N_i is the solubility of the element i expressed as an atomic fraction and T is the temperature in °K. From these and previously reported solubility data, the relative partial molar enthalpies shown in Table I-2 have been calculated for the simple eutectic-type binary systems indicated.[17]

Eleven liquid Pu-Co-Ce alloy fuels in tantalum capsules have been irradiated to 2.6 at.% burnup under conditions similar to those expected in the Fast Reactor Core Test Facility.[18] The fuel-container interface temperature was maintained below 725°C but above the fuel freezing point of approximately 440°C. The capsules operated at an

*Unless otherwise designated, all compositions are understood to be by wt.%.

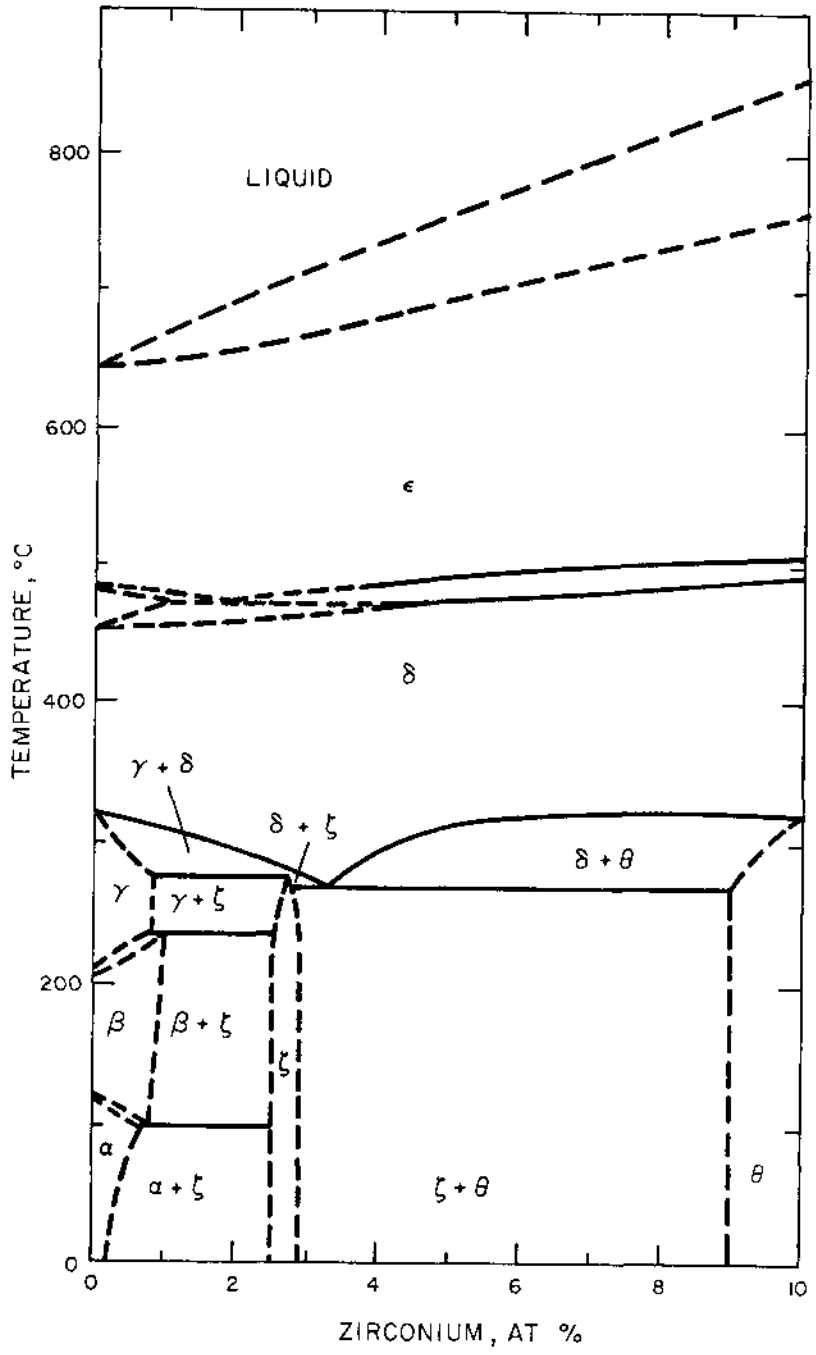

Fig. I-3 Plutonium-rich end of the Pu-Zr equilibrium diagram.[15]

Table I-1 AVERAGE SOLUBILITIES OF SELECTED ELEMENTS IN LIQUID PLUTONIUM[16]

Temperature, C	Average solubility, at.%							
	Ti	V	Cr	Mn	Zr	Nb	Mo	Tm
700	5.44	1.02	1.62	--	2.10	1.10	1.57	2.35
750	9.72	1.34	2.23	--	3.44	1.44	2.11	3.08
800	22.50	1.67	3.26	--	5.42	1.69	2.65	4.09
850	26.07	2.29	4.35	30.8	8.03	2.05	3.08	5.04
900	28.81	2.96	5.59	--	12.4	2.68	3.64	6.79
950	33.31	3.78	6.94	45.7	18.0	3.14	4.58	7.25
1000	37.17	4.46	8.58	53.6	--	3.71	--	8.48

Table I-2 RELATIVE PARTIAL MOLAR ENTHALPIES OF SELECTED ELEMENTS IN LIQUID PLUTONIUM[17]

Element	ΔH_i, kcal/mole
Tungsten	22.0 ± 0.1
Tantalum	16.6 ± 0.1
Niobium	11.1 ± 0.1
Vanadium	11.0 ± 0.1
Molybdenum	10.3 ± 0.1
Chromium	9.5 ± 0.1
Thulium	9.2 ± 0.2

average specific power of 150 watts/g of plutonium. Presumably, postirradiation observations will be described in a future report.

Argonne and Battelle-Northwest are initiating a program to determine the mechanism that controls swelling in U-Pu-base fuels and to establish the effects of temperature, pressure, burnup, and fuel composition on the swelling rate.[19a] Injection-cast and heat-treated specimens will be irradiated isothermally and at constant pressure within a range of temperatures from 400 to 800°C and a range of pressures from 50 to 5000 psi. Specimens of uranium, U-5Pu, U-14Pu, and U-14Pu-12Zr have been prepared and are being encapsulated. Irradiation is expected to begin shortly as reactor space becomes available.

A single unit process for the rapid production of plutonium metal from the oxides has been reported by Lawrence Radiation Laboratories.[20] The process consists of (a) the reduction of the plutonium oxides by calcium metal, (b) the extraction of the CaO reaction product with molten calcium chloride, and (c) the quantitative separation of the two immiscible molten-metal phases by the immiscible salt solution. Yield efficiencies of 99.96% are reported, with a batch cycle time of 15 min independent of batch scale.

(D. F. Askey)

Plutonium Compounds

Oxides. Oak Ridge[21] has established the feasibility of producing PuO_2 from PuF_6. The product from these experimental runs was confirmed by X-ray diffraction examination. A limitation of the vapor fabrication of PuO_2 was recognized as the conversion of PuF_4 to PuF_6, although this aspect of the process was not a part of the experimental process studied.

Spherical particles of PuO_2 have been prepared in two laboratories[22,23] by the sol gel technique. Mound Laboratory[22] has evaluated $^{238}PuO_2$ particles and determined a crush strength of 1260 g and a density of 10.8 g/cm^3 for 250 to 400-μ spheroids which had been calcined at 1200°C. At Karlsruhe[23], PuO_2 microspheres were prepared and reduced in hydrogen at 1750°C to obtain particles with a final O/Pu ratio of 1.67 to 1.73. These particles were subsequently coated with carbon and silicon carbide. Mound Laboratory[24] has also established the impact characteristics of plasma-formed $^{238}PuO_2$ microspheres under simulated reentry conditions. The particle size distribution before and after impact at 105 ft/sec is shown in Table I-3.

Table I-3 EFFECT OF IMPACT ON PARTICLE-SIZE DISTRIBUTION OF PuO_2[24]

Diameter, μ	Distribution before impact, wt.%	Distribution after impact, wt.%		
		Capsule 18	Capsule 20	Capsule 24
177-210	8.16	9.4	7.7	5.7
149-177	21.22	25.2	18.3	14.8
125-149	16.53	18.1	15.9	12.1
105-125	18.98	12.6	14.1	14.2
77-105	21.63	19.8	24.3	24.6
44-77	13.47	10.4	16.9	23.1
20-44	0.00	3.02	0.73	3.8
10-20	0.00	0.26	0.08	0.19
<10	0.00	0.03	0.06	0.08

Argonne[25] has measured the high-temperature properties of PuO_2. The heat capacity of PuO_2 was given as:

$$C_p = 22.18 \times 2.080 \times 10^{-4}\ T - 4.935 \times 10^5\ T^{-2} \quad .$$

An extrapolation of this relationship to higher temperatures resulted in a value of 23 ± 1 cal/(mole)(°K) at the melting point, 2663 ± 20°K. Mass-spectrometric studies performed in iridium effusion cells yielded partial heats of sublimation in kcal/mole for the vapor species: 138.5 ± 1.5 for PuO_2, 127.0 ± 3.5 for PuO, and 136 for plutonium. The temperature dependence of the partial pressures of $PuO_2(g)$ and PuO(g) are shown in Fig. I-4. The thermal diffusivity for PuO_2 has also been found[19b] to be 0.0148 cm^2/sec [at 400°C, 0.00503 at 1500°C, and 0.00400 at 2000°C.

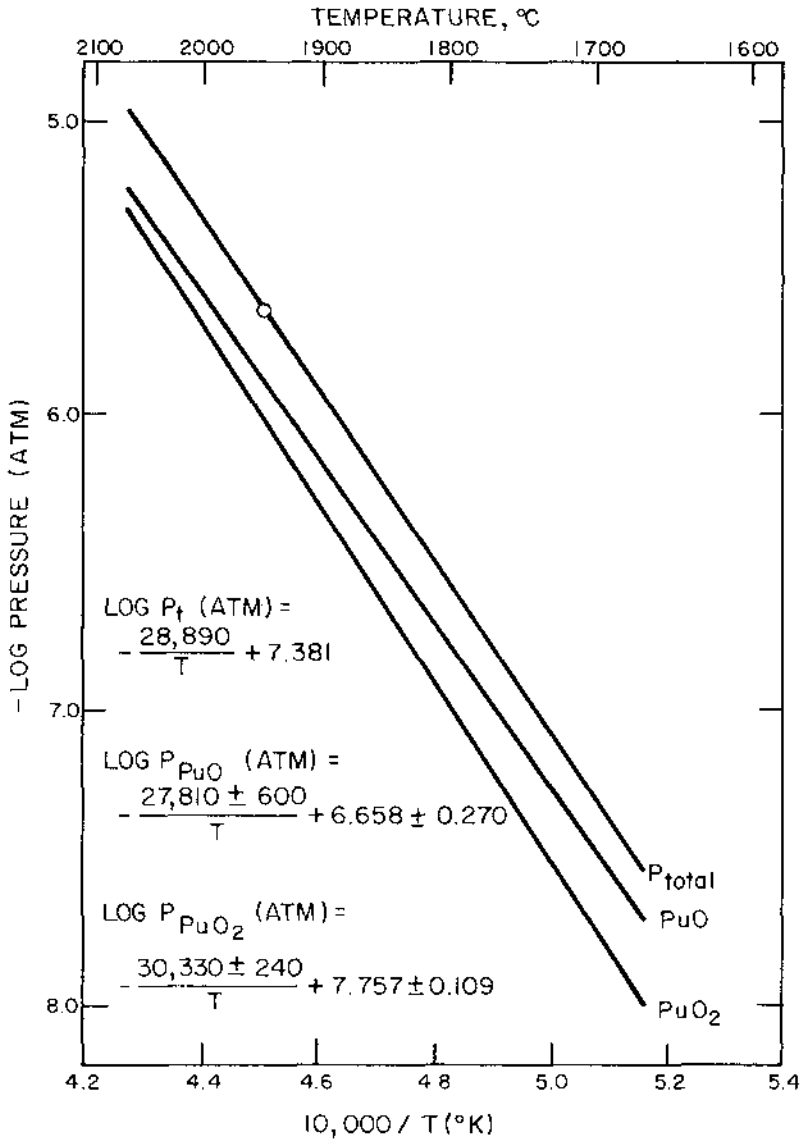

Fig. I-4. Temperature dependence of the partial pressures of $PuO_2(g)$ and $PuO(g)$.[25]

Mound Laboratory[26] has reviewed the methods applied for the dissolution of PuO_2. The solubility rate was found to be directly related to the method of oxide preparation and to the processing temperatures.

A mechanical blending powder route for preparing mixed UO_2-20 to 25 PuO_2 pellets has been established by Battelle-Northwest[27] as the process for producing FFTF fuel. The specified limits for these pellets are 93 to 95% of theoretical density and a 50-μ maximum diameter for PuO_2 particles. Nuclear Materials and Equipment Corp.[28] has investigated the incorporation of burnable additions, such as methyl cellulose, sucrose, dextrose, and carbowax, into mixed oxides for porosity and density control. Final densities in the range of 85 to 92% of theoretical were obtained with 1.5 to 3.0 wt.% additions.

The effects of selected metallic and nonmetallic impurities on the sintered density of mixed oxides and the retentive ability of the oxides during sintering were studied at Nuclear Materials and Equipment Corp.[29] The chemical analysis before and after sintering showed that only two impurities, silicon and chromium in concentrations of 5000 ppm, decreased the sintered density. Losses of 2 to 7% in density were observed, depending upon the particle size of the impurity.

Babcock and Wilcox[30] has evaluated both gel additions and mixed sol blending as techniques for producing UO_2-PuO_2 particles. Gel-addition chemistry studies have involved techniques for improving the pickup of tri- or quadrivalent plutonium by in situ changes of pH and plutonium valence. Adjustments of this type increased the pickup from the range of 4 to 5% to between 7 and 10%, which is about half that required for fast-reactor fuel. Mixed sols usually undergo segregation unless strongly agitated. UO_2-20PuO_2 particles with 95% of theoretical density and 44 to 500-μ particle size were obtained after sintering at 1250°C in N_2-6 vol.% H_2. Oak Ridge[21] has also investigated mixed sol techniques for mixed oxide preparation. The product is further jet milled, cold pressed, and sintered into cylindrical pellets. Final densities in the range 85 to 90% of theoretical have been achieved.

The diffusion of uranium in PuO_2 and plutonium in UO_2 has been determined at Karlsruhe[31] by electron-microprobe analysis. The diffusion of these species has been given as: $D_U = 9.25 \times 10^{-5} \exp(-67,800/RT)$ cm^2/sec and $D_{Pu} = 12.4 \times 10^{-5} \exp(-64,900/RT)$ cm^2/sec. Similar investigations carried out at Harwell[32] on mechanically blended powders showed PuO_2-rich areas to be 20 to 40 μ after the first sintering at 1550°C in CO_2 and 10 to 15 μ after a second milling and sintering step. British investigators[33] have also developed a direct alpha-spectrometric technique to examine fabricated and irradiated fuel materials. The advantage of this system is its ability to separate the contribution by various alpha emitters.

The thermal diffusivity and thermal conductivity of UO_2-20PuO_2 as a function of temperature and stoichiometry has been measured by the French.[34] The effect of oxygen content is greatest in the lower temperature range (100 to 1000°C) and indicates that the conductivity decreases as the O/M ratio decreases. The most drastic shift in thermal conductivity is accompanied by a decrease in stoichiometry from 2.00 to 1.98. Battelle-Northwest[35a] has also investigated these properties for UO_2-25PuO_2. The same general trend but a more gradual decrease with respect to oxygen content was reported. In addition, the mixed oxide composition with an O/M of 1.97 exhibited good

compatibility characteristics with 304 stainless steel after 1000 hr at 650 and 1000°C in either helium- or sodium-bonded assemblies.

Argonne[36] has utilized the Förster resonance technique to establish room-temperature elastic and anelastic properties for UO_2-20PuO_2 (O/M = 1.98). Within the density range studied (80 to 85% of theoretical), the Young's modulus and shear modulus appeared to be linearly dependent upon density. The Young's modulus ranged from 1250 to 1500 kbars, and shear modulus ranged from 450 to 600 kbars. Los Alamos[14b] has determined the heat of fusion for UO_2-20PuO_2 (O/M = 1.97) to be 19.4 kcal/mole by differential-thermal-analysis techniques. The solidus and liquidus temperatures were observed at 2780 and 2820°C, respectively.

Battelle—Northwest[37] has studied the effects of stoichiometry (O/M = 2.00, 1.99, 1.97, and 1.94) on the melting heat rating of UO_2-25PuO_2. In the hypostoichiometric region, the melting heat rating decreased by 3.2% for an O/M of 1.99 and by 5.5% for an O/M of 1.94. The insensitivity of relative heat rating to decreasing O/M is consistent with a decrease in thermal conductivity and a compensating increase in melting point. General Electric[38] has determined the melting points of irradiated mixed oxides. The melting point of UO_2-25PuO_2 after 85,000 Mwd/tonne decreased 50°C and that of UO_2-20PuO_2 after 55,000 Mwd/tonne decreased 100°C. UO_2-25PuO_2 irradiated to 250,000 Mwd/tonne indicated a temperature decrease of 60°C. A decrease in the melting point of 50°C was reported to decrease the effective thermal conductivity ($\int k d\theta$) to melting by ~0.5 watt/cm. Also, the transient-failure threshold for irradiated UO_2-28PuO_2 fuel after burnup to 70,000 Mwd/tonne was identified[39] at approximately 50 vol.% molten fuel. The primary mechanism for failure was specified as internal pressure caused by the sudden local release of contained fission gases during the excursion.

Harwell[40] has conducted sintering studies on the ThO_2-PuO_2 system. Sintering at 1600°C in argon resulted in densities of 94% of theoretical but poor solid-solution formation. Sintering in air or wet hydrogen yielded good solid solution but poor density, in the range of 85% of theoretical. The British[41] have also compiled the physical properties of various plutonium and mixed compounds.

Carbides. Argonne[42] has developed a fluidized-bed process for the preparation of UC-15PuC. Carbide powder of controlled stoichiometry was produced by carburization of hydrided metal or alloy at 750 to 850°C with mixtures of methane and hydrogen. The composition of the carbides from a series of experiments is shown in Table I-4.

Compatibility results for UC-20PuC with various commercial cladding alloys have been presented by Latimer.[43] With hyperstoichiometric carbide at 800°C, no new phases were observed after 1000 hr with 304 stainless steel or Timken alloys 16-15-6 and 16-25-6. Tests involving alloys having higher nickel contents, such as Incoloy-800, Hastelloy-X, and Inconel-625, have shown some reaction with both the mixed monocarbide and sesquicarbide. Reaction layers for (U, Pu)C ranged from 3 to 180 μ after 1000 hr at 800°C.

Los Alamos[14b] has developed an arc-melting and hydrogen-treatment process to prepare single-phase UC-20PuC. The monocarbide with a C/(U + Pu) ratio of 0.97 ± 0.01 was readily obtained by hydrogen treatment at 850°C. A reaction time of 0.6 hr/g

was necessary to remove the initial 3% excess carbon. Melting temperatures of UC-PuC solid solutions in the compositional range up to 50 wt. % PuC were also determined and the resulting solidus-liquidus relationship is shown in Fig. I-5. Neutron-diffraction studies with Pu_2C_3 were performed to establish a postulated antiferromagnetic transition at 120°K, but this transition was not experimentally observed. Compatibility results for (U, Pu)C sodium bonded with 316 stainless steel showed that there was no reaction between the fuel and cladding after 1000 hr at 750°C.

Table I-4 ANALYSIS OF (U, 15Pu)C PREPARED BY THE METAL-METHANE FLUIDIZED-BED PROCESS[42]

Conditions: Temperature 800°C
Pressure 2 atm
Gas composition H_2-6.2 vol. % CH_4

Charge weight, g	Product composition			
	Carbon, wt. %	Oxygen, ppm	Nitrogen, ppm	Hydrogen, ppm
300	4.92	340	1700	--
300	5.00	260	800	55
400	4.93[a]	190	500	180
400	4.76[a]	320	300	>250
400	4.75[a]	270	900	>200

a Products treated with hydrogen at 800°C to reduce carbon content.

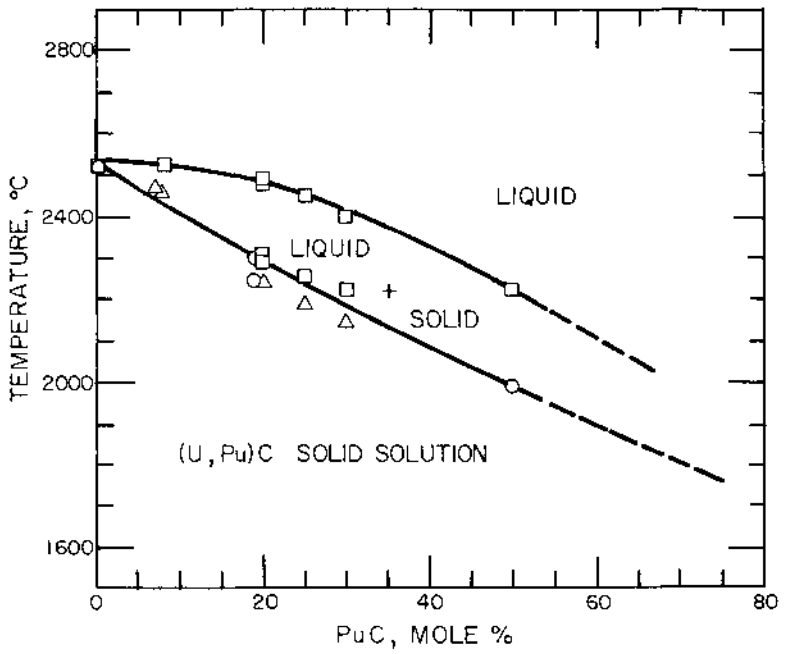

Fig. I-5 Melting temperatures of UC-PuC solid solutions.[14b] (M/C ratio = 0.95 - 1.00.) ○, metallographic observations; DTA observations: △, arc-melted samples; □, pellets.

Atomics International[44] has investigated plutonium losses during arc melting of UC-20PuC. These losses were calculated as a function of the blanket atmosphere and the melt geometry. Los Alamos[45] has also compiled a survey of the properties and irradiation behavior of carbide fuels.

Nitrides. A study of mixed nitrides (UN-20PuN) for fast-reactor application has continued at Battelle-Columbus.[46] Vapor-pressure determinations for the mixed nitrides indicated that the activity of plutonium is 0.2, and it does not appear to be dependent upon temperature. For PuN, the heat of formation was found to be -76 kcal/mole. A ΔH°_{298} of 158.6 kcal/mole was obtained for the reaction PuN = Pu(g) + 1/2 N_2(g). The plutonium partial pressure for the mixed nitride and PuN is shown in Fig. I-6. Compatibility studies with slightly hyperstoichiometric UN-20PuN have indicated no reaction between the high-density fuel pellets and 304 stainless steel after 10,000 hr at 700 and 800°C. Compatibility results for 316 and Oak Ridge stainless steel, Inconel 625, Incoloy 800, and vanadium were also obtained. Helium- and sodium-bonded specimens were irradiated to burnups in the range 34,000 to 55,000 Mwd/tonne, and the observed swelling rates (4.2 to 9.6 vol.%) indicate that a 10-mil gap is sufficient to accommodate fuel swelling to burnups well in excess of 100,000 Mwd/tonne. Stoichiometric (U-Pu)C was also prepared in this study in a conventional arc melter under 1-atm nitrogen pressure. The carbon concentration in these materials ranged from 3.15 to 3.50 wt.%.

Los Alamos[14b] determined the thermodynamic properties of PuN by galvanostatic and mass-spectrometric techniques. The emf from a cell consisting of PuN(s), Pu(s,l)/$PuCl_3$, LiCl-KCl/PuN(s), and N_2(g) was measured over the temperature range from 680 to 1040°C. The Gibbs free energy of formation for PuN was reported as:

$$-\Delta G^\circ_T = 73.8 - 0.0225T \text{ kcal/mole}$$

Vapor-pressure results were in good agreement with the Battelle-Columbus results for the partial pressure of plutonium over PuN.

Battelle-Northwest[35a] observed that sodium-bonded UN-20PuN is compatible with 304 stainless after 1000 hr at 1000°C. The parameters were given for a carbothermic process to produce the mixed nitrides from oxides. After sintering to densities in the range of 87 to 95% of theoretical, the impurity levels were found to be 1800 to 8900 ppm for oxygen and 1000 to 6000 ppm for carbon. Thermal diffusivity was measured and a thermal-conductivity relationship was established as shown in Fig. I-7.

(M. D. Houston)

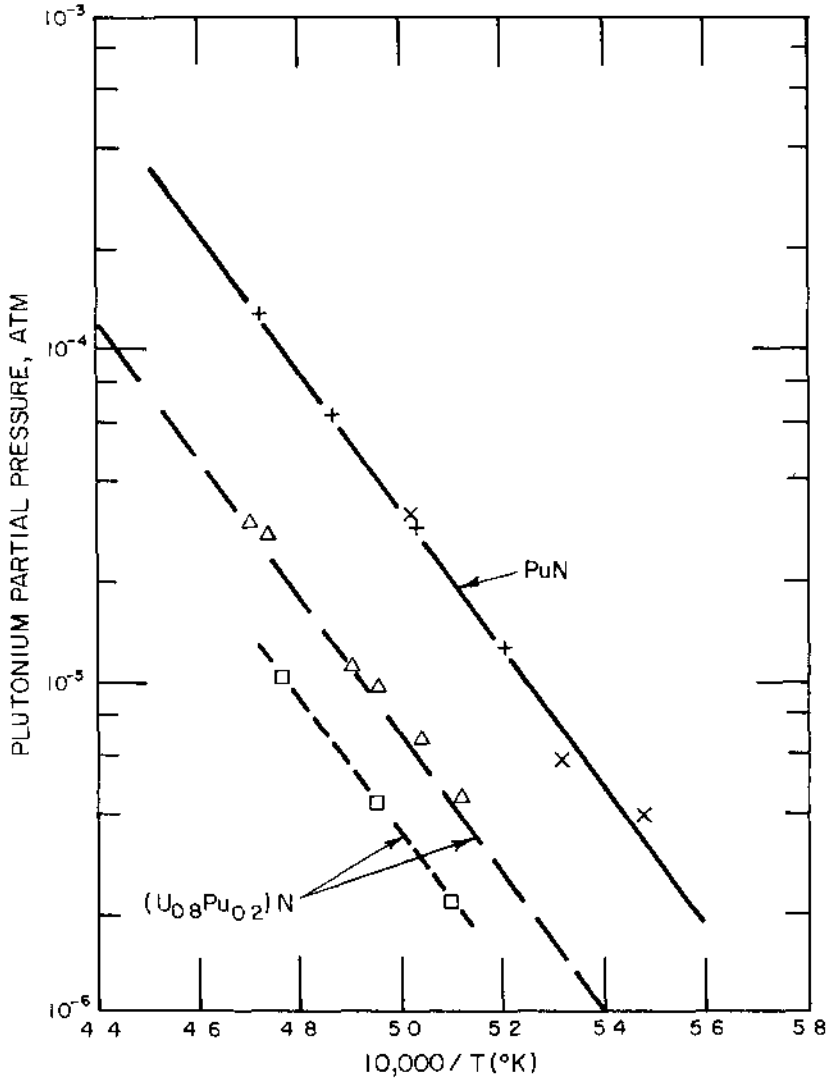

Fig. I-6 Vapor pressure of PuN and $(U_{0.8}Pu_{0.2})N$.[46] △, 1-mm-diameter orifice; □, 2-mm-diameter orifice.

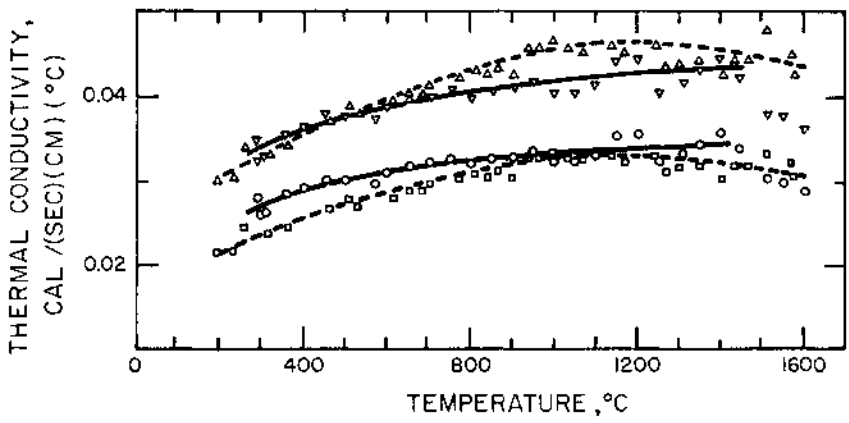

Fig. I-7 Calculated thermal conductivity of $(U_{0.20}Pu_{0.80})N$ samples.[35a] Metal-hydride (UPu)N: □, 86% theoretical density; △, corrected to 100% theoretical density. Carbothermic (UPu)N: ○, 89% theoretical density; ▽, corrected to 100% theoretical density.

3. Thorium

Battelle–Northwest has irradiated test fuel elements containing a Th-2.5U (93.2 ^{235}U)-1.0Zr alloy in the ETR up to 20,300 Mwd/ton (2.3 at.%) burnup.[35b] After 403 thermal cycles, the fuel has exhibited 3.8% swelling, as determined by weighing the fuel elements in water. Fuel temperatures were maintained between 350 and 600°C with a surface temperature of 295°C. No evidence of warpage, bowing, or distortion has been noted.

The dependence of the iodide process for refining thorium on the temperature of the crude metal, the deposition temperature, and the pressure of ThI_4 vapor has been studied by the Germans.[47] The speed of thorium transport showed a maximum at ThI_4 vapor pressure of about 0.06 torr. The occurrence of this transport maximum was attributed to the interplay of the two different transport reactions at the deposition wire. Depending on the total pressure, the speed of the transport is determined by either the phase-boundary reactions on the hot wire or diffusion and convection in the gas phase.

(R. L. Martin)

4. Metal-Ceramic Fuels

Dispersion Fuels (Less Than 50 vol.% Ceramic Phase)

Fuel elements containing powdered U_3O_8 or UAl_3 dispersed in aluminum powder were fabricated by Oak Ridge[48] for HFIR and ATR applications. These fuel elements were all of the flat-plate type and were manufactured by the picture-frame, hot-rolling technique. Factors which must be controlled in plate fabrication to prevent hot spots and potential melting during reactor operation are fuel loading and distribution, core thickness, quality of heat transfer bonds, and uniformity of plate curvature. Techniques to optimize these fuel plate characteristics are discussed.

NASA-Lewis researchers[49] used experimental thermal-strain data obtained by cycling tungsten and W-UO_2 composites to determine allowable temperature differences for equivalent thermal strain with a localized temperature perturbation and a uniform temperature gradient in operation. These temperature profiles result in the maximum and minimum thermal strains for typical reactor conditions. The allowable temperature difference for a local temperature perturbation is only one-half that for the uniform gradient.

Idaho Nuclear workers[50] observed that commercially manufactured U_3O_8 fuel elements and those manufactured at Oak Ridge have similar performance characteristics. The U_3O_8 reaction with aluminum proceeded at a slightly faster rate in the commercial plates. For UO_2 and UAl, the incorporation of the proper amount and distribution of porosity was found to limit fuel swelling from solid fission products during irradiation. Swelling from fission gas was not observed.

Compatibility studies with a tungsten-clad cermet fuel of molybdenum and Tm_2O_3 have been conducted at Los Alamos.[51] The tests were run at 2000°C for 1000 hr in vacuum (pressure not given). No reaction between the cermet fuel components or between the fuel and the cladding was observed. The conclusion was that at temperatures up to 2000°C, these components were compatible. Some loss of Tm_2O_3 by vaporization was noted. By increasing the thickness of the tungsten cladding, this loss was reduced to a low level, less than 0.5 wt.% in 1000 hr.

(J. T. Smith)

Cermet Fuels (Over 50 vol.% Ceramic Phase)

Transport rates of krypton through high-density powder-metallurgy W-60 vol.% UO_2 cylindrical cermet fuel cores are being measured at General Electric.[52] The cermet specimen is subjected to a krypton pressure gradient of approximately 0.8 atm and the permeated gas is collected in internal gas counting bulbs. Results from several measurements on a single cermet specimen showed that throughout the history of the specimen, transport rates were lower at elevated temperatures. This effect suggests a closure of some growth damage (fuel particle cracking or separation) with increased

temperature over the first 11 to 12 cycles. A decrease in transport rates at both high and low temperatures was noted. However, additional cycling resulted in an increase in transport rates to values greater than those obtained initially. A diametrical growth of 0.4% was measured for the specimen after Cycle 17. The increase in transport rates may indicate considerable grain growth and attendant embrittlement of the tungsten matrix.

Tensile and creep-rupture properties of molybdenum and tungsten matrix – UO_2-ThO_2 cermets have also been determined at General Electric.[53] Testing atmosphere had a pronounced effect on creep strength as demonstrated by lower creep deformation rates obtained in He-5 vol.% H_2 than in helium only. It was believed that specimens tested in helium maintained a higher stoichiometric (O/U) ratio than those tested in the mixture of helium and hydrogen. Tensile data for tungsten matrix and molybdenum matrix cermets are given in Tables I-5 and I-6, respectively. The higher ductility of molybdenum compared with that of tungsten results in higher ultimate tensile strengths at low temperatures for the molybdenum matrix cermets. At temperatures of approximately 1370°C and above, however, tungsten matrix specimens exhibit higher ultimate tensile strengths.

Tungsten cermets with UC, UN, and UO_2 were irradiated at 1600°C and above, at linear heat-generation rates approximating 2.5 kw/ft by Battelle–Columbus.[54] For high-density cermet specimens, diametral and volumetric swellings generally exceed approximately 8 and 20%, respectively, after accumulated burnups of 1×10^{20} fissions/cm^3. While a stabilization of cermet swelling has been observed for cermets containing UN or UO_2, cladding strain at the time of stabilization has generally been of a magnitude sufficient to cause cladding failure. An investigation is in progress to see whether making the cermet fuel porous and surrounding it with a thick cladding for restraint will minimize radiation-induced swelling. Results of some experiments along these lines are shown in Figs. I-8 and I-9. It seems apparent that a considerable dilution in fissile density by fuel porosity and cladding material is required before the swelling of cermet fuels at high temperature is reduced to tolerable levels.

General Electric has fabricated and measured several properties of Mo-UO_2 cermets intended for Pulse Reactor experiments.[55] Properties which have been measured include sonic velocity, thermal expansion, thermal conductivity, Young's modulus (in compression), and fatigue strength. Cermets containing different fuel loadings and particle sizes were fabricated for testing. The thermal conductivity of a UO_2-40Mo cermet (150-μ fuel particles) was measured by the radial-heat-flow method and the data obtained were fit to the following equation:

$$k = 16.539 + 2.649 \times 10^{-3}\ T$$

where k = thermal conductivity in Btu/(hr)(ft)(°F) and T = temperature in °F over the range 750 to 1700°F (400 to 927°C).

(R. A. Smith)

Table I-5 TENSILE DATA FOR W-(UO_2-ThO_2) COMPOSITE MATERIALS TESTED IN HELIUM[53]

Specimen[a] composition	Density, % of theoretical	Temp., °C	Strain rate, 10^{-3}/min	Ultimate strength, kg/mm^2	Elastic modulus, 10^3 kg/mm^2	Elongation,[b] %
W-(36UO_2-4ThO_2)	95.9	25[d]	0.75	6.7	21.3	Nil
	95.7	25[d]	0.75	7.9	18.3	Nil
	95.7	25[d]	0.75	7.8	20.4	Nil
	--	1100	0.114[d]	15.0	17.2	0.4
	--	1100	0.114[d]	10.4	29.3	--
	--	1100	0.114[d]	8.2	19.4	--
	--	1100	0.114[d]	11.8	32.3	0.2
	--	1100	0.114[d]	7.0	13.8	0.2
W-(45UO_2-5ThO_2)	94.5	25[c]	0.75	5.6	18.2	Nil
	95.7	25[c]	0.75	4.6	19.1	Nil
	95.5	25[c]	0.75	5.2	16.3	Nil
W-(54UO_2-6ThO_2)	94.2	25[c]	5.0	4.0	8.6	Nil
	94.8	25[c]	5.0	3.7	10.3	Nil
	94.9	25[c]	0.75	7.5	16.1	0.1[e]
	95.0	25[c]	0.75	8.5	15.7	0.1
	95.2	25[c]	0.75	6.3	17.8	0.1[e]
	94.7	816	5.0	10.3	14.2	0.2[e]
	94.9	816	5.0	10.4	15.7	0.4
	95.3	816	5.0	10.8	--	0.3
	94.0	1093	5.0	6.6	17.7	0.3[e]
	95.7	1093	5.0	11.0	--	0.5
	94.8	1093	5.0	9.8	--	0.4[d]
	95.2	1093	28.0	7.9	9.6	0.4
	95.0	1370	5.0	13.6	--	0.4
	96.7	1370	5.0	12.5	--	0.7[d]
	95.9	1370[f]	20.0	15.0	--	0.3
	95.2	1370[f]	5.0	14.7	--	0.2
	95.5	1370[f]	5.0	13.3	--	0.4
	94.9	1370[f]	10.0	15.9	--	0.2
	94.9	1650[f]	5.0	11.6	--	0.7
	95.6	1650[f]	5.0	11.7	--	0.7[e]
	95.2	1650[f]	5.0	10.7	--	0.9
	95.5	1650[f]	8.0	10.0	--	0.6[e]
	95.4	1650[f]	10.0	11.1	--	0.4
	95.8	1650[f]	50.0	13.3	--	0.6
	95.6	1650	50.0	13.4	5.4	1.6

a Specimens were 0.32 cm in diameter.
b In 2.54-cm gage length.
c Tested in air.
d Crosshead speed in 10^{-3} cm/min.
e Failed outside gage length.
f Tested in helium + 5 vol.% hydrogen.

Table I-6 TENSILE DATA FOR Mo-($54UO_2$-$6ThO_2$) MATERIAL[a] TESTED IN HELIUM[53]

Specimen density, % of theoretical	Temp., C	Ultimate strength,[b] kg/mm^2	Elastic Modulus, 10^3 kg/mm^2	Elongation,[c] %
92.4	25[e]	5.0	11.4	Nil
--	816	9.4	6.9	0.4[e]
--	1093	10.2	--	0.3
94.0	1093	11.6	13.8	0.2[e]
--	25[c]	7.5	--	0[g]
94.2	25[c]	8.3	14.2	0[g]
98.4	25[c]	8.7	14.2	0[g]
93.8	816	10.3	--	--
94.0	816	10.1	--	0.4[e]
--	816	10.5	11.6	Nil
93.2	1093	6.7[f]	2.4	0.5[e]
93.2	1093	11.3	--	0.1[e]
95.4	1093	11.4	--	0.2[e]
--	1093	12.7[f]	--	0.5[e]
--	1093	11.6	--	0.4
93.9	25[d]	7.2	--	0.1[e]
--	1093	12.1	--	0.3[e]
93.8	1093	9.0	--	0.1[e]
--	1093	11.1	--	0.1[e]
96.3	25	10.9	--	0.2
96.5	816	12.9	--	0.3[e]
96.5	1093	12.3	--	0.3[e]
96.5	1093	16.7	--	0.3[e]
96.4	1370	12.8	--	0.7
96.5	1370	12.8	--	0.6
96.3	1650	10.3	--	5.6
96.4	1650	8.7	--	6.2
96.5	1650	7.1[f]	--	3.8
96.9	1650	8.2	--	1.8

a Specimens were 0.32 cm in diameter.
b Strain rate was 0.005 min^{-1} unless otherwise noted.
c In 2.54-cm gage length.
d Tested in air.
e Failed outside gage length.
f Strain rate was 0.0025 min^{-1}.

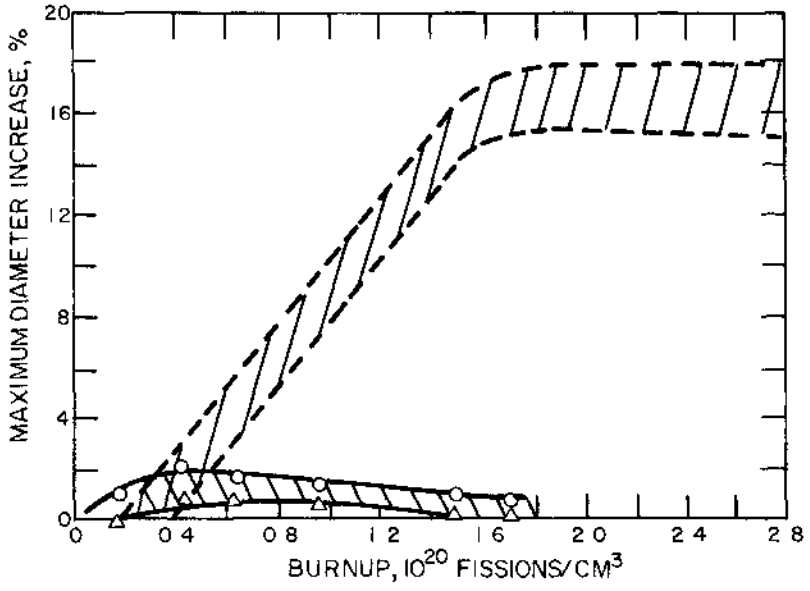

Fig. I-8 Effect of burnup on diametral swelling of W-UO_2 cermets.[54] Surface temperatures for the cermets ranged from 1600 to 1800°C. ZZZ, W-50 vol.% UO_2, 20-mil cladding; ▨: o, W-42 vol. % UO_2, 28% porosity 40-mil cladding, vented; △, W-42 vol. % UO_2, 28% porosity, 40-mil cladding.

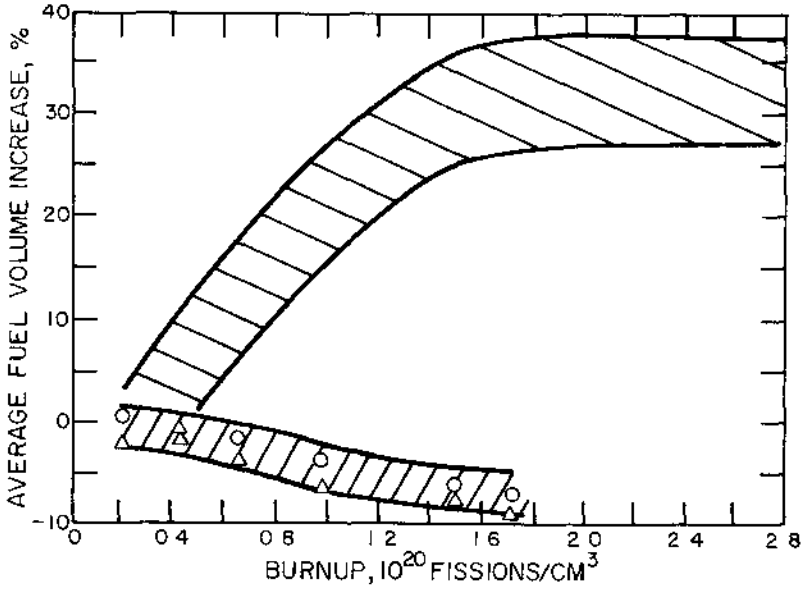

Fig. I-9 Effect of burnup on volumetric swelling of W-UO_2 cermets.[54] ▨, W-30 vol.% UO_2, 20-mil cladding; ▨: o, W-42 vol. % UO_2, 28% porosity, 40-mil cladding, vented; △, W-42 vol. % UO_2, 28% porosity, 40-mil cladding.

[redacted]

5. Coated-Particle Fuels

Development of processes for the coating of nuclear-fuel particles appears to be at a low rate of effort. However, evaluation of coated products of existing processes is receiving significant attention. At Gulf General Atomic, studies of defective PyC-coated particles, which include an SiC-barrier coating, are being intensified because of the proven significance of defective coatings in fission-product release.[56a] Quantitative information on the contribution of various types of defective coated particles to fission-product release is being obtained.

Detailed studies of the thermal stability of TRISO-coated particles[57] are being undertaken (1) to determine mode of failure, (2) to estimate more accurately the time-temperature limitation, and (3) to determine methods of improving thermal stability. Observations of the release of metallic fission products from TRISO-coated particles have indicated that defects in the SiC layer are responsible for the major amount of the metallic-element release.[58] A burn-leach test for the detection of damaged or absent SiC layers on TRISO-coated particles is being developed to provide a rapid method for determining defective SiC layers in production batches of these particles.

Results of microprobe analyses of irradiated TRISO particles suggest that the mechanism that produced the amoeba effect in BISO particles may also play a role in TRISO particles.[58,59] Precipitation of carbon on the side of the core opposite the core-coating interaction is similar in both particles. The formation of mobile silicon compounds with the fission products ruthenium, thorium, and technetium at the reaction zone may affect the temperature limits of the TRISO particles. The reaction between core and coating was observed after irradiation at 1300°C but was not detected after irradiation at 600°C.[60]

At Oak Ridge, 20-μ-thick SiC coatings were applied to 14 kg of ThO_2 for use in fuel-reprocessing studies. Deposition efficiencies of 60 to 75% and rates of 0.35 to 1.0 μ/min were obtained at 1500 to 1600°C with methyltrichlorosilane as the coating reactant.[61] At General Atomic, SiC coatings deposited from the coating reactant methyldichlorosilane were compared with SiC coatings deposited from methyltrichlorosilane.[56a] The bend strengths were nearly equal. It was also observed that intergranular pores and cracks were present in the SiC coatings. The frequency of flaws was found to vary between coating runs, and this could account for the variability in strength of SiC from different coating runs made at nearly identical conditions.

(N. D. Veigel)

6. Uranium and Thorium Oxides

Properties and Behavior of Uranium and Thorium Oxides

At General Electric,[63] thermal-conductivity measurements were performed on 82, 86, and 91% dense UO_2 at temperatures between 800 and 2000°C in an argon atmosphere

by means of the radial heat-flow technique. The thermal-conductivity values for UO_2 to within ±10% were related to the temperature (T) and the density (D) by the equation

$$k = 0.0130 + \frac{1}{T\,(0.4848 - 0.4465D)} \text{ watt/(cm)(°C)}$$

for T between 800 and 2000°C and D between 82 and 95% of theoretical.

Henney and Jones[64] employed an optical interferometric technique to study the growth of grain-boundary grooves and the decay of surface scratches on UO_2 at 1100 to 1700°C. The surface diffusion coefficient for $UO_{2.005}$ was found to follow the relationship

$$D_S = 1.3 \times 10^8 \exp\,[-(110,000 \pm 15,000)/RT]\ cm^2/sec$$

between 1200 and 1400°C. It was noted that the rate of grooving increased markedly as the oxygen content of the UO_2 increased.

(R. H. Barnes)

Preparation of Fuel Bodies

The addition of 0.1 to 4.0 wt.% iridium to UO_2 powder to inhibit columnar grain growth at 1800°C is the subject of a U.S. patent.[65] Equiaxed grain growth from 10 to 25 μ occurred in the iridium-containing specimens, while pure UO_2 specimens prepared in the same manner exhibited a columnar grain growth about 250 μ in length with a 40-μ equiaxed diameter.

A British patent[66] describes the preparation of hollow spherical UO_2 particles. The starting UO_2 powder is first oxidized at 180 to 300°C, mixed with a small amount of $CaO\text{-}TiO_2$ powder, granulated, and spheroidized in an oxyacetylene flame at 3000°C. Upon cooling, the spheroids are reduced to stoichiometric proportion in hydrogen. The resultant particles are characterized by high density and closed internal porosity.

(T. R. Wright)

7. Carbide and Nitride Fuels

Properties and Behavior

The quasi-ternary systems UC-ZrC-"CeC" and UN-ZrN-CeN have been examined by Holleck and Wagner at several temperatures.[1b,67] The tentative sections obtained at 1400, 1500, and 2000°C are shown in Figs. I-10 and I-11, respectively.

The Germans[68] have studied alloy formation in UN systems with TiN, HfN, and ZrN. Complete solubility between UN and ZrN was confirmed. Complete solubility between UN and HfN was also observed at 2000 C. The solubility of TiN in UN was found to be 1 mole % at 1700°C, 2 mole % at 2000°C, and 4 mole % at 2400°C.

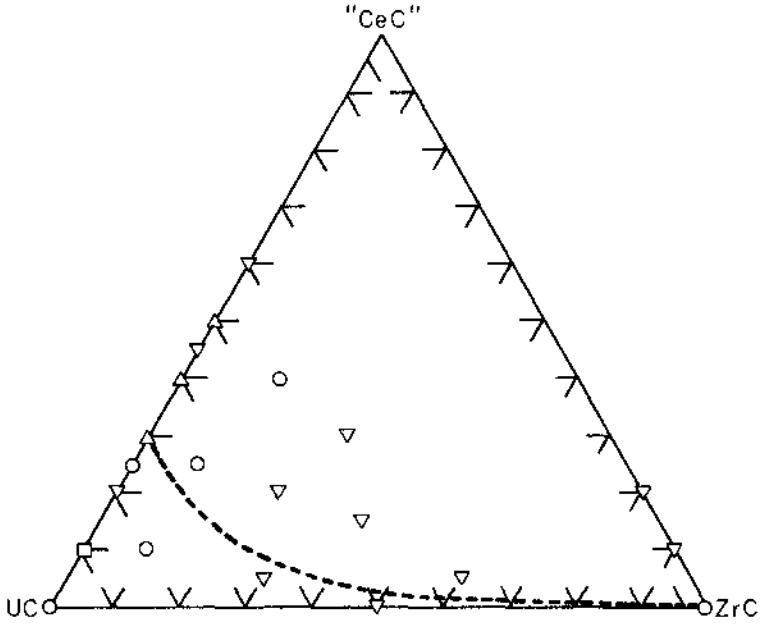

Fig. I-10 Tentative section of the UC-ZrC-"CeC" diagram at 1400 and 1500° C.[67] Single-phase structure: □ , 1400° C; ○ , 1500° C. Two-phase structure: △ , 1400° C; ▽ , 1500° C.

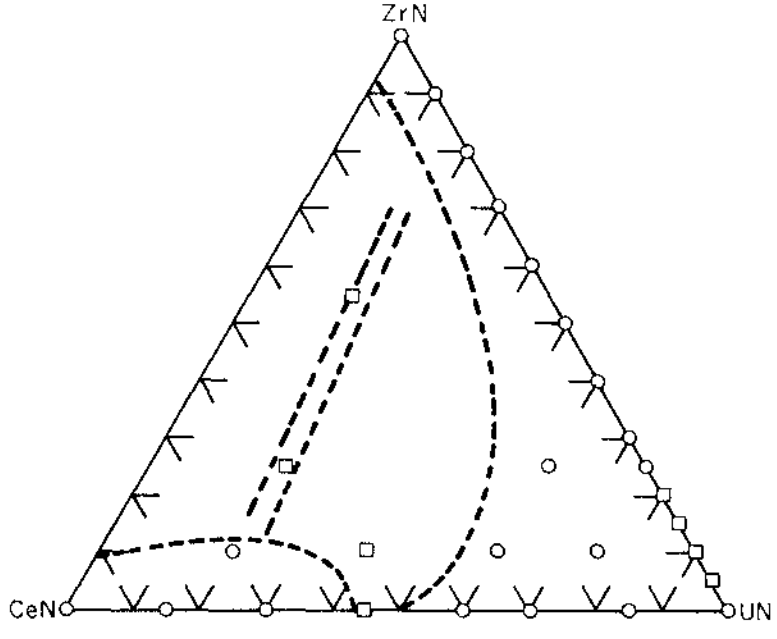

Fig. I-11 Tentative section for the UN-ZrN-CeN system at 2000° C.[67] ○ , single-phase structure; □ , two-phase structure.

The reactions of nonmetallic compounds of uranium were investigated by Imoto et al.[1c] The solubility of UB in UN was estimated to be about 12 mole % at 1500°C. Reaction of silicon with UN produced a solid solution containing a maximum of 28 mole % USi. Excess silicon resulted in the formation of a mixture of this solid solution, $UN_{0.72}Si_{0.28}$, plus U_3Si_5.

Gorle et al.[1d] examined the compatibility of stainless steel with UC stabilized with chromium and vanadium. The results were not entirely consistent, but certain combinations apparently were compatible at 800°C. A new phase, possibly UVC_2, was tentatively identified; on the basis of the compatibility results, the tentative constitution diagram shown in Fig. I-12 was proposed.

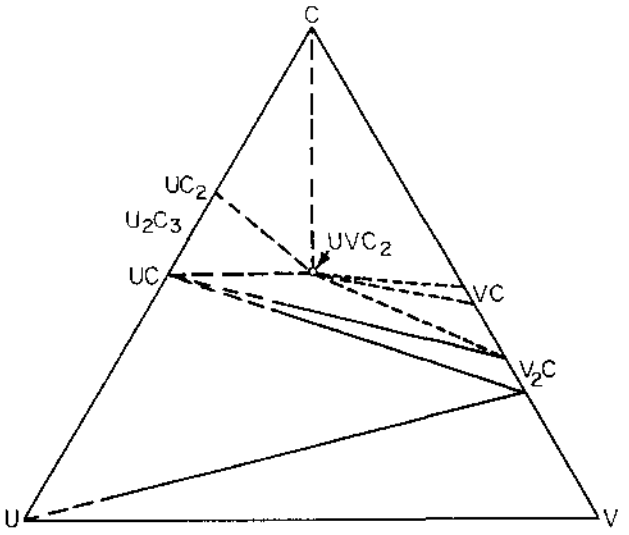

Fig. I-12 Proposed U-C-V phase diagram.[1d]

The determination of the partial pressure of nitrogen over U_2N_{3+x} has been exceptionally difficult. Two independent investigations of this pressure have succeeded in widening the range of scatter of data already in the literature.[1e,69] This discrepancy may be due to variation of the exact composition of the samples.

Naoumidis and Stöcker[1f] heated UC under nitrogen at atmospheric pressure to obtain a mixture of $UC_{0.02}N_{0.98}$ and graphite. Without removing the graphite, the pressure was then reduced and the mixture heated to equilibrium at various temperatures and pressures to determine the stability of UC-UN solid solutions. It was assumed that the $UC_{0.02}N_{0.98}$ proceeded to equilibrium by the reaction $UC_{0.02}N_{0.98} \rightarrow U(C,N) + N_2$ and that no U(C, N) reacted with carbon to form UC_2 or U_2C_3. Since such back reactions to form UC_2 or U_2C_3 are possible and since the pressures obtained were more than an order of magnitude higher than theoretical estimates, it seems likely that the U(C, N) compositions formed at equilibrium contained less uranium and more nitrogen than assumed.

The elastic constants of single crystals of UN were determined by an ultrasonic-vibration method at room temperature.[70] Young's modulus was found to be 38.4×10^6 psi; the shear modulus was 15.1×10^6 psi; and Poisson's ratio was 0.27.

The compressive creep behavior of UC has been examined at temperatures from 1200 to 1600°C and at stresses from 3000 to 10,000 psi.[71] The equation which best fits all the data over this range is:

$$\dot{\epsilon} = 1.8 \times 10^{-3}\ \sigma^3 \exp(-90{,}000/RT) \quad .$$

A comparison of these data for UC at 6000 psi with data in the literature for UN and UO_2 at 6000 psi shows a remarkable correlation (Fig. I-13). Since these uranium compounds all have cubic crystal structures and since diffusion of uranium probably controls creep by the vacancy mechanism, such a correlation may be expected.

(W. Chubb)

Preparation and Fabrication

Gorle et al.[1g] investigated the reduction of pressed pellets of hyperstoichiometric UC to the single-phase monocarbide by heat treating in a reducing hydrogen atmosphere. The reduction in pure hydrogen, $UC_2 + 2H_2 \rightarrow UC + CH_4$, starts around 300°C and is very rapid at 550°C. However, reduction of the monocarbide also occurs, $UC + 2H_2 \rightarrow U + CH_4$, and proceeds so rapidly that it is difficult to stop the reaction before formation of a hypostoichiometric product. Diluting the hydrogen with argon reduces the reaction rate considerably and offers the possibility for a controllable commercial process.

The inclusion of methane (CH_4) in the hydrogen atmosphere at a concentration intermediate to that required for equilibrium of the two reactions appears more promising. It was shown that a CH_4 concentration of 5000 to 8000 ppm (by volume) produced single-phase UC, with the reaction rate practically independent of the concentration. Residual oxygen in the compound can promote the formation of free uranium during subsequent fabrication; therefore, both the oxygen content and the fabrication process must be considered in determining the optimum gas mixture.

Single-phase, high-density UC has been fabricated by warm pressing a stoichiometric mixture of UC_2 and uranium powders at 1000°C to obtain a density roughly equal to that of the monocarbide and then reactive sintering at temperatures as low as 1400°C for 2 hr to form the monocarbide.[72] A density of 98% of theoretical is easily attained by this procedure, but further work is required to optimize the parameters of the process.

(J. T. Lowder)

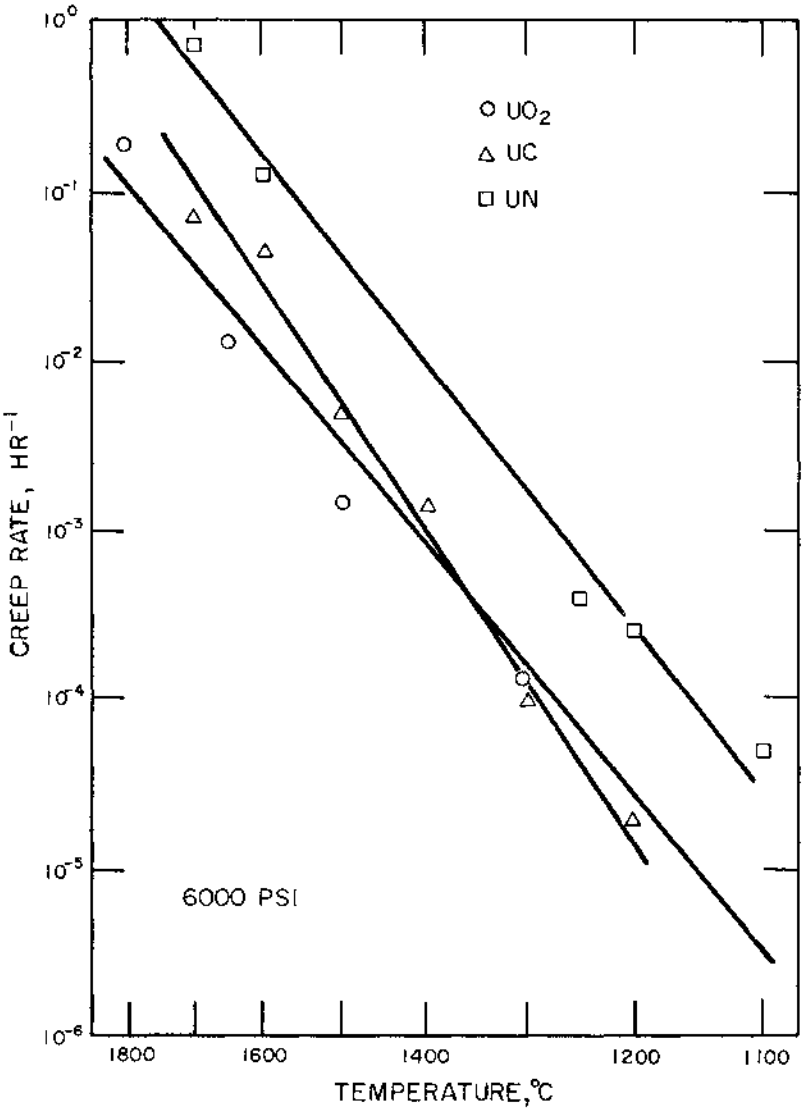

Fig. I-13 Creep rates of ceramic fuels as a function of temperature at 6000 psi.[71]

8. Basic Studies of Irradiation Effects in Fuel Materials

Metals

Computer analyses can be effective in dealing with some of the complex problems associated with radiation damage in crystals. Klimenkov et al.[73] conducted a study in which one of the techniques reduces to an examination of a small region in an infinite crystal around the initial location of a primary displaced atom. The remainder of the crystal is replaced by an elastic continuum and the motion of the atoms in this crystal region is described by classical equations. The size assigned to the region and its shape are determined by the energy of the displaced atom, the computer memory capacity, and the basic content of the problem to be solved.

A computer program, FIGS (Fission Gas Swelling) has been developed at General Electric[74] to study the high-temperature fission-gas swelling of matrix-type fuel elements. The Foreman-type analytical model was modified for this use, providing a method which is a conservative technique for estimating swelling.

A computer program, BEMOD, has been written at Argonne[19c] to model the behavior and to estimate the lifetime of a metallic fuel element during irradiation. An empirical "equation of state" was assumed to represent the compressible fuel. In this equation the volume of a section of fuel rod was assumed to be a function of burnup, ambient pressure, and average temperature. This assumption was based upon several parameters determined from swelling experiments made under pressure. The BEMOD code is being used to compare the predicted behavior of a fuel element with actual behavior in order to determine the adequacy of the code in describing the behavior of the cladding, fuel, and fuel element.

Computer simulations of radiation-damage events in a lead iodide crystal have been carried out by Torrens and Chadderton.[75a] Calculations were restricted to one plane of the lattice, and emphasis was placed on obtaining a qualitative model for the behavior of knocked-on atoms of energies which might result from secondary fission-fragment damage, rather than on accurate quantitative results. In particular, the importance of directional events such as focusing and channelling was investigated.

The damage produced in a single crystal by the excited electrons energized by a fission fragment has been described by Chadderton et al.[75b] on the basis of a simple classical model. An "average" primary electron, or delta particle, possesses a typical energy of some 80 ev which is communicated to the lattice, first by electron-electron interactions and then by electron-phonon interactions. It was concluded that the nature of the fission-fragment damage observed in crystals by electron microscopy will depend primarily upon (1) the rate at which secondary electrons are produced by primaries, (2) the effective range of the secondaries, (3) the activation energies for defect-creating processes, (4) whether the crystal is an element or compound, and (5) the activation energy for defect migration.

Lidiard and Nelson[76] have noted that a strain field generally exists around gas bubbles even in thermodynamic equilibrium. The existence of this strain field leads to

a small attraction between bubbles but in typical practical situations, this effect is significant for bubble migration only when the bubbles are close together compared to their radii.

In metals irradiated at low temperatures and subsequently subjected to high-temperature treatment, the resulting defects involve the formation of three-dimensional clusters of vacancies (i.e., cavities or pores). This formation is due to the heat-induced relaxation of the local shear stresses that had been generated in the crystal by previous irradiation. A mathematical formulation of this problem has been developed by Lyubov and Semenov[77] regarding the metal crystal as a continuum obeying the macroscopic theory. The macroscopic defects (pores) occur only at high temperatures, and they influence the strength characteristics of the material by restricting, in particular, the migration of dislocations.

The relation between grain-boundary migration and the distribution of inert gas in aluminum has been investigated by Kawasaki.[78] It was concluded that under the given experimental conditions, the sweeping of inert gases by moving grain boundaries did not have a significant effect. It was not clear in this study whether inert-gas bubbles were formed or not.

Ceramics

An analytical study of pore migration in ceramic fuel elements has been conducted by Nichols.[79] For the case in which the dominant mechanism of material transport is evaporation-condensation, it was shown that a spherical pore migrates up a thermal gradient without distortion. A second-order effect predicts distortion of an initially spherical shape, the pore tending to elongate along the thermal gradient. Some speculations concerning the origin and stability of the lenticular voids sometimes observed were also reviewed.

The release of fission products from coated fuel particles is being evaluated at Gulf General Atomic.[56b] Estimation of fission-product release has been attempted using the SLIDER code. This code consists of a numerical solution of Fick's law in spherical coordinates, continuity equations, a representation of fission-product decay and birth rates as a function of position, and a thermodynamic description of fission-product behavior at interfaces. These studies are related to safety evaluation of an HTGR reactor system.

Carroll et al.[80] have shown that at relatively high fission densities, the fission-gas release from UO_2 is accelerated as the fission density is increased. It was noted that most UO_2-fueled, water-cooled power reactors operate in fission-density regions in which the fractional fission-gas release rate is decreasing or is constant with an increase in fission rate. However, some gas-cooled and fast sodium-cooled reactors are planned for operation in the region in which fractional release will increase with higher fission densities.

The microstructures of irradiated UO_2 fuel pellets have been examined by Manley[81] using transmission electron microscopy. He observed, for example, that gas bubbles were often associated with black dots which were probably solid fission products. Bubbles not associated with black dots were found to migrate by a surface diffusion process.

Evidence that a fission-gas re-solution process must operate during irradiation was also found.

Samples of UO_2 and UC were irradiated by Kingery et al.[82] at liquid-nitrogen temperature and then annealed at either 21 or 400°C. Density changes during these anneals were measured to high precision and compared with the corresponding changes in lattice parameter determined by others. For UO_2 irradiated to 0.86×10^{16} fissions/cm^3, the density changes determined by the two methods were in agreement, but at 0.83×10^{17} fissions/cm^3 the density decrease measured directly exceeded that calculated from parameter changes. It was concluded that interstitials produced by fission damage recombine to form dislocation loops.

The effect of the migration of fission products on measurements of burnup in fuel elements has been studied by Miller et al.[83] Migration of fission products along the length of a fuel element was demonstrated using a gamma spectrometer with a Ge-Li detector. It appears that this technique may also give information regarding operating temperatures and the state of the fuel without destroying the fuel element.

In radioactive substances under the effect of their own radiation, point defects of structure (vacancies and interstitial atoms) occur in concentrations considerably higher than they do when the substances are in thermodynamic equilibrium. The energy of these structural defects ("stored" energy) increases the free energy of the irradiated substance, which may cause a change in some of its physical and chemical properties. Gagarinskii et al.[84] investigated a method for the thermal analysis of the accumulation of structural defects in the tetraiodide of ^{233}U under the effect of self-irradiation. Influences on the temperature of the phase transition were also evaluated.

The processes of radiation damage in ceramic materials of interest in nuclear technology have been reviewed by Lidiard.[85] The growth of gas bubbles in nuclear fuels is one of the topics discussed.

(A. J. Markworth)

I. FUEL AND FERTILE MATERIALS

REFERENCES

1. Thermodynamics of Nuclear Materials, 1967, International Atomic Energy Agency, Vienna, 1968.

   a. D. Cerovic and M. M. Ristic, Thermodynamic Characteristics of Grain Growth in α-Uranium, pp. 727-733.

   b. H. Holleck and W. Wagner, Ternary Phase Relationships of Oxygen, Nitrogen, and Carbon with Uranium, Cerium, and Zirconium, pp. 667-681.

   c. S. Imoto et al., Reactions of Various Nonmetallic Compounds, pp. 381-383.

   d. F. Gorle et al., Preparation Processes and Stabilization of Uranium Monocarbide, pp. 481-496.

   e. F. Mueller and H. Ragoss, Disorder in Cubic Uranium Sesqui-Nitride, pp. 257-264.

   f. A. Naoumidis and H. J. Stöcker, Stability of UC-UN Solid Solutions in the Presence of Free Carbon, pp. 287-360.

   g. F. Gorle, W. Timmerman, F. Casteel, J. Vangeel, and M. Braber, pp. 481-486.

2. M. H. Yoo, Slip Modes in Alpha Uranium, J. Nucl. Mater., 26: 307-318 (1968).

3. I. Saxl and J. Otruba, Mobilities of Dislocations in α-Uranium, J. Nucl. Mater., 26: 325-330 (1968).

4. J. S. Daniel, F. Jean-Louis, and P. Lacombe, The Temperature Dependence of Slip in α-Uranium, J. Nucl. Mater., 26: 319-325 (1968).

5. I. Saxl, J. Kocik, and J. Otruba, Extended Dislocations and Stacking Faults on {110} and (001) Planes of α-Uranium, J. Nucl. Mater., 25: 172-178 (1968).

6. F. N. Rhines, Structural Changes Associated with High-Temperature Deformation of Uranium, USAEC Report NLCO-988, University of Florida, April 1968.

7. A. F. Smith, The Recrystallization of β-Quenched Uranium Containing Iron and Aluminum, J. Nucl. Mater., 26: 341-344 (1968).

8. A. F. Smith, The Precipitation of Aluminum from Supersaturated Solution in α-Uranium, J. Nucl. Mater., 27(2): 194-200 (August 1968).

9. M. Fource, J. P. Lauque, M. Colombie, and J. Decours, Influence of Boron on Crystallization of α-Phase Alloys of Uranium, J. Nucl. Mater., 26: 185-203 (1968).

10. J. Lehmann, Study of Uranium-Molybdenum Alloys, Arch. Hutn., 13(1): 3-16 (1968).

11. G. Petzow, A. O. Sampaio, and M. DeLourdes Pinto, Phase Equilibria in the Systems U-UMn_2-UFe_2 and UAl_2-UMn_2-UFe_2, J. Nucl. Mater., 26: 331-337 (1968).

12. B. S. Wyatt, The Effect of Carbon on the δ-Peritectoid Reaction in Uranium-Silicon Alloys, J. Nucl. Mater., 27: 201-215 (1968).

13. R. L. Moment, Evaluation of Modified Solidification Techniques for Growth of Large Crystals of Pu-3.3 Atom Percent Gallium Alloy, J. Crystal Growth, 2: 15-25 (1968).

14. Los Alamos Scientific Laboratory, Quarterly Status Report on the Advanced Plutonium Fuels Program April 1 – June 30, 1968, and Second Annual Report, FY 1968, USAEC Report LA-3993-MS, (a) pp. 105-109, (b) pp. 29-35, 43-49, 57, Sept. 12, 1968.

15. J. M. Taylor, A Study of Phase Equilibria with Plutonium-Zirconium Alloys, USAEC Report BNWL-402, Battelle–Northwest, September 1968.

16. D. F. Bowersox and J. A. Leary, The Solubilities of Selected Elements in Liquid Plutonium II., Titanium, Vanadium, Chromium, Manganese, Zirconium, Niobium, Molybdenum, and Thulium, J. Nucl. Mater., 27: 181-186 (1968).

17. D. F. Bowersox and J. A. Leary, The Enthalpies of Selected Elements in Liquid Plutonium, USAEC Report LA-3951, Los Alamos Scientific Laboratory, July 22, 1968.

18. R. L. Cubitt, G. L. Ragan, and D. C. Kirkpatrick, Thermal Irradiation of Liquid Plutonium-Alloy Fuels, USAEC Report LA-3832, Los Alamos Scientific Laboratory, June 4, 1968.

19. Argonne National Laboratory, Reactor Development Program Progress Report, May 1968, USAEC Report ANL-7457, (a) pp. 4-5, (b) p. 106, (c) pp. 103-104, July 2, 1968.

20. W. Z. Wade and T. Wolf, Production of Plutonium Metal by Direct Reduction of the Oxide, USAEC Report UCRL-50403, University of California, Lawrence Radiation Laboratory, Feb. 22, 1968.

21. P. Patriarca (Comp.), Fuels and Materials Development Program, Quarterly Progress Report for Period Ending March 31, 1968, USAEC Report ORNL-TM-2217, pp. 26-29, 129-151, Oak Ridge National Laboratory, June 1968. (Official Use Only)

22. D. L. Plymale and W. H. Smith, The Preparation of Pu-238 Dioxide Microspheres by the Sol-Gel Process, USAEC Report MLM-1450, p. 7, Mound Laboratory, Sept. 30, 1967.

23. K. P. Louwrier, T. Steemers, and E. Zamorani, Formation of Colloidal Solutions of Pu(IV) and the Conversion into PuO_2 Microspheres, German Report EUR-3737 e, Nov. 27, 1967.

24. P. H. Bonnell, Particle Sizing of Plutonium Dioxide Microspheres After Impact, USAEC Report MLM-1499, Mound Laboratory, Dec. 11, 1967.

25. Argonne National Laboratory, Reactor Development Program Progress Report, April 1968, USAEC Report ANL-7445, pp. 124-127, June 12, 1968.

26. W. S. Gilman, A Review of the Dissolution of Plutonium Dioxide. Part II, USAEC Report MLM-1513, p. 12, Mound Laboratory, Aug. 7, 1968.

27. C. A. Burgess, J. E. Hanson, and B. R. Haywood, FFTF Fuel Development Program, USAEC Report BNWL-SA-1750, Battelle – Northwest, Mar. 27, 1968.

28. Nuclear Materials and Equipment Corp., Development and Testing of PuO_2-UO_2 Fast Reactor Fuels, Progress Report, April 1 – June 30, 1967, USAEC Report NUMEC-3524-39, p. 19.

29. Nuclear Materials and Equipment Corp., Development and Testing of PuO_2-UO_2 Fast Reactor Fuels, 12th Quarterly Report, January – March, 1968, USAEC Report NUMEC-3524-50, pp. 16-23. (Official Use Only)

30. E. H. Dewell (Comp.), Gel-Addition Process Chemical Studies, Quarterly Progress Report No. 7, February – April, 1968, USAEC Report BAW-3714-7, pp. 2, 3, 5, 41, Babcock and Wilcox Co., July 1968.

31. R. Theisen and D. Vollath, Plutonium Distribution and Diffusion in UO_2-PuO_2 Ceramics, German Report KFK-696, March 1967.

32. K. Bischoff, J. D. L. Harrison, and P. E. Potter, The Preparation and Characterization of Sintered Uranium-Plutonium Oxides, British Report AERE-R-5774, April 1968.

33. J. K. Butler and D. Clarke, Alpha Scanning of Solid Surfaces and Measurement of Plutonium Migration in Irradiated Ceramic Fuels, British Report TRG-Report-1656 (D), Mar. 5, 1968.

34. J. C. Van Craeynest and J. C. Weilbacher, Study of the Thermal Conductivity of Mixtures of Uranium and Plutonium Oxides, J. Nucl. Mater., 26: 132-136 (Jan. 9, 1968).

35. J. J. Cadwell, D. R. de Halas, R. E. Nightingale, and D. C. Worlton, Reactor Fuels and Materials Development Programs for Fuels and Materials Branch of USAEC Division of Reactor Development and Technology, Quarterly Progress Report, January – March 1968, USAEC Report BNWL-768, (a) pp. 5.2, 5.9, 6.7, (b) pp. 8.1-8.2, Battelle – Northwest, June 1968. (Official Use Only)

36. Argonne National Laboratory, Reactor Development Program Progress Report, June 1968, USAEC Report ANL-7460, pp. 102-103, July 29, 1968.

37. J. A. Christensen, Nonstoichiometry Effects on the Melting Heat Rating for UO_2-25 wt. % PuO_2 Fast Fuels, Trans. Amer. Nucl. Soc., 11(1): 131 (1968).

38. J. L. Krankota and C. N. Craig, Melting Point of High Burnup PuO_2-UO_2, Trans. Amer. Nucl. Soc., 11(1): 132 (1968).

39. J. E. Hanson and J. H. Field, Experimental Studies of Transient Effects in Fast Reactor Fuels, Series III, Pre-Irradiated Mixed Oxide (PuO_2-UO_2) Irradiations, USAEC Report GEAP-4469, General Electric Co., Advanced Products Operation, July 1967.

40. J. R. McLaren, The Sintering Behavior PuO_2-ThO_2, British Report AERE-M-1964, January 1968.

41. B. J. Seddon (Comp.), Physical Properties of Some Plutonium Ceramic Compounds: A Data Manual, British Report TRG-Report-1601(R), Dec. 18, 1967.

42. Argonne National Laboratory, Chemical Engineering Division Research Highlights, May 1967 – April 1968, USAEC Report ANL-7450, pp. 55-61.

43. T. W. Latimer, Compatibility of (U. Pu) Carbides with Selected Commercial Austenitic Alloys, Trans. Amer. Nucl. Soc., 11(1): 99-100 (1968).

44. Atomics International, AEC Unclassified Programs, Quarterly Technical Progress Report, January – March, 1968, USAEC Report AI-AEC-12680, pp. 151-152.

45. F. B. Litton, The Properties and Irradiation Behavior of Carbide Fuels: A Literature Survey, USAEC Report LA-3799, Los Alamos Scientific Laboratory, Oct. 6, 1967.

46. D. L. Keller, Progress Relating to Civilian Applications During July 1967 – June 1968, USAEC Report BMI-1845, pp. A12, A24, A35, A60, A85, Battelle – Columbus, July 1, 1968.

47. J. Gerlach, F. Pawlek, and H. Probst, Contribution to the Thermal Dissociation of Thorium Tetraiodide, J. Less-Common Metals, 14: 355-366 (March 1968).

48. G. M. Adamson, Jr., Fabrication of Research Reactor Fuel Elements, USAEC Report ORNL-TM-2197, Oak Ridge National Laboratory, June 1968.

49. I. B. Fiero, Establishing Allowable Temperature Gradients for Tungsten-UO_2 Fuel Elements Using Cyclic Strain Data, Report NASA-TND-4279, National Aeronautics and Space Administration, Lewis Research Center, January 1968.

50. G. W. Gibson and M. J. Graber (Eds.), Annual Progress Report on Reactor Fuels and Materials Development for FY 1967, USAEC Report IN-1131, pp. 37-39, Idaho Nuclear Corp., February 1968.

51. Los Alamos Scientific Laboratory, Quarterly Status Report on the Space Electric Power R & D Program for Period Ending January 31, 1968, USAEC Report LA-3882-MS, pp. 15-17, Feb. 29, 1968. (Classified)

52. General Electric Co., Nuclear Materials and Propulsion Operation, AEC Fuels and Materials Development Program Progress Report No. 68, USAEC Report GEMP-68, pp. 61-62, Aug. 31, 1967. (Classified)

53. J. B. Conway and W. H. McCullough, Summary Report - High Temperature Materials Engineering Properties Evaluations, USAEC Report GEMP-530, pp. 5-25, General Electric Co., Nuclear Materials and Propulsion Operation, Aug. 18, 1967. (Classified)

54. D. L. Keller and W. Chubb, Developments in the Technology of Nuclear Fuels During August 1967 through July 1968, USAEC Report BMI-1848, pp. 54-62, Battelle - Columbus, Aug. 1, 1968. (Classified)

55. J. F. Collins and P. N. Flagella, Fabrication and Measurement of Properties of Mo-UO_2 Cermets, USAEC Report GEMP-545, General Electric Co., Nuclear Materials and Propulsion Operation, July 7, 1967.

56. Gulf General Atomic, Inc., HTGR Base Program Quarterly Progress Report for the Period Ending May 31, 1968, USAEC Report GA-8662, (a) pp. 103-105, (b) pp. 11-18, June 28, 1968.

57. Gulf General Atomic, Inc., Public Service Company of Colorado Plant Research and Development Program Monthly Progress Report for May 1968, USAEC Report GACD-6900(5-68), pp. 23-24.

58. Gulf General Atomic, Inc., Public Service Company of Colorado Plant Research and Development Program Monthly Progress Report for June 1968, USAEC Report GACD-6900(6-68), pp. 22-24.

59. Gulf General Atomic, Inc., Public Service Company of Colorado Plant Research and Development Program Monthly Progress Report for July 1968, USAEC Report GACD-6900(7-68), pp. 21-22.

60. Gulf General Atomic, Inc., Public Service Company of Colorado Plant Research and Development Program Monthly Progress Report for August 1968, USAEC Report GACD-6900(8-68), p. 19.

61. A. W. Savolaenen (Comp. and Ed.), Gas-Cooled Reactor Program Semiannual Progress Report for Period Ending March 31, 1968, USAEC Report ORNL-4266, pp. 3-5, Oak Ridge National Laboratory, September 1968.

63. R. R. Asamoto, F. Anselin, and A. E. Conti, Effect of Density on the Thermal Conductivity of Uranium Dioxide, USAEC Report GEAP-5493, General Electric Co., Advanced Products Operation, April 1968.

64. J. Henney and J. W. S. Jones, Surface-Diffusion Studies on UO_2 and MgO, J. Mater. Sci., 3: 158-164 (March 1968).

65. C. A. Elyard and T. J. Potter, Sintered Uranium Dioxide-Iridium Composition and Method of Preparation, U.S. Patent 3,342,744, to UKAEA, Sept. 19, 1967.

66. Nuclear Fuel Particles, British Patent 1,109,621, to USAEC, Apr. 10, 1968.

67. H. Holleck and W. Wagner, Ternary Phase Relationships of Oxygen, Nitrogen, and Carbon with Uranium, Cerium, and Zirconium, German Report EURFNR-387, September 1967.

68. H. Holleck, E. Smailos, and F. Thuemmler, Mixed Crystal Formation in the Quasibinary Systems of UN and the Mononitrides of Group IVA, TiN, ZrN, and HfN, German Report KFK-721, January 1968.

69. A. Naoumidis and H. J. Stöcker, Thermodynamics of $UN_{1.5}$ - $UN_{1.75}$, Proc. Brit. Ceram. Soc., No. 8: 193-200 (June 1967).

70. University of California, Lawrence Radiation Laboratory, Advanced Space Nuclear Power Program, Quarterly Report, January - March, 1968, USAEC Report UCRL-50004-68-1, p. 17.

71. D. E. Stellrecht, M. S. Farkas, and D. P. Moak, Compressive Creep of Uranium Carbide, J. Amer. Ceram. Soc., 51: 455-458 (August 1968).

72. J. K. Moorthy and B. D. Zope, Preparation of High Density Uranium Monocarbide (UC) Pellets by Reactive Sintering of a Mixture of Uranium Dicarbide and Uranium Metal Powders, Indian Report BARC-319, 1967.

73. V. I. Klimenkov, V. V. Kirsanov, and Z. Ya. Osipova, Computer Investigation of Radiation Damage in Crystals, At. Énerg. (USSR), 23(4): 356-358 (October 1967).

74. J. E. McConnelee, High Temperature Fission Gas Swelling of Matrix Type Fuel Elements, USAEC Report TID-24386, General Electric Co., Nuclear Materials and Propulsion Operation, March 1966. (Classified)

75. AIME Symposium on Radiation Effects, Asheville, N. C., 1965, Met. Soc. Conf., Vol. 37, 1967.

    a. I. McC. Torrens and L. T. Chadderton, On Correlated Collisions in Hexagonal Compound Lattices, pp. 57-73.

    b. L. T. Chadderton, D. V. Morgan, I. McC. Torrens, and D. Van Vliet, On the Electron Microscopy of Fission Fragment Damage, pp. 183-196.

76. A. B. Lidiard and R. S. Nelson, Gas Bubbles in Solids, Phil. Mag., 17: 425-429 (1968).

77. B. Ya. Lyubov and L. P. Semenov, Pore Formation in Irradiated Metals, Fiz. Metal. Metalloved., 25(2): 307-313 (1968).

78. S. Kawasaki, The Effect of Grain-Boundary Migration on the Xenon Distribution in Aluminum, J. Nucl. Mat., 26(3): 338-340 (June 1968).

79. F. A. Nichols, Pore Migration in Ceramic Fuel Elements, J. Nucl. Mat., 27(2): 137-146 (August 1968).

II. MODERATOR AND CONTROL MATERIALS

1. Graphite

The fluctuations in area density over a disc of high-density graphite 45 mm in diameter and 14 mm thick were measured by the British[1] using a 147-Mev proton beam as the nondestructive probe. An accuracy of ±0.08 kg/m^2 at each point and a spatial resolution of 3 mm were reported. The technique is considered capable of giving an accuracy of ±0.003 kg/m^2 or ~1% of the value of fluctuation, whichever is greater, and a spatial resolution of less than 1 mm for samples up to 100 to 200 kg/m^2 thick.

Information on carbon-base materials for superheat service in reactor cores was compiled by Canadian researchers.[2] It was noted that the present electrographites do not meet the requirements for this application without improvements in such properties as fracture toughness and oxidation resistance.

The oxidation of a variety of PyC-coated fuel-particle types by water vapor has been investigated at Oak Ridge.[3] Flowing He-H_2O mixtures having water-vapor concentrations of 250 to 1000 ppm and a total pressure of 1 atm were studied at 1100 to 1400°C. Rates of reaction of water vapor with pyrolytic carbon coatings were determined from continuously recorded weight changes and from analysis of effluent gases for reaction products. The extent of coating failure was determined from the quantity of uranium and/or thorium leached by acid from the oxidized fuel particles. Differences in oxidation rates were observed for the various batches of coated particles which could not be correlated satisfactorily with the density, anisotropy, and crystallite size of the coatings. Percentages of failed coatings at constant burnoff also varied from batch to batch.

Diffusion data for Cs, Sr, Ba, and Eu in pyrolytic carbon were reviewed by Gulf General Atomic.[4] A linear relation between diffusion coefficients and atomic radii of the metals was suggested by the results as illustrated in Fig. II-1. All the diffusion experiments were carried out using either metal chloride or oxide sources. Since it was shown that the diffusion coefficients for cesium in pyrolytic carbon were higher with a Cs_2O source than with a CsCl source, the question exists as to how well the data apply to reactor calculations where the diffusion sources could be expected to be the metals or metal carbides.

The Japanese[5] have investigated the effects of irradiation on hard carbons (such as the low-permeability glassy carbons). The radiation contraction of hard carbon was found to be isotropic and nonannealable and X-ray diffractions of the material indicated changes similar to graphitization without high-temperature heat treatment. The permeability of reactor graphite impregnated with hard carbon was observed to increase with irradiation.

A pressure cell with a resistance-heated graphite test specimen in a helium atmosphere was used to determine the triple point of four grades of graphite to 1000 atm absolute.[6] The triple-point pressure was determined to be 103 atm for all four grades. The temperature varied for each grade as follows: 7529 ± 19°R for AGOT, 7606 ± 60°R for LANG, 7629 ± 30°R for AGSR, and 7738 ± 45°R for AGKS. The solidus-liquidus interface from the triple point to 1000 atm was also experimentally determined for the

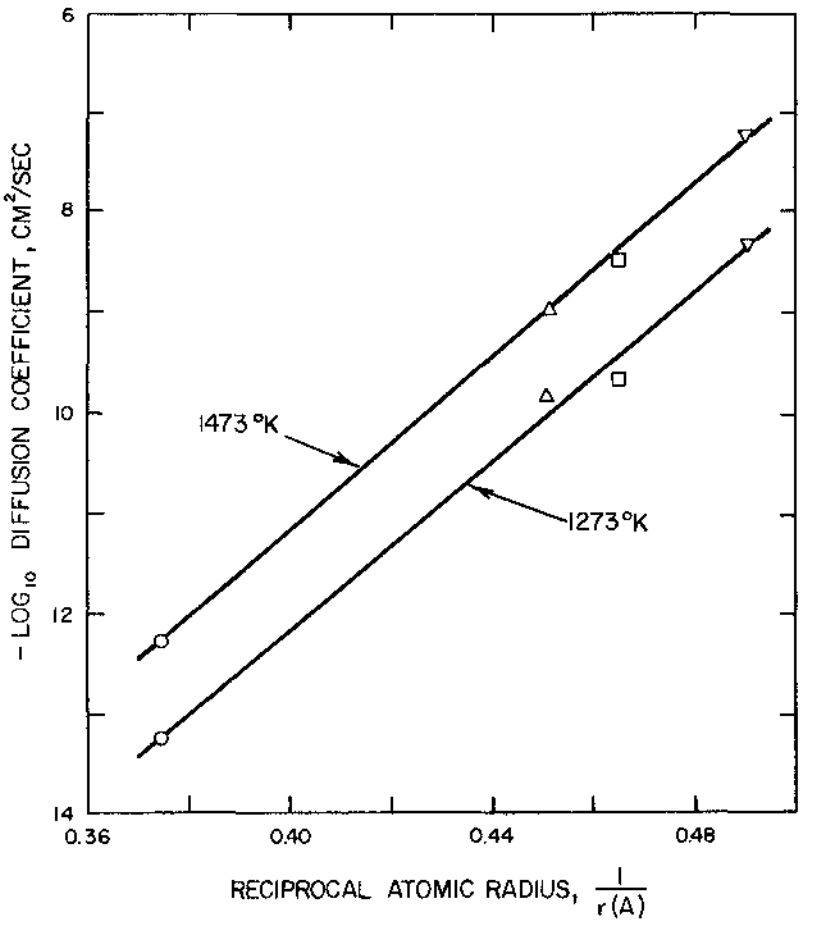

Fig. II-1 Comparison of calculated and measured diffusion coefficients for transport in isotropic pyrocarbon.[4] —, calculated; measured: ○, cesium data; △, barium data; □, strontium data; ▽, europium data.

LANG graphite. The melting point increased with increasing pressure from 7645°R at 103 atm to 7750°R at 1000 atm.

The increasing importance of nondestructive testing of graphites is reflected in an ASTM publication[7] which presents the papers on nondestructive testing of nuclear graphite from a symposium held in June, 1967.

Experiments and analyses to establish the power-density and thermal-stress limitation of graphite fuel elements in Rover reactor cores have been summarized.[8] Significant experimental improvements, modification, and advances in analytical techniques were noted. The effect of temperature on the correlation between the calculated stress and the experimental data at fracture was also established.

(M. C. Brockway)

2. Beryllium and Beryllium Alloys

Mechanical Metallurgy

Divergent X-Ray Beam Studies. The ductile-brittle behavior of beryllium is being studied at Rutgers[9] by characterizing the slip activity and substructural changes which lead to room-temperature cleavage failure and the substructure induced by deformation at higher temperatures. A divergent X-ray beam apparatus was used to obtain the strain configurations in single crystals. Changes in the deficiency conics in the forward-transmission region provided a measure of the substructural changes induced by deformation. When the conic sections of the Kossel-type patterns were sharp and continuous, the crystal was relatively free of defects. Broadening, diffuseness, or discontinuities in the curves indicated the development of a defect structure in the crystal. Also, variations in background intensity allowed foreign particles 1 μ or less in diameter to be observed. Compression specimens oriented for basal slip indicated the formation of tilt and twist boundaries in the early stages of deformation. Reversing the slip direction by rotating the compression specimen resulted in partial restoration of some deformed regions.

Flow Stress for Prism Slip. The flow and fracture characteristics of zone-purified beryllium and beryllium-rich alloys were studied by London and Damiano.[10] Single-crystal-deformation studies of prism slip on zone-refined (12-pass) material and on a 0.68 wt.% copper alloy indicated a flow-stress temperature inversion from 25 to -150°C, with a lower flow stress being observed at the lower temperature. Slip-trace observations suggested that the character of the slip process changed so that prism glide was facilitated at the lower temperatures. Transmission electron microscopy showed that as the temperature was lowered from 25 to -150°C, the frequency of thermally activated cross slip from the prism to the basal plane decreased. Thus, the normally measured flow stress for prism slip in beryllium at room temperature is anomalously high because of rapid work hardening resulting from the thermally activated cross-slip process.

Beryllium Brittleness. Franklin Institute has continued to investigate factors relating to the brittleness of beryllium.[11] The studies are divided into three relatively distinct phases: (1) bicrystal and related behavior, (2) prestraining effects, and (3) theoretical analysis relating to the mechanical behavior of beryllium.

Bicrystal tests have been performed at temperatures up to 350°C on specimens which exhibited little ductility at room temperature. Although macroscopic compatibility can be satisfied in beryllium bicrystals, failure by cleavage on the (0001) plane or $(1\bar{1}20)$ planes is the result of a crack-nucleation mechanism at bend planes arising after some plastic flow. The crack leading to failure then continues by rapid propagation under the influence of a large normal stress. Room-temperature tensile tests on textured polycrystalline material revealed that cracks originate at bend planes for which the normal stress (0001) plane was greatest. It was suggested that the increased ductility with temperature of the bicrystals is associated with the blunting of the (0001) and $(11\bar{2}0)$ cracks, possibly by local pyramidal slip. Polycrystalline samples that also exhibited increased ductility at temperatures of 200 to 350°C were found to contain cracks that do not readily propagate, suggesting a similar blunting mechanism.

Elastic constants of beryllium and its alloys were calculated from the theory of the electronic structure of metal. Using Gilman's expression for the surface energy and calculating the value of the alpha parameter (representing the range or relaxation distance of the atomic forces) for the various crystallographic planes, the surface-energy value obtained for the (0001) plane was lower than that for the $(10\bar{1}0)$ plane. These results agree with experimental observation but are in contrast to the lower value of the surface energy for the $(10\bar{1}0)$ planes obtained by Gilman.

A theory developed by Armstrong[12] for the ductile-to-brittle transition in hexagonal close-packed metals has been applied to limited tensile data on beryllium. The ductile-brittle behavior was related to the critical resolved shear stress for the various deformation systems in single crystals. The theory predicts that at small grain sizes

$$T_c = A + Bd^{1/2}$$

where T_c is the transition temperature, d is the average grain diameter, and A and B are constants that depend on the material. These constants are determined by the following parameters:

(1) Preferred orientation

(2) Fracture characteristic of the material

(3) Slip process within the grains

(4) Accommodating plastic flow mechanism at the grain boundaries.

Fracture Toughness. The influence of loading rate and testing temperature on the fracture toughness of AMS 7902 beryllium sheet has been studied at Boeing.[13] Center-crack and semielliptical part-through crack specimens were tested at variable stress rates. The results of these tests are presented in Fig. II-2. Cyclic tensile loading tests were also performed with center-crack specimens at a constant frequency of 30 cps. These tests appear to support the Corten-Shoemaker hypothesis that an Arrhenius-type

relationship exists among strain rate ($\dot{\epsilon}y$), frequency factor (A), absolute temperature (T_R), and fracture toughness (K_{Ic}). Only large changes in loading rate had an appreciable effect on K_{Ic}. For severe stress environments, a minimum K_{Ic} was found which was relatively insensitive to further reduction in testing temperature and increases in stress rate. This minimum of 11 ksi$\sqrt{in.}$ is recommended as a design K_{Ic} value.

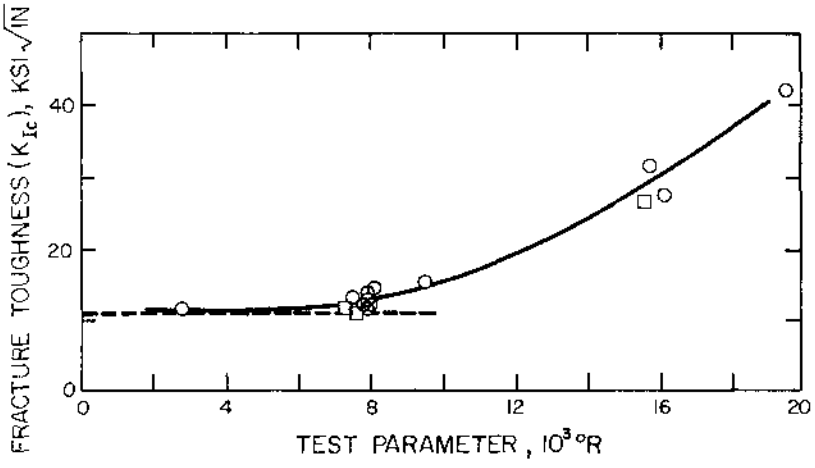

Fig. II-2 Effect of temperature and strain rate on fracture toughness of AMS 7902 beryllium.[13] ○, center-crack specimens; □, surface part-through specimens. P (parameter) = $T_R \ln \frac{A}{\dot{\epsilon}_y}$ where T_R is absolute temperature, °R; A is frequency factor, 10^3 sec^{-1}; and $\dot{\epsilon}_y$ is strain rate in y direction, sec^{-1}.

Physical Metallurgy

Recovery and recrystallization studies of beryllium sheet with additions of 3.3 wt.% copper or 4.2 wt.% nickel were performed at Franklin Institute.[10] The optical microstructure of specimens heat treated in the 600 to 650°C range exhibited very little change, while a heat treatment of 700°C for 15 min produced recrystallization. Transmission electron microscopy revealed that a wide range of substructures were produced in the recovery heat-treatment range of 600 to 650°C even though the optical microstructure failed to reveal significant responses. Bend and tensile tests showed that the greatest ductility was observed for recovered rather than recrystallized material and that recrystallization also caused a decrease in strength. Thus, for improved mechanical properties, it appears to be preferable to heat treat beryllium in the recovery range rather than at recrystallization temperatures.

The Russians[14] investigated self-diffusion in polycrystalline beryllium by using the ^7Be isotope. Curves were constructed of the specific activity as a function of the diffusion quadratic for temperatures of 650, 800, 900, 1000, and 1200°C. The diffusion coefficient as a function of temperature was calculated to be:

$$D = 0.36 \exp(-38,400/RT) \text{ cm}^2/\text{sec}$$

Powder Metallurgy

The effects of powder particle size on the physical behavior of press-forged beryllium have been investigated by the Army.[15] A single lot of electrolytic beryllium powder was sized to fractions of nominally minus 43 μ and minus 20 μ. This provided approximately an equivalent metallic-impurity content for the two fractions, with powder-surface area and resulting oxide distribution in the densified beryllium being the main variables. The total oxide content was similar for the two powder fractions (1.0 wt.% oxide for the minus 43-μ powder and 2.2 wt.% oxide for the minus 20-μ powder). Both powders were vacuum hot pressed to block, and 2-in. cubes were machined for press forging to a 1/2-in. height. Prior to forging, the specimens were solutionized at 1900°F (1040°C) for 6 hr and quenched in flowing argon.

After forging at 1400, 1600, 1800, and 1900°F (760, 870, 980, and 1040°C), specimens were either aged at 1400°F for 8 hr and furnace cooled or solutionized at 1900°F for 6 hr and quenched in flowing argon. The impact strength, as shown in Fig. II-3, was influenced by powder particle size; the minus 20-μ material exhibited a resistance to impact considerably greater than that exhibited by the minus 43-μ material. Forging or heat treatment at the higher temperatures substantially decreased these effects. The tensile strengths, as shown in Fig. II-4, have similar trends but to a lesser extent. Metallographic examination of samples produced with both powder sizes revealed little difference in that all exhibited similar grain sizes and the oxide particles were concentrated in network-like zones. Thus, the oxide dispersoid appears to influence beryllium beyond the normally considered grain-refinement strengthening.

Corrosion

Corrosion of beryllium by water vapor (5 and 30 mm Hg) at 600 to 800°C was studied with a Gulbransen-type microbalance.[16] At 600°C oxidation followed the parabolic rate law during an initial period, after which the pattern became exponential. At 650 and 700°C, the oxidation at first proceeded exponentially and later became linear with time. The latter step was accompanied by breakaway of the oxide film. At 800°C, the oxidation obeyed the rectilinear rate law throughout the course of the experiment. Electron metallography indicated that the logarithmic-rate behavior can be attributed to the generation of blisters at the oxide-metal interface and that the ensuing rectilinear pattern stems from breakaway of the oxide film.

(F. T. Zurey)

3. Solid Hydrides

Hydrided Zr-U Alloys

Pressure-temperature isochores for the Zr-U-H system have been extended to 1300°C in measurements at General Atomic.[17] The compositions covered the H/Zr range from 1.50 to 1.70 with a uranium content of 8 wt.% for most of the work, although some data were obtained for the pure ZrH. Equilibrium dissociation pressures at high temperatures for H/Zr compositions from 1.60 to 1.70 agreed with values extrapolated

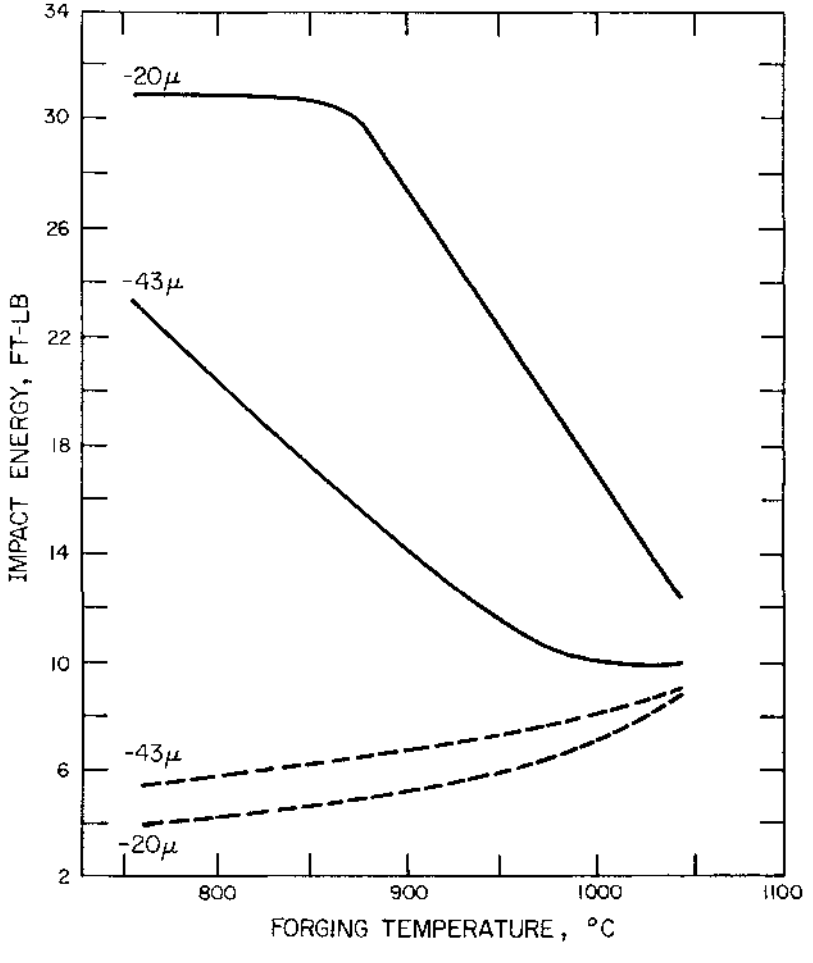

Fig. II-3 Impact resistance of forged beryllium powder block.[15] ——, 1400°F treatment; – – –, 1900°F treatment.

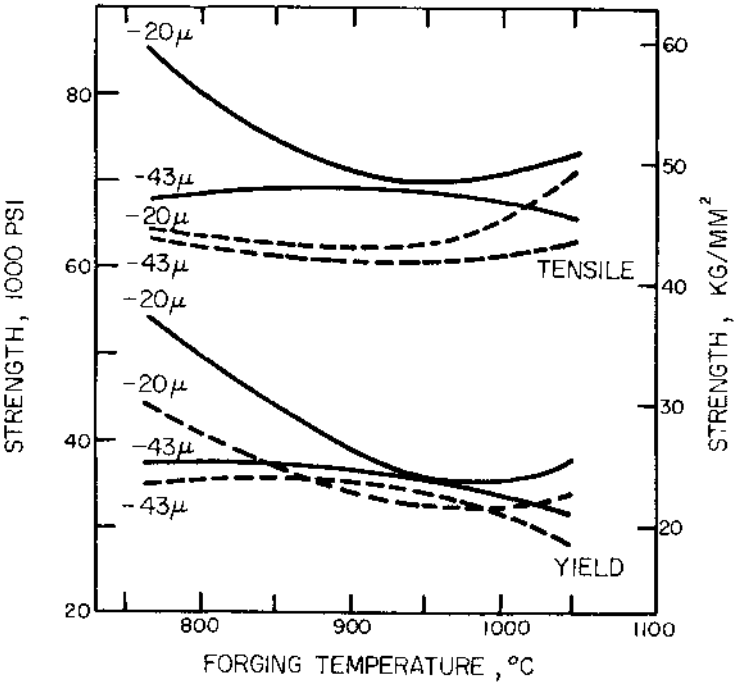

Fig. II-4 Yield and tensile strength of forged beryllium powder block.[15] ——, 1400°F treatment; – – –, 1900°F treatment.

from data previously determined for temperatures below 900°C. However, for the H/Zr range from 1.50 to 1.55, the equilibrium pressures at temperatures above 1000°C were found to be significantly lower than the extrapolated values.

Fully enriched test fuel elements containing 8 wt.% uranium and having H/Zr ratios from 1.60 to 1.65 were loaded in the TRIGA Mark F reactor and pulsed. After 400 pulses, selected fuel elements were declad and examined metallographically. These examinations showed that fuel-body performance at temperatures up to the design point of 1000°C was satisfactory in that no evidence of interaction between the cladding and the fuel was observed. Peak gas pressures measured during the pulses were less than 40 psig, which was well below the upper boundary indicated by the equilibrium pressure data.

Yttrium Hydride

A U.S. patent for a moderator-fuel element based on YH_2 has been granted to the Atomic Energy Commission of France.[18] The element consists of molybdenum-coated fuel particles dispersed in the YH_2 moderator. The fabrication method disclosed requires that ground yttrium metal be mixed with the coated fuel particles, and the mixture then sintered. The sintered product is placed in a can of molybdenum or other refractory alloy and then hydrided. A British patent has also been obtained on the process.[19]

Rare-Earth Hydrides

The light rare-earth metals form a single-phase dihydride which expands without structural change to the trihydride composition as hydrogen is added. However, the heavy rare earths undergo a structural change in going from the dihydride to the trihydride. For this reason a typical heavy rare earth, erbium, has been studied in detail with respect to its hydride phases. At the same time that work was being conducted at Denver Research Institute,[20] Russian investigators[21] were also studying the Er-H system. Pressure-temperature-composition data were obtained at Denver over the composition range from pure metal to ErH_3, while the Russian investigators used X-ray diffraction techniques to study the same compositions. Both groups used the best erbium metal available, which was 99.9 wt.% in the case of the U.S. investigators and 99.5 wt.% for the Russian workers.

Because the approaches in the two studies were different, and the data are presented differently, it is difficult to compare results. In addition, the X-ray data were taken at room temperature, while the isotherms were derived at high temperatures. However, both studies showed that as hydrogen is absorbed by the hexagonal erbium metal, a face-centered cubic phase characterized as ErH_2 is formed. The Russian investigators found a two-phase region, consisting of Er-H solid solution and ErH_2, from 7 to 66 at.% hydrogen at room temperature. From 500 to 950°C in the Denver work, this two-phase region appeared in the range 28 to 33 at.% hydrogen and extended to 66 at.% hydrogen. Both groups found a narrow range of homogeneous ErH_2 between 66 and 68 at.% hydrogen. Another two-phase region, consisting of ErH_2 and ErH_3, was located between 68 and 73 at.% hydrogen at room temperature and from 68 to 75 at.%

hydrogen at the higher temperatures. Finally, the single-phase ErH_3 was noted from 73 to 75 at.% hydrogen at room temperature.

The Russian workers determined the lattice parameter of the ErH_2 phase to be $a_o = 5.125$ A, which is in good agreement with unpublished work cited by the Denver group. However, the Russians claimed that the ErH_3 is rhombic, while the others reported a hexagonal close-packed structure for ErH_3, with $a_o = 3.63$ A and $c_o = 6.54$ A. Considering that some of the other rare-earth trihydrides have been found to have the hexagonal structure, it seems likely that the Russians have indexed the structure incorrectly.

The isotherm work also permitted calculation of thermodynamic properties of the Er-H system. The differential heats and entropies of reaction were calculated to be:

	$Er_{ss} + ErH_2$	$ErH_2 + ErH_3$
Heat of reaction, kcal/mole H_2	-52.6 ± 0.3	-19.8 ± 0.2
Entropy of reaction, cal/(mole H_2)(°C)	-35.2 ± 0.3	-30.1 ± 0.4
Log dissociation pressure, torr	$-\frac{11,500 \pm 70}{T} + 10.57$	$-\frac{4320 \pm 50}{T} + 9.46$

The integral free energies, enthalpies, and entropies of mixing determined for the Er-H system are shown in Table II-1.

Table II-1 INTEGRAL FREE ENERGIES, ENTHALPIES, AND ENTROPIES OF MIXING IN THE Er-H SYSTEM AT 923°K[20]

Composition, H/Er ratio	$-\Delta G^M$, kcal/ gram atom soln	$-\Delta H^M$, kcal/ gram atom soln	$-\Delta S^M$, cal/ (°K)(gram atom soln)
0	0	0	0
0.05	0.71	1.05	0.37
0.10	1.27	2.00	0.79
0.15	1.75	2.88	1.22
0.20	2.19	3.70	1.64
0.25	2.55	4.47	2.08
0.30	2.87	5.20	2.52
0.35	3.17	5.91	2.96
0.40	3.43	6.57	3.40
0.45[a]	3.70	7.21	3.80
1.80[a]	6.10	15.60	10.30

a Solubility boundaries of the two-phase region, $Er_{ss} + ErH_{1.80}$.

The character of the Er-D system was also established at Denver Research Institute.[22] The only observable difference in the pressure-temperature-composition data was a shift to higher pressures in the dueterium curves compared with the hydrogen curves. The solubility boundaries for the Er-D system were the same as those for the Er-H system, within experimental error. The heats of reaction and entropies of reaction were also very close to those found with hydrogen:

	$Er_{ss} + ErD_2$	$ErD_2 + ErD_3$
Heat of reaction, kcal/mole H_2	-53.0 ± 0.2	-20.0 ± 0.1
Entropy of reaction, cal/(mole H_2)(°C)	-36.3 ± 0.2	-31.0 ± 0.2
Log dissociation pressure, torr	$-\frac{11,570 \pm 40}{T}$ + 10.81	$-\frac{4380 \pm 30}{T}$ + 9.66

The integral values for the thermodynamic quantities involving the Er-D system are presented in Table II-2.

Table II-2 INTEGRAL FREE ENERGIES, ENTHALPIES, AND ENTROPIES OF MIXING IN THE Er-D SYSTEM AT 923°K[22]

Composition, D/Er ratio	$-\Delta G^M$, kcal/ gram atom soln	$-\Delta H^M$, kcal/ gram atom soln	$-\Delta S^M$, cal/ (°K)(gram atom soln)
0	0	0	0
0.05	0.68	1.02	0.37
0.10	1.23	1.96	0.79
0.15	1.77	2.91	1.22
0.20	2.00	3.52	1.65
0.25	2.56	4.49	2.09
0.30	2.90	5.23	2.53
0.35	3.19	5.94	2.98
0.40	3.42	6.59	3.44
0.45[a]	3.64	7.22	3.88
1.80[a]	5.87	15.80	10.78

a Solubility boundaries of the two-phase region, $Er_{ss} + ErD_{1.80}$.

Ternary Hydrides

Ternary systems with zirconium, hydrogen, and either carbon or nitrogen were studied by R. A. Andrievskii et al.[23] Ternary compounds were formed by hydriding ZrC and ZrN at about 1000°C. A wide range of homogeneity was observed and lattice-parameter values were determined for compositions approximating $ZrC \cdot ZrH_{1.5}$ and up

to $ZrC \cdot ZrH_2$; these values were very close to the values a_o = 3.3467 A and c_o = 5.4898 A reported by Atomics International[24] for this hexagonal lattice.

With nitrogen, the composition $ZrN_{0.4}H$ was obtained, and the hexagonal lattice constants were a_o = 3.285 A and c_o = 5.470 A. These values are slightly lower than those observed previously in structures with less nitrogen. The Russians also measured the electrical resistivity of both sets of ternary compounds and obtained values of the order of 1000 μohm-cm, which indicates that the compounds are defect structures.

(H. H. Krause)

4. Metallic Poison Materials

Calhoun and Fascia[25] determined that a minimum of 10% cold work is necessary before grain refinement in hafnium can be obtained by recrystallization. The smallest grain size was obtained by a high degree of cold work followed by low-temperature annealing. The final grain size was primarily dependent on the amount of cold work and to a lesser degree on the working temperature or the annealing temperature. Fig. II-5 illustrates the relationship between final grain size, cold work, and annealing temperature. Increased oxygen content results in significant hardness increases at lower temperatures, but above 600°C the microhardness of hafnium appeared to be independent of oxygen content.[26]

(M. Kangilaski)

5. Dispersions and Nonmetallic Poisons

Boron and Boron Compounds

Two methods were developed at Oak Ridge[27] that can be used to transform the more readily available low-density amorphous boron to a higher density, high-purity crystalline boron powder. In the first method, amorphous boron-metal powder was placed in high-purity (HPR-grade) boron nitride containers and heated to 2000 to 2150°C in a tungsten-susceptor induction furnace with an argon atmosphere. In the second method, the boron-metal powder was passed through a sheath-stabilized helium plasma flame onto a water-cooled target to produce an essentially massive body. Amorphous normal boron as produced by the reduction of the oxide (B_2O_3) by magnesium metal was crystallized and purified to greater than 99 wt.% boron by both of these methods. Electrolytic-cell-produced amorphous ^{10}B metal powder was crystallized and purified to greater than 97 wt.% boron by both methods.

Mound Laboratory[28] studied the packing characteristics of irregularly shaped crystalline boron particles in the size range 20 to 105 μ. The particles were sized into seven successive groups and revealed many of the same packing characteristics as found for spheres. Maximum densities achieved with these powders were slightly lower than those for spheres and were not consistently repeatable.

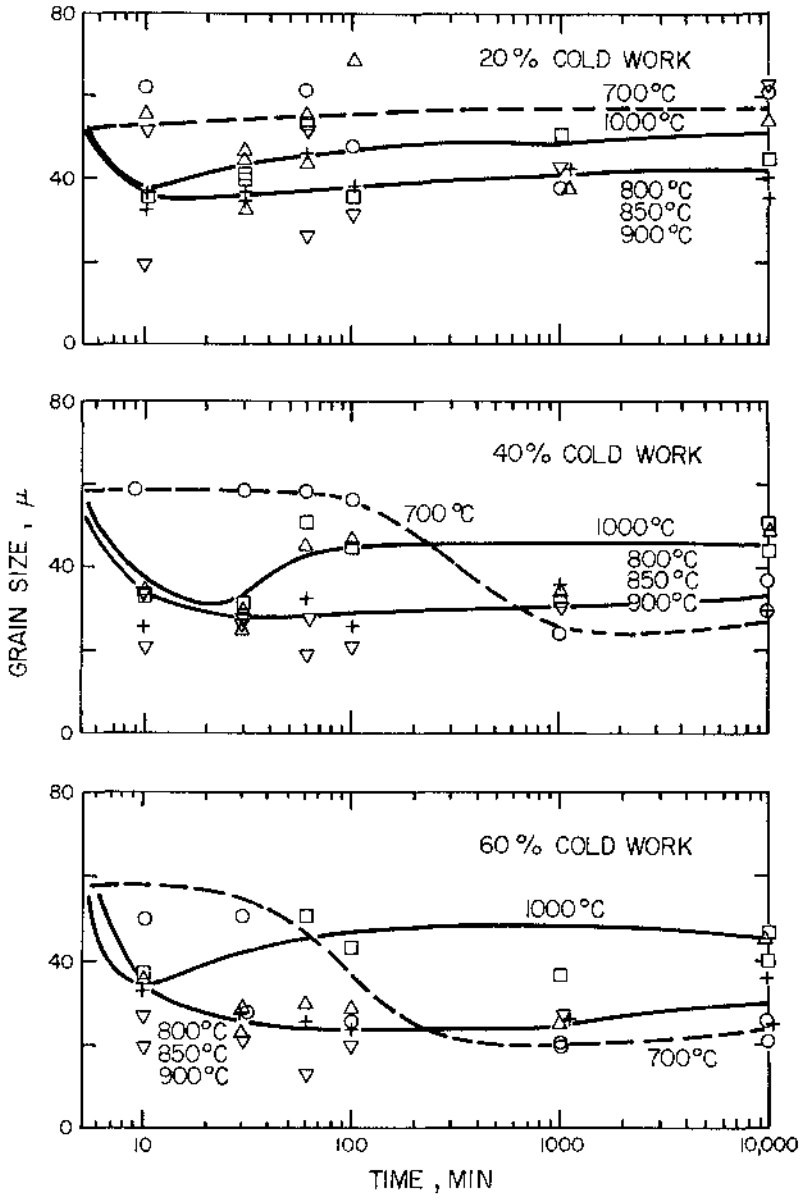

Fig. II-5 Effect of heat treatment on the grain size of hafnium cold-rolled at 25°C.[25] ○, 700°C; ▽, 800°C; △, 850°C; +, 900°C; □, 1000°C.

Russian workers[29] irradiated various boride samples to determine the effect of lattice damage from the ^{10}B isotope in the natural boron. The samples were approximately 8 mm in diameter and 10 to 15 mm long. Irradiation to 10^{20} neutrons/cm^2 (thermal) at <100°C caused samples of ZrB_2, CrB_2, and LaB_6 to shatter into bits, but merely produced cracks in TiB_2 and $(TiCr)B_2$ specimens. The radiation stability of the substance was correlated with the modulus of elasticity. A maximum lattice expansion of 3.1 vol.% was observed in the case of TiB_2, while ZrB_2 showed a lattice expansion of only 0.9 vol.%.

A British patent[30] claims that the mechanical properties of particles of boron or boron-containing compounds such as B_4C are improved by vapor coating with an inner layer of SiC and an outer layer of TiC by the fluidized-bed process. The coated particles are then dispersed in a metal matrix and fabricated into control elements by conventional techniques.

The shrinkage behavior of TaB_2 powder compacts in vacuum at 1100 to 2100°C was examined by investigators at Lockheed.[31] A density of 94% of theoretical was obtained by sintering for 1/2 hr at 2100°C. It was found that initial-stage sintering occurs by either a volume or grain-boundary diffusion mechanism with an activation energy of approximately 90 kcal/mole. It was also noted that compacts of a powder mixture of TaB_2 plus boron in excess of stoichiometry expanded upon sintering.

A review of the properties and reactor performance of boron carbide has been compiled by Battelle-Northwest[32] to assess its potential for fast-reactor application. Data from 34 references concerning the irradiation behavior of B_4C with respect to gas release, swelling, mechanical integrity, and dimensional stability in thermal reactors to 500°F (260°C) and for burnups to 50% of the ^{10}B isotope in natural boron were included. It was concluded, however, that realistic performance evaluation of B_4C requires testing in a fast-neutron environment at the temperatures of interest.

Rare Earths

The HfO_2-Sm_2O_3 diagram in the solid-phase region rich in HfO_2 was investigated by the Russians.[33] The diagram of HfO_2-Sm_2O_3 was compared with that of ZrO_2-Sm_2O_3. During the interaction of HfO_2 with Sm_2O_3, solid solutions are formed with a composition close to 33 mole % Sm_2O_3 and 67 mole % HfO_2. On further reaction with excess HfO_2, equilibrium reaction products were formed.

(D. E. Lozier)

II. MODERATOR AND CONTROL MATERIALS

REFERENCES

1. R. A. Bell, P. J. Clements, and A. Langsford, A Nondestructive Measurement of the Fluctuations in Area Density of a Graphite Block Using a 147 Mev Proton Beam, British Report AERE-R-5732, May 1968.

2. I. D. Peggs, Carbon, Graphite, and Some Carbides for Superheat Service: Literature Survey, Canadian Report AECL-3069, March 1968.

3. J. E. Baker and L. G. Overholser, Oxidation of Pyrolytic-Carbon-Coated Fuel Particles by Low Concentrations of Water Vapor, USAEC Report ORNL-TM-2199, Oak Ridge National Laboratory, Apr. 10, 1968.

4. Gulf General Atomic, Inc., HTGR Base Program Quarterly Progress Report for the Period Ending May 31, 1968, USAEC Report GA-8662, pp. 30-41, June 28, 1968.

5. T. Masuyama, Radiation Damage of Low Permeability Graphite and Hard Carbon, Japanese Report NSJ-Tr-102 [translated from Nippon Genshiryoku Gakkaishi, 8: 185-194 (1966)].

6. G. J. Schoessow, Graphite Triple Point and Solidus-Liquidus Interface Experimentally Determined up to 1000 Atmospheres, Report NASA-CR-1148, National Aeronautics and Space Administration, Lewis Research Center, July 1968.

7. Nondestructive Testing of Nuclear Graphite, Amer. Soc. Testing Materials, Special Tech. Pub., No. 439 (July 1968).

8. R. G. Lawton and W. R. Prince, Rover Graphite Fuel Element Thermal Stress Experiments and Analyses, USAEC Report LA-3849-MS, December 1967. (Classified)

9. H. Glass, E. Levine, G. Luetjering, and S. Weissmann, Ductile-Brittle Behavior of Beryllium, Interim Progress Report, October 15, 1967 – April 15, 1968, Rutgers University, May 1968.

10. G. London and V. Damiano, Flow and Fracture Characteristics of Zone Purified Beryllium and Selected Beryllium Rich Alloys, Report F-C2031, The Franklin Institute Research Laboratories, June 1968.

11. G. L. London and V. V. Damiano, Investigations Relating to the Brittleness of Beryllium, Bi-Annual Report, August 1, 1967 – February 1, 1968, The Franklin Institute Research Laboratories.

12. R. W. Armstrong, Theory of the Tensile Ductile-Brittle Behavior of Polycrystalline H.C.P. Materials, With Application to Beryllium, Acta Met., 16: 347-355 (March 1968).

13. F. A. Pall, The Influence of Strain Rate and Temperature upon the Fracture Toughness of AMS 7902 Beryllium, Report D2-113565-1, The Boeing Co., May 22, 1967.

14. G. S. Pavlinov, G. V. Grigor'ev, and Yu. G. Sevast'yanov, Beryllium Self-Diffusion, Fiz. Metal. Metalloved., 25: 565-567 (March 1968).

15. J. Greenspan, Some Effects of Powder Particle Size on the Physical Behavior of Press-Forged Beryllium, Report AMMRC TR 68-08, Army Materials and Mechanics Research Center, May 1968.

16. M. Sasabe and S. Nomura, High Temperature Oxidation of Beryllium in Water Vapor, Nippon Genshiryoku Gakkaishi, 10: 319-324 (1968).

17. M. T. Simnad and J. B. Dee, Equilibrium Dissociation Pressures and Performance of Pulsed U-ZrH Fuels at Elevated Temperatures, in Thermodynamics of Nuclear Materials 1967, pp. 513-27, International Atomic Energy Agency, Vienna, Austria, 1968.

18. A. Bourrasse, Y. Carteret, J. Elston, and R. Lucas, Moderator-Fuel Element, U. S. Patent 3,342,692, Sept. 19, 1967.

19. A. Bourrasse, Y. Carteret, J. Elston, and R. Lucas, Moderator-Nuclear Fuel Element, British Patent 1,107,300, Mar. 27, 1968.

20. C. E. Lundin, Erbium-Hydrogen System, Trans. Met. Soc. AIME, 242(5): 903-907 (May 1968).

21. Z. M. Azarkh and P. I. Gavrilov, X-ray Phase Analysis of the Erbium-Hydrogen System, Kristallografiya, 12(6): 1070-1072 (November-December 1967).

22. C. E. Lundin, Thermodynamics of the Erbium-Deuterium System, Trans. Met. Soc. AIME, 242(6): 1161-1165 (June 1968).

23. R. A. Andrievskii, E. B. Boiko, and V. P. Kalinin, Ternary Compounds in the Zr-H-C and Zr-H-N Systems, Kristallografiya, 12(6): 1068-1070 (November-December 1967).

24. Atomics International, Quarterly Technical Progress Report, AEC Unclassified Programs, July-September 1965, USAEC Report NAA-SR-11650, Dec. 22, 1965.

25. C. D. Calhoun and J. R. Fascia, Recrystallization Behavior of Hafnium, USAEC Report KAPL-3353, Knolls Atomic Power Laboratory, January 1967.

26. A. I. Evstynkhin, I. P. Barinov, and I. I. Korobkov, Properties of Iodine-Type Hafnium and Alloys in the Zirconium-Hafnium System, High Purity Metals and Alloys, pp. 23-30, Consultants Bureau, New York, 1967.

27. P. E. Trent, Crystallization and Purification of Boron Metal Powder, USAEC Report Y-1614, Union Carbide Corp., Y-12 Plant, July 8, 1968.

28. J. W. Voigt, Tap Density Values from Irregular Boron Particles, USAEC Report MLM-1458, Mound Laboratory, June 7, 1967.

29. G. V. Samsonov, M. S. Kovalchenko, V. V. Ogorodnikov, and A. G. Krainij, Radiation Stability of Borides, At. Energ., USSR, 24: 191-192, February 1968.

30. J. Rich and G. Arthur, Boron Containing Materials, British Patent 1,106,291, Mar. 13, 1968.

31. A. G. Elliot and H. W. Lavendel, Sintering of TaB_2, in Proceedings of the International Conference on Sintering and Related Phenomena, pp. 565-579, Gordon and Breach, Science Publishers, New York, 1967.

32. T. W. Evans, The Effects of Irradiation on Boron Carbide, USAEC Report BNWL-679, Battelle-Northwest, February 1968.

33. E. N. Isupova, V. B. Glushkova, and E. K. Keler, Investigation of the System HfO_2-Sm_2O_3 in the Solid Phase in the Region Rich in HfO_2, Izv. Akad. Nauk SSSR, Neorg. Mater., 4: 399-405 (March 1968).

III. CLADDING AND STRUCTURAL MATERIALS

1. Corrosion by Aqueous and Gaseous Media

Corrosion of Zirconium Alloys

The effect of heat transfer and isothermal conditions on the corrosion and hydriding of Zircaloy-4 tubing in a pressurized-water system has been studied at Westinghouse.[1] Bulk-water temperatures ranged from 600 to 640°F (316 to 338°C) and metal surface temperatures were 20 to 80°F (11 to 44°C) higher. Heat fluxes were 3420 to 13,000 Btu/(hr)(sq ft) under forced-convection conditions and 20,000 Btu/(hr)(sq ft) under nucleate-boiling conditions. The oxidation rate was directly proportional to the cladding surface temperature in all heat-transfer systems studied. Hydrogen absorption was the same in the nucleate-boiling systems as in the forced-convection systems and was homogeneous throughout the tube cross sections. There were no abnormal hydride-platelet clusters in the microstructures.

Knolls researchers[2] have investigated the effect of silicate ions released from spent ion-exchange resins on the high-temperature steam corrosion of Zircaloy. In 14-day tests at 750°F (400°C) in 1500 psi steam, corrosion rates were accelerated for Zircaloy sensitized by slow cooling from 1650°F (900°C) with 0.12 ppm silicon in the water and for reactor-grade Zircaloy with 1.3 ppm silicon in the water.

Corrosion of Aluminum Alloys

A new accelerated stress-corrosion laboratory test for aluminum alloys has been developed by Kaiser.[3] The test consists of a 1-week immersion of chemically etched C-ring or round tensile specimens in a 1 NaCl-2 $K_2Cr_2O_7$ (by wt.) solution at pH 4 and 60°C. The accelerated-test results were correlated with marine and industrial exposures and with the 3.5 NaCl (by wt.) alternate-immersion test. Good correlation was obtained for the susceptible tempers of 2014, 2019, and 2024 alloys. However, the outdoor environments were more prone to cause stress-corrosion cracking than was the new accelerated test at the lower stress levels with 7039, 7075-T651, and 7079-T651 alloys.

Corrosion of Iron-Base Alloys

Steel. The oxidation of mild and low-alloy steels at 500°C in CO_2 containing small amounts of CO and H_2O has been studied at Harwell.[4] Oxide scales were double layered and oxygen transport in the nonprotective oxides was believed to be by gas diffusion through open pores. Oxygen transport in the protective oxides was believed to occur across closed pores that formed as the result of the condensation of vacancies produced by cation diffusion through the film. Nonprotective oxidation occurred at high CO_2 pressures in the presence of water vapor. The adverse influence of water vapor was enhanced by deposits of gold, platinum, and carbon on the metal surface. These elements appeared to increase oxidation by chemical reaction rather than by mechanical effects in the oxide film.

Stainless Steels. The structure and composition of thin films formed on an Fe-15Cr-4Al-1Y* alloy during oxidation in CO_2 at 800 to 1000°C have been determined by the British.[5] X-ray diffraction revealed $FeCr_2O_4$ spinel, Al_2O_3, and Y_2O_3. Neither of the latter two phases appeared to form a solid solution with any other component of the oxide film. Over the exposure period of 0.1 to 1000 hr, the rate-controlling step was attributed to self-diffusion of Al^{3+} in Al_2O_3. No other phase contributed significantly to the oxidation behavior of the alloy, except for Y_2O_3, which apparently improved scale adhesion.

The oxide-scale formation on superheater alloys exposed up to 36 months in high-temperature steam has been investigated for the ASME.[6] Commercial superheater-tubing specimens were exposed to 2000-psi steam in a large steam-generating plant. Ferritic materials were exposed at 1100 and 1200°F (595 and 650°C) and austenitic materials were exposed at 1200, 1350, and 1500°F (650, 730, and 815°C). A subsurface layer and a surface layer of the oxide scales formed on both grades of materials. Apparently the subsurface layer was formed by inward diffusion of anions of oxygen and the surface layer by the outward diffusion of cations of iron and manganese. The subsurface layer was dense and consisted of oxides of the alloying elements of the base metal. Concentrations of these alloying elements in the subsurface layer were higher than those in the base metal. The surface layer was primarily iron oxide and contained many voids and pores. After an 18-month exposure at 1350°F, the average scale thickness on 310 stainless steel, Incoloy 800, and Inconel 600 was <1.5 mils compared with 4 to 5 mils for most of the other austenitic materials and 15 to 25 mils for the ferritic alloys at 1200°F.

The effectiveness of phosphates in inhibiting stress-corrosion cracking of austenitic stainless steel as related to the N-Reactor has been studied at Battelle-Northwest.[7] Autoclave tests were conducted for 8 months in 100-psi water containing 0 to 1000 ppm phosphate, 0 to 100 ppm sulfite, 0 to 15 ppm hydrazine, 2 ppm morpholine, and no added chloride (chloride ranged from <0.05 to 1.84 ppm). After a 4-month exposure, stress-corrosion cracking occurred in 304-stainless-steel tubing taken from the N-Reactor in all solutions not containing phosphate. Small cracks were found in the N-Reactor tubing exposed in two of the five phosphate-treated waters after 6 to 8 months. No cracks were found in solution-treated or sensitized 304-stainless-steel sheet material, Inconel-600 N-Reactor tubing, Incoloy 800, or A212 carbon steel.

"Straining"-electrode experiments on Fe-Cr-Ni alloys have been conducted at The Ohio State University to test the hypothesis that the tip of an advancing stress-corrosion crack is dynamically strained, thereby producing sufficiently high current densities to propagate the crack by electrochemical dissolution.[8] At strain rates of up to 6%/min very little change was observed in the current density in the active region during straining. In the lower range of passive potentials, the current density with the straining electrode was not appreciably increased over that with a static electrode. At the critical potential for current increase in the passive region, the current density with the straining electrode was greatly increased over that with a static electrode. This potential was less than the pitting potential. The largest differences between the critical and pitting potentials were observed for H_2SO_4 and H_2SO_4 + KCl solutions, while the smallest differences were observed for H_2SO_4 + KBr or KI. The latter two were also

*Unless otherwise designated, all compositions are considered to be in wt.%.

less prone to produce stress-corrosion cracking. Nickel in H_2SO_4 + KCl solutions showed no significant difference between current density with the straining electrode and that with the static electrode over the whole range of potentials in the passive range.

Corrosion of Nickel- and Cobalt-Base Alloys

Oxidation studies of Hastelloy X for periods of up to 12,500 hr in air at temperatures from 1300 to 2000°F (705 to 1095°C) have been performed by Aerojet-General.[9] The primary mode of oxidation at 1600°F (870°C) and lower was by thin, intergranular penetration. At 1750°F (955°C) and higher, internal oxidation occurred as a uniform band of small oxide particles distributed intergranularly beneath the metal-oxide interface. The oxidation produced a duplex oxide consisting of a Cr_2O_3 inner layer and a $MnCr_2O_4$ spinel outer layer. The oxidation resistance of the Hastelloy X increased as the spinel:Cr_2O_3 ratio increased, and the amount of spinel formed increased with increasing manganese content in the alloy.

The oxidation behavior of Hastelloy N is being studied at Oak Ridge.[10a] The addition of silicon to the alloy markedly improved its oxidation resistance, particularly at 982°C, at which temperature the oxidation rate decreased linearly from about 500 mg/(cm^2)(1000 hr) at <0.05% silicon to about 15 mg/(cm^2)(1000 hr) at 0.6% silicon. At 760°C, the oxidation rate at silicon contents >0.05% was <10 mg/(cm^2)(1000 hr). Titanium in the range of 0 to 1% had little effect on the oxidation behavior of the Hastelloy N.

The oxidation behavior of nickel- and cobalt-base alloys was determined at Savannah River in connection with encapsulating ^{60}Co heat sources.[11] Specimen performance was evaluated on total penetration, which was based on surface-scale thickness (including that which spalled) and depth of intergranular penetration and alloy depletion. After exposures of 9400 to 10,000 hr at 1000°C, TD nickel-chromium was the most resistant material, having a total affected zone of 2.4 mils. Inconel 600, Tophet C, Hastelloy C, GE2541, Haynes 25, and Hastelloy X had affected zones of 8 to 12 mils and were considered acceptable.

The cause of cracking failures of K-Monel bolt studs on autoclaves and pumps has been investigated at Petten, Holland.[12] The cracks were intergranular and analyses indicated that there was an increase in sulfur and copper content at the grain boundaries. The source of the sulfur was the fatty ingredient in the paste of a high-temperature lubricant that decomposed to liberate sulfides or sulfur at vessel-operating temperatures of 360 to 400°C.

Corrosion of Other Alloys

Corrosion and wear surveillance in the Plutonium Recycle Test Reactor through December, 1967, has been described by Battelle–Northwest.[13] Measurements on coupons exposed in the primary system (water at 265°C and 1070 psi) and in the moderator calandria showed negligible corrosion (<0.004 mil/month) for stainless steel, Zircaloy, and aluminum. Continuous measurements by electrical-resistance probes in the moderator, reflector, top and bottom shield, and core-blanket helium systems indicated negligible corrosion (<0.005 mil/month) for the aluminum and carbon-steel probes. Inspection inside the steam generator revealed that the tube bundle and shell were in good condition.

Electrical-resistance probes indicated moderate corrosion rates (0.10 to 0.19 mil/month) in the biological- and thermal-shield systems. Elbows on three steam-generator vent lines were replaced because of failure resulting from localized (trench) corrosion and high stress levels. Two tubes were sealed in the primary-treatment heat exchanger because of leaks which apparently were caused by wear from rubbing against a baffle plate.

Galvanostatic polarization techniques have been used to determine electrochemical corrosion rates of the SNAP-21 radioisotopically fueled power system in seawater at the Naval Radiological Defense Laboratory.[14] A galvanic series was determined and galvanic currents were measured between coupled materials. On the basis of these results, complete penetration of components would be predicted as follows: aluminum insulation and ring, < 1 year; U-8 wt.% Mo alloy biological shield, 3 years (2.5 in.); copper insulation and cold frame, 3 years; stainless-steel liner, ~ 200 years (0.125 in. thick); and Hastelloy C fuel container, ~600 years (0.25 in. thick).

The crevice corrosion of titanium in 150°C salt solutions has been investigated by Oak Ridge.[15] Results indicated that crevice corrosion under these conditions begins as a result of a differential aeration cell and continues because of an acid concentration developed in the small volume within the crevice. Crevice attack was not specific to chloride solutions but also occurred in iodide, bromide, and sulfate solutions. The more concentrated salts produced the more severe attack. Results of electrochemical polarization studies indicated that alloys which remain passive in nonoxidizing acid salts, such as those containing palladium, molybdenum, or nickel, should be more resistant to crevice attack.

(W. E. Berry)

Corrosion of Refractory Metals

The French[16] have investigated the oxidation of tungsten and rhenium in the temperature range 1127 to 2227°C at oxygen pressures between 5×10^{-6} and 3×10^{-4} torr. The oxidation rate exhibited a maximum as a function of pressure because of the production of atomic oxygen above 1727°C.

The diffusion of oxygen in niobium oxides has been studied at McMaster University.[17] Single crystals of α-Nb_2O_5 were grown by the Verneuil technique and machined into cylinders; electrical conductivity then was measured as a function of temperature between 600 and 1000°C and oxygen pressure between 10^{-16} and 1 atm. By following the resistance change as a function of time on changing the environmental pressure, the diffusion coefficient of oxygen was determined at varying degrees of oxide nonstoichiometry. Diffusion was several hundred times slower in the oxide with the highest degree of nonstoichiometry. A similar study on γ-Nb_2O_5 scale stripped from oxidized niobium was conducted, but absolute measurements could not be made because of cracking. Nevertheless, the results indicated similar behavior for both α- and γ-Nb_2O_5.

The Russians[18] have investigated the oxidation of binary Nb-Ta alloys at 550 to 1050°C. For alloys up to 30 at.% tantalum, a decrease in oxidation rate with increasing temperature was noted in the temperature ranges 600 to 700°C and 800 to 1000°C. For alloys containing 30 to 100 at.% tantalum, the decrease was noted only in the lower temperature range. The temperature at which the rate was observed to decrease was related to the oxide-film composition.

Various aspects of tantalum oxidation have been studied. Growth characteristics, morphology, and crystallography of tantalum oxide in the initial stages of formation after 10 min at 500°C in 1 atm oxygen have been determined.[19,20] The data indicated that formation of TaO_y plates occurred by martensitic transformation. Geometrical effects of oxidation of tantalum tubes at 825 to 930°C in 0.53 atm oxygen have also been described.[21] These results suggest that the major stress generated at the oxidizing surface was in the adherent part of the oxide scale rather than in the surface-metal layers affected by solution of oxygen. A tetragonal phase with a = 13.32 and c = 6.12 A has been detected in the Ta-O system by electron diffraction.[22]

Adsorption and decomposition of various gases on tungsten have been the subjects of a number of investigations. These studies include the following: (1) adsorption and decomposition of NH_3 on (211) surfaces at 25 to 1000°C using flash desorption and mass spectrometry, low-energy electron diffraction, and measurements of work-function change,[23] (2) adsorption of CO on (211) surfaces at 25 to 900°C using LEED,[24] (3) chemisorption of N_2O on tungsten filaments at 25 to 1500°C,[25] (4) adsorption of oxygen on (110), (211), (111), (100) surfaces at -195 to 1500°C using field-emission microscopy.[26]

(B. C. Allen)

2. Corrosion by Nonaqueous Liquids and Vapors

Corrosion by Sodium

It has long been recognized that mass transfer in liquid metal systems can stem from either temperature gradients or concentration gradients. The latter may be significant in high-temperature molten-metal systems where the circulating fluid encounters more than one construction material. A good example would be a sodium-cooled reactor system made of stainless steel, which contains fuel elements clad with a nickel-base alloy or a refractory metal. West German workers studied this dissimilar-metal mass-transfer phenomenon by exposing nickel alloys and molybdenum alloys to flowing sodium in isothermal stainless-steel loops.[27] They found that this caused iron-rich microcrystals (10^{-3} to 10^{-2}-mm diameter) to grow at the grain boundaries of the nickel- and molybdenum-alloy specimens. Microprobe studies showed that the crystals had the atom ratios Fe:Mo ≈ 1:1 on molybdenum, Fe:Ni ≈ 2:1 on Incoloy 800, and Fe:Ni = 6:1 to 10:1 on Incoloy 626. Constituents of the stainless steel other than iron were also present in the microcrystals, but in much smaller amounts.

Several studies have given evidence that exposure to hot sodium produces irreversible effects at the grain boundaries of stainless steels. For example, workers at Argonne noted that 304-stainless-steel specimens treated with a modified Strauss reagent underwent much larger increases in electrical resistivity if they had previously been exposed to 1200°F (650°C) sodium than if they had been sensitized in air.[28] To learn more about such grain-boundary effects, Stanford Research workers exposed thin foils of 304 stainless steel to 1200°F sodium for periods up to 110 hr, cleaned the foils thoroughly by repeated washings with solvent in a Soxhlet extractor, and then examined them by transmission electron microscopy.[29] They noted severe grain-boundary attack and the presence of precipitates on the surface, as well as along and within the grain boundaries. The precipitates, which definitely stem from the prior sodium exposure, do not appear to be

sodium or sodium oxide. Work is in progress on their identification, and preliminary X-ray indications are that they could be $Cr_{23}C_6$, Cr_3C_2, Cr_2N, or some combination of these.

At Brookhaven,[30] a 1655-hr forced-convection sodium-loop run was completed with specimens of HS-25, UMCO-51, Mo, 321 stainless steel, and 304 stainless steel inserted in the all-stainless-steel loop. In the test section the sodium was heated from 710 to 760°C while flowing over the specimens at 22 ft/sec. The oxygen content of the sodium was 4 ± 2 ppm for the first 900 hr, dropping steadily thereafter to ~1 ppm by the end of the test. The molybdenum specimens showed no measurable weight changes. The corrosion rates of the remaining materials decreased with time, leveling off to essentially steady values of <1.5 mils/year by the end of the test.

A second loop was run for 335 hr under the same conditions, except that the oxygen level was maintained below 1 ppm by hot trapping at 650°C and the specimens were made of V-20Ti, Nb-1Zr, Mo-0.5Ti-0.06Zr (TZM), V-15Ti-7.5Cr, V-15Cr-5Ti, and 321 stainless. The molybdenum alloy showed essentially no weight change and the Nb-1Zr gained only 0.1 to 0.2 mg/cm^2. The vanadium alloys gained on the order of 1 to 2 mg/cm^2, and the 321 stainless steel lost about the same amount. In each case the weight change increased with increasing temperature in the range 720 to 760°C.

Continuing their biaxial-stress-rupture studies on 304 and 316 stainless steels in high-purity sodium (~10 ppm oxygen) and helium (99.99% pure), researchers at Atomics International[31] confirmed the fact that sodium does not degrade the mechanical properties in tests up to 3000 hr at 1200°F (650°C) and 1000 hr at 1400°F(760°C). Further, the use of 10 to 15% cold work reduces the long-term stress-rupture resistance of both steels, enhancing precipitation within grains, weakening the grain boundaries, and promoting sigma-phase and grain-boundary-void formation during stress-rupture testing. At 1000°F (540°C), 10 to 15% cold-worked 304 stainless steel has higher long-term rupture strength than comparable worked 316 stainless steel. At 1200°F the opposite is true. Figure III-1 shows some of the creep-rupture results.

Battelle-Columbus has issued a comprehensive review[32] of the properties and technology of candidate cladding materials for the liquid-metal-cooled fast-breeder reactor (LMFBR). Materials covered are selected austenitic stainless steels, nickel

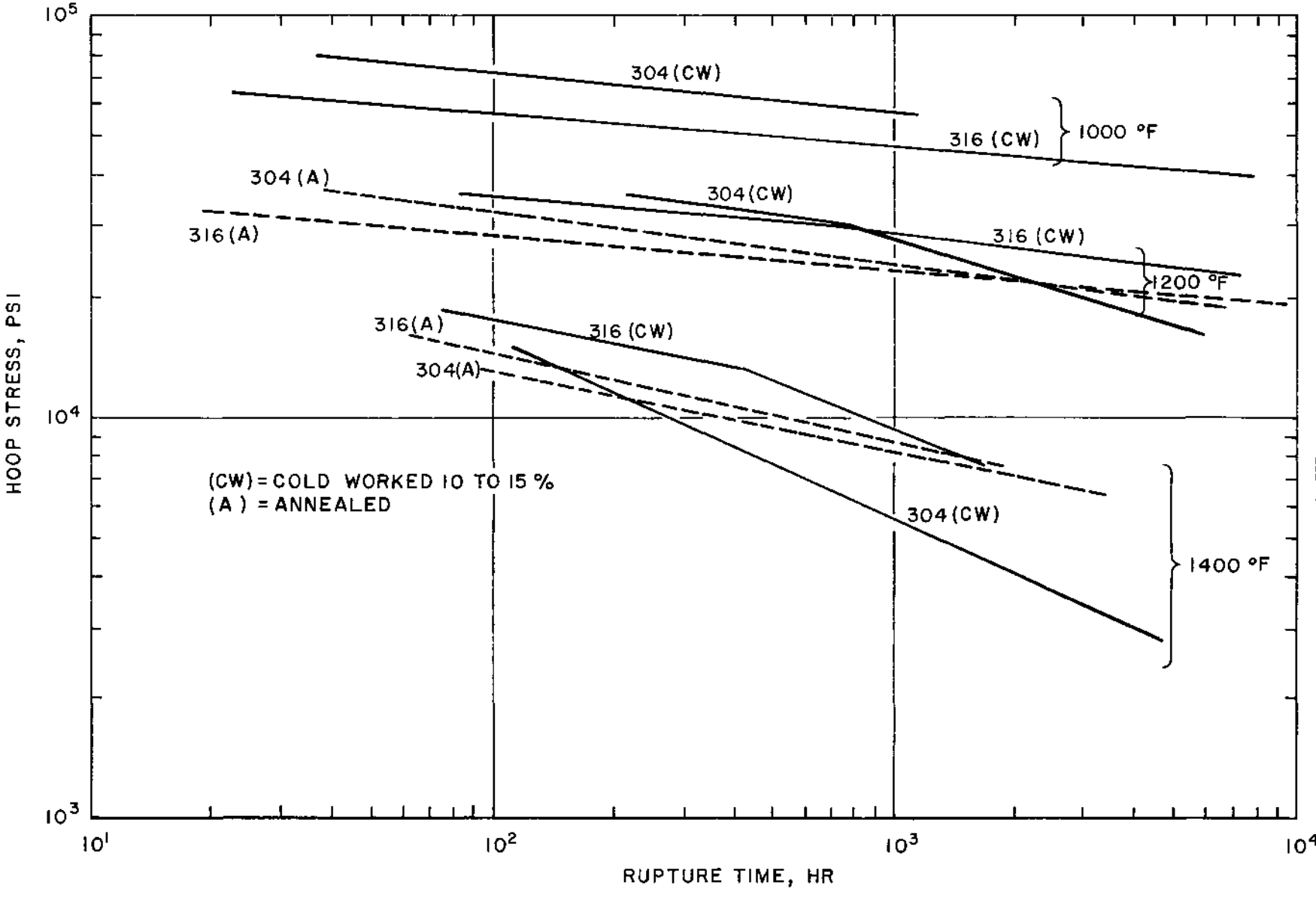

Fig. III-1 Stress-rupture properties of 304 and 316 stainless steels in 1000, 1200, and 1400°F sodium.[31]

Workers at Argonne[34a] measured the solubility of nitrogen in molten sodium as a possible aid in the understanding and control of nitriding in sodium systems, and also in connection with the possible use of nitrogen-containing blanket gases. The results of at least six measurements at each temperature and 10 atm pressure, using ^{15}N-tagged nitrogen, are tabulated below.

Temperature, °C	Solubility/atm pressure, 10^{-12} g N_2/g Na
451	12±8
502	19±7
550	28±8
600	49±9

Furthermore, by noting that the stripped-gas samples contained essentially the same distribution of nitrogen isotopes as the gas used to saturate the sodium, it was concluded[35] that nitrogen dissolves diatomically in sodium.

After exposing vanadium wires to sodium at 700°C for 10 hr or more to equilibrate oxygen, Argonne workers were able to use the oxygen-concentration measurements to arrive at a distribution coefficient and an activity coefficient for oxygen in vanadium.[36a] The large negative deviation from Raoult's Law is illustrated in Fig. III-2. In this work, the standard state was selected as an oxygen-activity coefficient of unity in oxygen-saturated vanadium.

Corrosion by Potassium

Six alloys (318 stainless steel, HS-25, Hastelloys C, N, and X, and René 41) were evaluated at NASA's Lewis Research Center[37] for ability to withstand 1800°F (980°C) boiling potassium well enough for use in hardware for ground testing space-power-system components. Capsules machined from rod stock of the test alloys were exposed to 1800°F boiling-refluxing potassium and examined metallographically. All of the materials showed some evidence of corrosion. However, only the 318 stainless steel exhibited severe enough attack to be eliminated from further consideration. An interesting sidelight of this work is that the potassium, which contained no more than 20 ppm of oxygen initially, showed up to 500 ppm of oxygen after the test. The source of the oxygen is unknown, but the greatest pickup occurred in the capsules that were attacked the most. The materials could be arbitrarily ranked into three groups. Most resistant were René 41 and HS-25; next were Hastelloys N, C, and X (in that order); and finally, 318 stainless steel.

Investigators at EIMAC conducted studies[38] to find an electrical insulator with sufficient strength and corrosion resistance to protect the alternator windings in a potassium-vapor turboalternator space power system. High alumina and beryllia modulus-of-rupture bars were exposed for 500 hr to potassium vapor at up to 870°C and 2-atm pressure in Nb-1Zr capsules, then tested in cross bending. Control samples were heated similarly in vacuum and tested. It was found that potassium attacks the grain boundaries of the ceramics, owing largely to the presence of silica. For long-term usefulness at 870°C, ceramics must contain considerably less than 500 ppm silica.

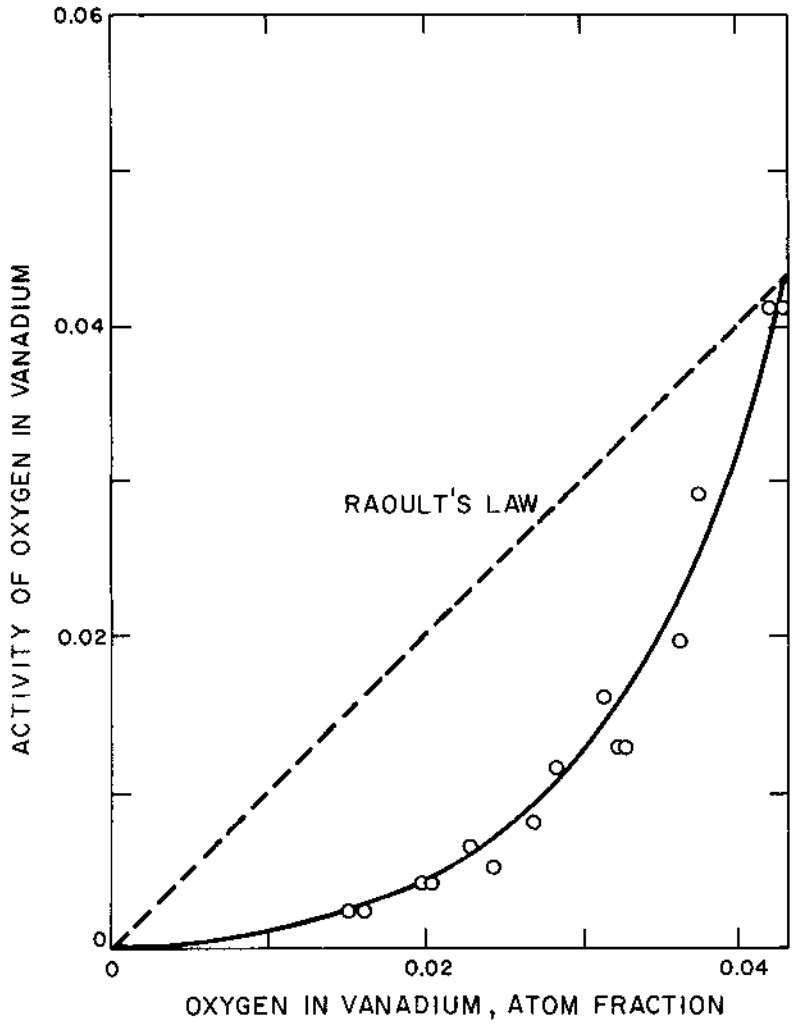

Fig. III-2 Activity of oxygen in vanadium at 700°C.[36a]

To aid in comparing cesium with potassium as the working fluid for space power plants, Oak Ridge investigators reviewed[39] all experience to date concerning erosion in steam, mercury-vapor, and potassium-vapor turbines. Analytical and experimental studies of turbine-bucket erosion and cavitation damage are described and summarized in tables and curves.

Corrosion by Mercury

In the SNAP 2 version of the Mercury Rankine Power Conversion Program, reactor-heated NaK is pumped through a NaK-to-mercury boiler and the mercury vapor drives a turbogenerator unit. The extensive mercury-corrosion tests conducted under this program have been summarized in several topical reports by TRW Equipment Laboratories.[40,41] In addition to over 1 million hr of capsule and loop testing, more than 30,000 hr of boiler-test operation were accumulated. Figure III-3 shows a representative mass-transfer pattern in one of the HS-25 test boiler tubes after 2200 hr of operation. This was the result of selective leaching of various elements from the HS-25. The deposits are predominantly cobalt (95 wt. %), with some iron; the leached zone is depleted in nickel, chromium, and cobalt, and somewhat enriched in tungsten.

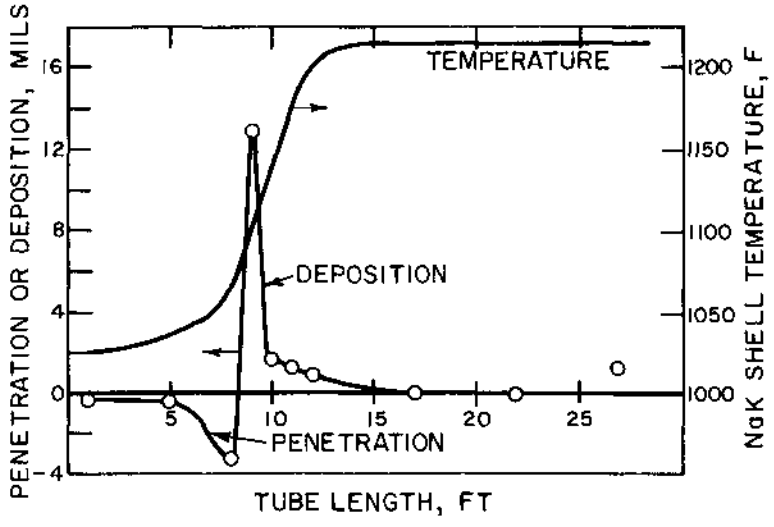

Fig. III-3 Corrosion-temperature correlation for NaK-heated HS-25 mercury boiler tube.[40]

The corrosion products carried by the mercury pose a major system-design problem because of their tendency to deposit in critical areas like mercury-lubricated sleeve-bearing surfaces, lubricant-line filters, the mercury pump, and the turbine nozzles and vanes. These corrosion products have been identified as ferrites, possessing a spinel structure of either the γ-Me_2C_3 or Me_3C_4 type. Their effects can be minimized by operating the boiler and condenser for at least 200 hr, then flushing with clean mercury and recharging before operating the turboalternater unit. This preconditioning eliminates the bulk of the corrosion products, which drop to a steady-state concentration of around 0.01 ppm in the liquid after reaching a much higher value in the first 100 to 200 hr. Since

the major source of corrosion products is the boiler, maintaining a high vapor quality (over 95%) at the exit will minimize carryover.

Containers for Molten Uranium

A study at Ames Laboratory[42a] to evaluate yttrium metal as a container material for molten-uranium-alloy fuels has been concluded. Iron additions (0.02 to 10 wt.%) to the U-5Cr (eutectic) alloy were found to lower the melting point. The predicted solubilities of yttrium in molten uranium, UCr, and UCr-1Fe at 950°C are 0.042, 0.029, and 0.024 wt.%, respectively, suggesting that the UCr-Fe alloy should be the least corrosive of the three. Actually, capsule tests showed solution attack of yttrium to be slightly greater by UCr-1Fe than by UCr. With the latter alloy the yttrium-capsule walls suffered about 20 mils of penetration after 3000 hr at 950°C, making this combination appear less promising than it did in preliminary tests.

Corrosion by Organics

The terphenyl-cooled Piqua Nuclear Power Facility (PNPF) was forced to shut down early in 1966 as a result of fouling of the core by massive carbonaceous deposits. Careful study showed that oxygen exposure and subsequent contamination of the coolant were responsible, though little was known about the rate or the products of terphenyl oxidation – particularly in the presence of radiolysis products. As part of the Heavy-Water Organic-Cooled Reactor (HWOCR) program, workers at Atomics International studied the oxidation of Santowax OM (an orthorich terphenyl mixture) circulating at 350 to 620°F (175 to 325°C) in a small loop while up to 4 vol.% oxygen in argon was bubbled through it.[43] They found that at the higher temperatures the nonterphenyl impurities in the distilled Santowax OM caused the formation rate of oxygenated compounds to increase rapidly at first, then drop off gradually to a high steady-state rate. A film containing about 4 wt.% oxygen was found on the reaction vessel. The radiation dose of ~3 x 10^6 rad/hr from the ^{60}Co gamma source in the loop was apparently too low to influence the oxidation rate.

Thermal decomposition experiments on irradiated and unirradiated PNPF coolant were also completed. There was no change in composition of samples treated for up to 11 months at 550°F (290°C), but irradiated samples held at 750°F (400°C) for only 6 months were completely converted to high boilers (HB), coke, or gas. The disappearance of terphenyls from the unirradiated Santowax OM at the same temperature occurred much more slowly.

Fretting and wear tests of SAP (sintered aluminum powder) and Zircaloy-2-clad UO_2 fuel elements in organic coolants have been summarized by the Canadians.[44] Tests were conducted in Santowax OM with 30% high boilers at temperatures ranging from 316 to 399°C and with thermal cycling from about 340 to 93°C. After 1695 hr of operation and with 30 thermal cycles, an average of 9 rib-to-sheath fret marks were observed on each SAP-clad element. Maximum penetration was 3.4 mils or 14% of the wall thickness. After 1147 hr of operation and with 13 thermal cycles, an average of 5 wire-wrap-to-sheath fret marks were found on each Zircaloy-2-clad fuel element. Maximum penetration was < 1.5 mils or <6% of the wall thickness.

Results of loop experiments in Canada's NRU reactor using Santowax OM and HB-40 (hydrogenated terphenyls) to cool SAP-clad UC fuel bundles[45] showed considerable promise for this system. The fuel operated satisfactorily for 17 months at 20.8 kw/ft peak-power rating and reached a record burnup of 16,700 Mwd/tonne of uranium. Surface-film formation was effectively inhibited by maintaining a water concentration in the coolant above 50 ppm. Elaborate coolant cleanup was unnecessary. A small bypass flow through an attapulgus-clay column and glass-spool filter was adequate. Even after the cladding defected, it operated satisfactorily for 4-1/2 months without organic logging, fuel-coolant interaction, catastrophic cladding failure, or excessive radiation levels on the main-loop piping. Shutdown and fuel removal were scheduled and routine.

A British patent[46] has been obtained for Euratom on the use of NH_4OH and CO_2 additions to an organic coolant or moderator fluid to inhibit corrosion of magnesium or magnesium-alloy fuel claddings.

Corrosion by Fluoride Salts and Lead

A survey of metal-base structural materials for use in molten lead and fluoride salts at 500 to 1000°C has been published[47] by the Air Force Materials Laboratory. Mechanical properties, fabrication, and corrosion are the major items considered. The study was related to the Molten Salt Experimental (MOSEL) Reactor concept.

(E. M. Simons)

Metal-Water Reactions

The Nuclear Safety Information Center has published a comprehensive review of available data regarding the role of metal-water reactions during a loss-of-coolant accident in a light-water power reactor.[48] The physical chemistry of various metal-water and associated reactions was covered, with emphasis on the reactions of (1) zirconium or Zircaloy with water, (2) stainless steel with water, (3) aluminum with water, (4) UO_2 with water, and (5) hydrogen with air. Also, various data were applied to the analysis of reactions occurring during both nuclear-excursion accidents and loss-of-coolant accidents. It was concluded that metal-water reactions would contribute relatively little to the consequences of nuclear-excursion accidents.

In loss-of-coolant accidents, prompt initiation of emergency core-cooling systems would limit the amount of metal-water reaction to a low value. However, possible fragmentation of fuel pins having chemically reacted cladding makes it difficult to insure meeting of the AEC criterion that the cladding metal-water reaction be limited to negligible amounts. It was concluded that the amount of metal reacted prior to melting of the reactor core would be between 25 and 50% without any emergency core cooling. Hydrogen explosions, often discussed in safety analyses, were not considered credible since hydrogen produced by the metal-water reaction is assumed to be below its flammability limit or is assumed to burn upon release into the containment vessel.

Workers at General Electric have prepared a handbook-type report[49] for use in evaluating light-water cooled reactor loss-of-coolant accidents involving Zircaloy-4 and 304 stainless-steel-clad UO_2. Both boiling-water and pressurized-water reactors are covered. All property values were critically evaluated taking into consideration the meltdown environment of steam or steam and air. The physical properties discussed are: melting point, boiling point, heat of fusion, heat of vaporization, vapor pressure, phase transformations, coefficient of thermal expansion, density, total normal emittance, thermal conductivity, enthalpy, and heat capacity. The mechanical properties discussed are: tensile strength, ductility, compressive strength, and modulus of elasticity. In most instances, values are given as functions of temperature up to the melting point of the material. The kinetics of the oxidation of the cladding materials with steam are also discussed and equations are presented for calculation of oxidation rates under isothermal conditions in 1 atm steam. For Zircaloy-4 or zirconium with steam, the following equations are recommended.

Between 1000 and 1600°C,

$$\frac{W^2}{t} = 7.10 \times 10^5 \exp(-40,500/RT)$$

Between 1600°C and the melting point,

$$\frac{W^2}{t} = 1.5 \times 10^8 \exp \{(-60,600 \pm 5400)/RT\}$$

where W is the weight gain (oxygen pickup) per unit surface area in mg/cm^2, t is time in seconds, R is the gas constant in cal/(mole)(°K), and T is the absolute temperature. Similarly, for 304 stainless steel in steam above 1000°C

$$\frac{W^2}{t} = 2.4 \times 10^{12} \exp \{(-84,300 \pm 2400)/RT\}$$

Additional Transient Reactor Test (TREAT) photographic experiments were performed with Zircaloy-clad fuel rods containing UO_2 (5% enriched) pellets.[34b] These specimens were identical in composition and dimensions to the vibrationally compacted UO_2 fuel rods tested previously. Comparison of failure of pellets and power (Vibra-Pac) fuel from TREAT photographic tests (see Table III-1) suggested the existence of two modes of fuel failure, for both fuel types. The failure energies for these modes depend in part on the reactor period. The modes were defined as: (1) a prompt failure, which occurs during the power transient and is manifested by rapid pressurization within the fuel specimen followed by rupture of the cladding and injection of the fuel into the coolant; (2) a delayed failure, which occurs after completion of the transient and is due to the degradation of the cladding by metal-water reaction and fuel-cladding interaction. For reactor periods less than 80 msec, the failure threshold energies by both mechanisms were between 235 and 290 cal/g UO_2, independent of fuel type and enrichment. For longer reactor periods the energy required to initiate prompt failure was greater.

(J. M. Genco)

Table III-1 SUMMARY OF TREAT PHOTOGRAPHIC TESTS WITH ZIRCALOY-CLAD UO_2 FUELS[34b]

Fuel type	Enrichment, wt.% ^{235}U	Reactor period, msec	Total transient energy, cal/g UO_2	Energy at failure, cal/g UO_2	Mode of failure
Vibra-Pac	5	43	354	235	Prompt
Vibra-Pac	5	48	335	277	Prompt
Pellet	5	48	331	291	Prompt
Pellet	5	63	263	263	Delayed
Pellet	5	66	244	Did not fail	-
Vibra-Pac	5	67	258	258	Delayed
Vibra-Pac	5	71	233	Did not fail	-
Vibra-Pac	10	74	357	277	Prompt
Vibra-Pac	5	75	223	Did not fail	-
Pellet	10	80	450	295	Prompt
Pellet	10	107	330	330	Prompt
Pellet	10	108	290	290	Delayed

4. Radiation Effects in Structural Materials

The proceedings of the Symposium on Radiation Effects, held in September 1965, were published in Metallurgical Society Conferences, Vol. 37.[50] The 28 papers presented were concerned mainly with a basic understanding of radiation effects on metals. The 10th Symposium on Special Metallurgy Brittleness and Irradiation Effects held in Saclay, France, is the basis of another publication.[51] The 26 papers presented at this symposium dealt mostly with defects produced by irradiation at low temperatures. Most of the work presented was performed in France.

The results of in-pile creep test of various materials have been summarized by Battelle-Northwest.[52] It has been found that the creep rate of Zircaloy-2 and Zr-2.5 Nb at 300°C is higher in-pile than out-of-pile. At 350°C, the creep rates of these two materials may be higher or lower in-pile, depending on the stress and temperature. Austenitic stainless steels and nickel-base alloys exhibit no radiation-induced changes in creep rates, although the range of second-stage creep is drastically reduced because of decreased ductility. Stress-relaxation tests on zirconium alloys, stainless steel, and alpha iron during irradiation at 100°C indicate higher creep rates in-pile.

Zirconium Alloys

Proceedings of the Conference on Use of Zirconium Alloys in Nuclear Reactors at Marianske Lazne, Czechoslovakia, in October, 1966, have been published in two volumes.[53] These papers which are in several languages, contain data on corrosion, mechanical properties, hydride formation, and effects of irradiation on mechanical properties of Zircaloy and other zirconium alloys.

In-pile tensile tests were performed on Zircaloy-4 at 282°C using controlled constant strain rates[54a] from 1×10^{-4} to 5×10^{-6}/hr.[5] The results indicated that the in-pile yield strength of Zircaloy-4, both transverse and longitudinal to the rolling direction, is significantly increased by higher strain rates. However, the out-of-pile yield strength appears to be independent of strain rate for the longitudinal specimens tested.

Enhanced in-reactor relaxation has been observed in Zircaloy-4 and Zr-2.5Nb-0.5Cu.[55] This relaxation was found to be temperature dependent with a decrease apparent at lower radiation temperatures. The increased relaxation noted in cold-worked material was especially significant since it was earlier believed that cold work would enhance in-reactor creep resistance. The in-pile relaxation strain in Zircaloy-4 was sensitive to structure, increasing with both increasing amounts of prior plastic deformation and decreasing grain size. The in-pile relaxation behavior appears to be consistent with an accelerated thermal-creep model.

Specimens of Zr-0.5Nb-1.0Cr in the annealed, cold-worked, and as-quenched states were irradiated[56] at 50°C to fast fluences up to 1.25×10^{19} neutrons/cm^2. It was found that the annealed material underwent significant changes in room-temperature tensile properties as shown in Table III-2. However the room-temperature tensile properties of cold-worked (10 and 15%) and as-quenched material were not significantly changed by irradiation to a fast fluence of 1.6×10^{19} neutrons/cm^2. The effect of post-irradiation annealing on the tensile properties is illustrated in Fig. III-4.

Table III-2 EFFECT OF IRRADIATION ON TENSILE PROPERTIES OF ANNEALED Zr-0.5Nb-1Cr[56]

Specimen history	Yield strength (0.2% offset), 1000 psi	Ultimate strength, 1000 psi	Total elongation, %
Cold worked and annealed for 2 hr at 850°C followed by furnace cooling (100°C/hr).	41.1	57.1	
Irradiated to 1.45×10^{18} neutrons/cm^2	42.9	60.4	22
Irradiated to 6.0×10^{18} neutrons/cm^2	69.3	79.5	20
Irradiated to 9.5×10^{18} neutrons/cm^2	75.5	85.1	19
Irradiated to 12.5×10^{18} neutrons/cm^2	79.4	86.9	16

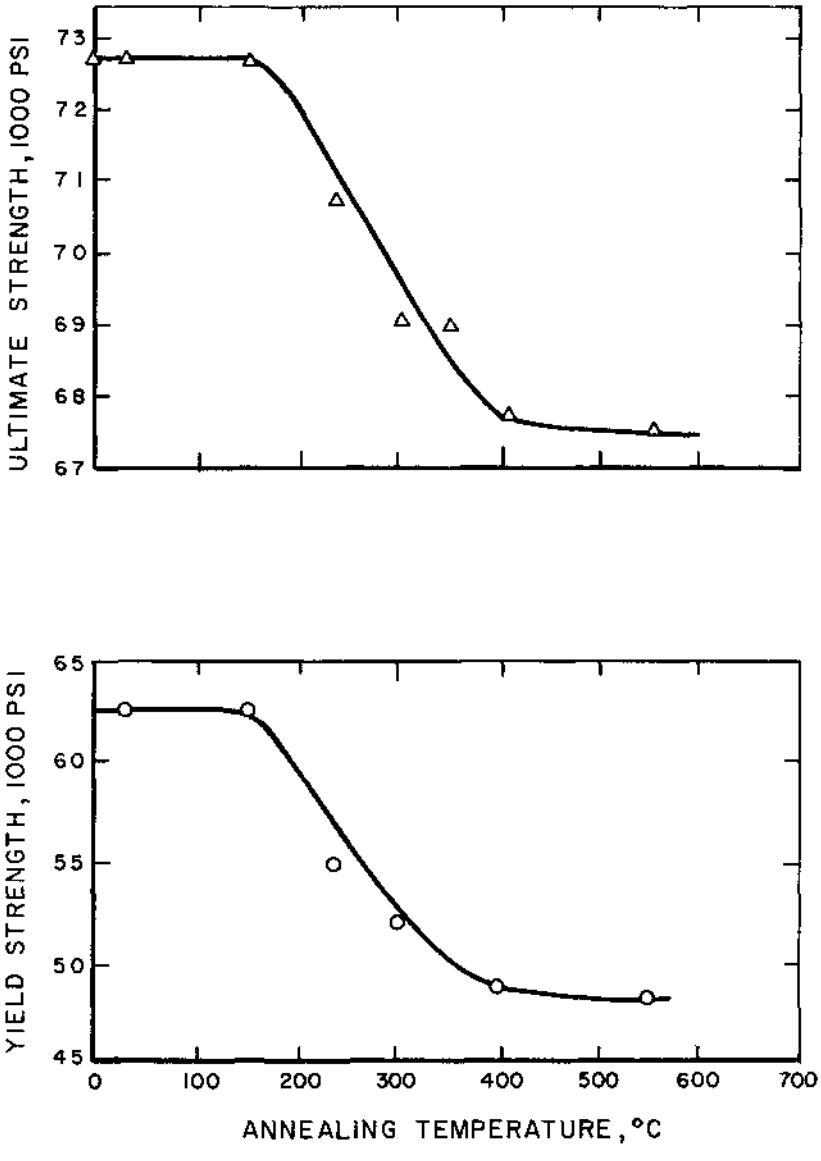

Fig. III-4 Isochronal annealing curves for Zr-0.5Nb-1Cr alloy irradiated to 5.5×10^{18} neutrons/cm^2.[56]

The effect of helium and lithium on the tensile properties of zirconium has been determined.[57a] The helium was introduced by irradiating a Zr-B alloy at 100°C until a helium content of ~2 cm^3/cm^3 of alloy (1.2×10^{-3} atom fraction) was obtained from the $^{10}B(n,\alpha)^7Li$ reaction. In postirradiation tensile tests the yield strength was only slightly affected, while the reduction-in-area values were drastically reduced at testing temperatures up to 500°C.

Stainless Steels and Superalloys

A large volume of research is being conducted on the radiation-induced embrittlement in stainless steels and nickel alloys at elevated temperatures. A thorough treatment concerning the effects of radiation on tensile properties of austenitic stainless steel has been presented by Battelle-Northwest.[58] The variables fluence, neutron spectrum, irradiation temperature, and testing temperature and possible mechanisms which may be responsible for the radiation-induced changes in tensile properties were considered. Specimens of 316 stainless steel were irradiated in the ETR at elevated temperatures (540 to 750°C), while 304 and 348 stainless-steel samples were irradiated in the same reactor at low temperatures (290°C), specimens of 304 and 348 stainless steel were also irradiated in EBR-II at 520°C. It was observed that the radiation-induced increase in yield strength was greater and persisted to higher testing temperatures with increasing fast fluence. As the testing temperature was increased to 750°C, the higher temperature irradiations caused larger increases in yield strength. The results of these tests are given in Fig. III-5. It was suggested that at lower irradiation temperatures, a large number of small defects are produced which are subsequently annealed out at the higher testing temperatures. Larger and more stable defects (cavities) are formed during irradiation at higher temperatures. Although these cavities do not cause as large an increase in yield strength as the smaller defects do, they are more stable at higher temperatures and consequently the radiation-induced yield-strength increase persists to higher test temperatures.

Postirradiation annealing for 1 hr at 1121°C was performed on the specimens which were irradiated in EBR-II at 520°C to a fluence of 1.1×10^{22} neutrons/cm^2 (>0.18 Mev). Testing of the annealed specimens at 500°C indicated that both the preirradiation

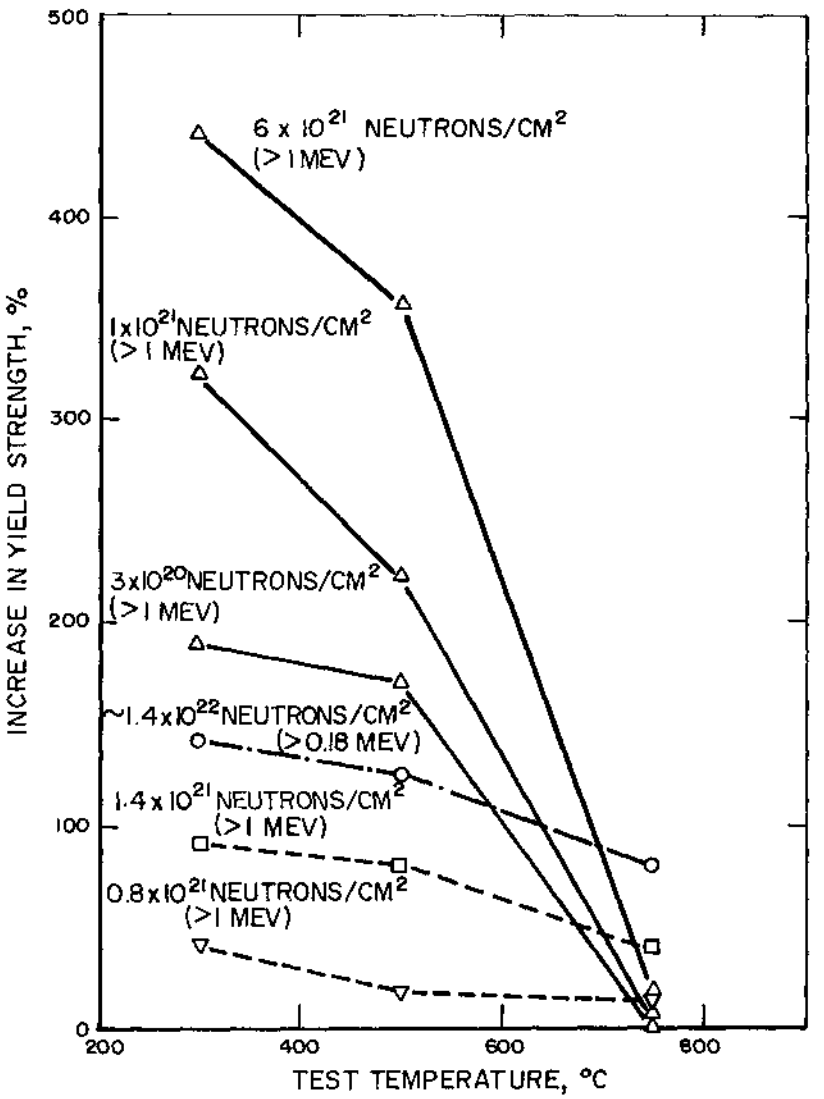

Fig. III-5 Effect of fast fluence and irradiation temperature on the yield strength of austenitic stainless steel.[58] △, ETR 304, 290°C; ○, EBR II 304, 540°C; □, ETR 316, 600°C; ▽, ETR 316, 700°C.

expect a uniform distribution of helium and thus little ductility loss in this stainless steel. However, it was found that this stainless steel exhibited greater ductility loss (total elongation being less than 1% at 650°C) than did stainless steels which had an equivalent amount of helium (~1 x 10^{-5} atom fraction) that originated either from a higher boron impurity or from cyclotron bombardment by alpha particles.

The loss in elevated-temperature ductility in 347 stainless steel irradiated to 2.2 x 10^{22} neutrons/cm^2 was also found to be independent of holding times from 4 min to 1 hr before testing at 650°C. These results indicate that the radiation-induced embrittlement at elevated temperature is not diffusion dependent. The extreme degree of radiation-induced loss in uniform elongation (from 18 to 0.7%) could not be explained by weakening of grain boundaries by helium bubbles. Rather, it was suggested that the extreme embrittlement could be caused by either (1) hardening of the grains by small helium bubbles or (2) extension of the ductility minimum as proposed by Rhines.[61] The ductility minimum occurs in many metals and alloys when grain-boundary shear takes place at elevated temperature and causes cracks at the grain boundaries. As the testing temperature is increased the cracks are healed by grain-boundary migration and the ductility of the material is increased. It was proposed that for the irradiated stainless steel the grain boundaries are pinned by helium bubbles or other transmutation products. Thus, the grain-boundary cracks are not healed by grain-boundary migration and fracture occurs with limited elongation.

French investigators[60b] found that increasing the carbon content from 0.04 to 0.07 wt. % in irradiated 316 stainless steel at 700°C resulted in a decrease in postirradiation elongation from 9 to 2.5% at 700°C. Previous studies indicated that the degree of radiation-induced embrittlement decreased with increasing carbon content.[62] However, it should be noted that the degree of embrittlement is very dependent on the morphology of carbide particles which may result from a given heat treatment.[64] The tensile specimens used to study the effect of carbon had been irradiated at 700°C to a fast fluence of 1 x 10^{21} neutrons/cm^2 and a thermal fluence of 1.7 x 10^{21} neutrons/cm^2. No helium bubbles were observed in the as-irradiated stainless steel tested at 700°C. However, annealing the irradiated stainless steel for 1 hr at 1100°C resulted in formation of helium bubbles in the grain boundaries, in twin boundaries, and on dislocations in the matrix. It was also found that the radiation-induced ductility reduction was more severe for specimens irradiated at 650°C than for those irradiated at 800°C, with the fast fluence being 1 x 10^{21} neutrons/cm^2 in both cases. The variation of grain size from 31 to 130 μ did not affect the postirradiation ductility at 700°C. This effect is in contrast to previous observations that the degree of radiation-induced embrittlement at elevated temperatures increased with increasing grain size.[65] Additions of niobium to the 316 stainless steel resulted in a material that was more resistant to radiation-induced embrittlement at elevated temperatures.

Stress-rupture tests were performed at 650 and 700°C for both unirradiated and irradiated (1 x 10^{21} neutrons/cm^2) 316 stainless steel.[60b] The creep rate for the irradiated material was factors of 2 to 10 higher than that for the unirradiated controls. Specimens irradiated at 80°C and annealed for 15 days at 650°C after irradiation exhibited higher creep rates than did specimens irradiated to equivalent fluences at either 550 or 650°C. These results are shown in Fig. III-6. Irradiation of stainless steel to a total fluence of 1.6 x 10^{22} neutrons/cm^2 in the Dounreay Fast Reactor was found to result in higher creep rates at 700°C as shown in Fig. III-7. However, in-pile uniaxial creep

tests resulted in lower ductilities at fracture but the creep rate itself did not seem to be affected by irradiation to 8×10^{19} neutrons/cm^2. The in-pile creep rate of tubular specimens appeared to be somewhat higher than the creep rate for uniaxial creep as shown in Fig. III-8.

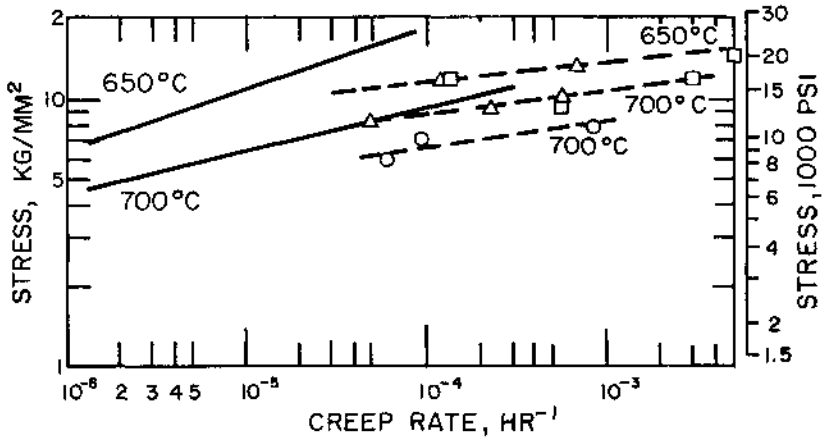

Fig. III-6 Creep rate of irradiated and unirradiated 316 stainless steel at 650 and 700°C.[60b] ——, thermal control data; – – –, irradiated: o, 10^{21} neutrons/cm^2 (>1 Mev) at 80°C + 15 days at 650°C; □, 7×10^{20} neutrons/cm^2 (>1 Mev) at 550°C; Δ, 10^{21} neutrons/cm^2 (>1 Mev) at 650°C.

Stress-rupture tests at 650°C have been conducted on 347 stainless steel irradiated to a fast fluence of 2.2×10^{22} neutrons/cm^2 in the ETR.[58] Irradiation reduced the rupture life of this material by a factor of about 6. However, the most significant irradiation effect observed was the reduction in elongation at rupture from 20 to about 0.2%. Microstructures of the fractured unirradiated specimen (20% elongation at fracture) showed considerable elongation of the grains and the presence of numerous cracks and voids at the grain boundaries. The fractured irradiated specimen (0.2% elongation at fracture) showed no elongation of the grains and no voids and cracks at the grain boundaries.[66]

Oak Ridge researchers[65] observed that fine-grain stainless steel was less susceptible to radiation-induced embrittlement at elevated temperatures. To study this effect further, Brookhaven workers[67] obtained a fine structure in 304 stainless-steel specimens by cold working to reduce the cross-sectional area by 92%. The specimens were then annealed at 760°C for 16 hr. This anneal was chosen to obtain a fully recrystallized structure that would be stable at 650°C. The recrystallized specimens were irradiated at 100°C to a fast fluence of 1.3×10^{20} neutrons/cm^2 (E > 0.82 Mev). Results of tensile tests on the irradiated and control specimens (Table III-3) indicate that irradiation does not significantly affect the strength at the different testing temperatures, but the ductility is noticeably reduced by irradiation.

To duplicate the radiation-induced embrittlement in stainless steel at elevated temperatures, specimens of 316 stainless steel were cold worked, annealed, and bombarded with alpha particles in a cyclotron.[68] A total of 4×10^{-5} atom fraction of helium was introduced into the steel while its temperature was kept below 150°C. One of the

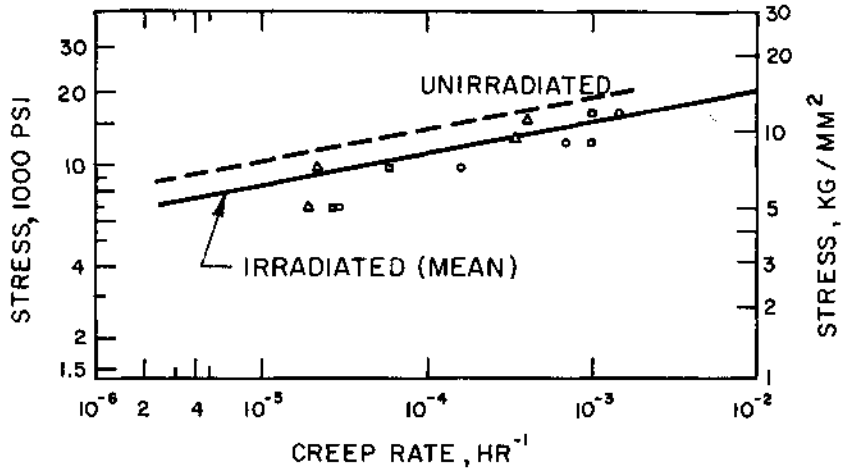

Fig. III-7 Creep rate of 316 stainless steel irradiated in Dounreay Fast Reactor to a total fluence of 1.6×10^{22} neutrons/cm^2 and tested at 700°C.[60b] All specimens annealed 1 hr at 1050°C (= A). △, A + 10% cold work + 100 hr at 800°C; ○, A + 100 hr at 800°C; □, A.

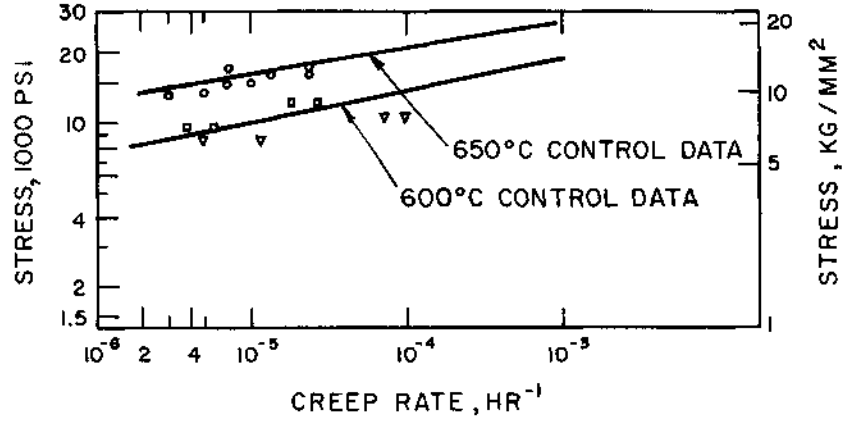

Fig. III-8 In-pile uniaxial and biaxial creep of 316 stainless steel at 650 and 700°C.[60b] Maximum fluence is 8×10^{19} neutrons/cm^2 (E > 1 Mev). In-pile uniaxial creep tests: ○, 650°C; □, 700°C. In-pile biaxial creep tests: ▽, 650 to 700°C.

microstructures exhibited $M_{23}C_6$ precipitates at the grain boundaries while the other microstructure contained both carbides and sigma phase. The presence of helium was found to have no effect on the yield or ultimate strength at the testing temperatures of 540 to 815°C. However, the total elongation was significantly reduced by the helium as illustrated in Fig. III-9. It was believed that helium formed bubbles on the grain-boundary carbide particles, thus reducing the ductility and greatly reducing the amount of grain-boundary sliding needed to form a void. A fine dispersion of sigma phase apparently trapped the helium bubbles, thus raising the temperature at which the ductility loss starts to take place.

Table III-3 TENSILE PROPERTIES OF HEAVILY COLD-WORKED[a] 304 STAINLESS STEEL[67]

Test temperature, °C	Yield strength, psi	Tensile strength, psi	Total elongation, %
	Unirradiated[b]		
25	55,000	115,000	47
650	23,300	31,500	76
750	10,200	13,000	53
800	6,600	8,650	83
	Irradiated to 1.3×10^{20} neutrons/cm^2 (E >0.82 Mev)[b]		
650	22,150	30,600	36
650	22,800	29,500	34
750	12,500	13,300	29.5
750	11,100	12,600	24
800	5,500	8,300	46.5

a Cold swaged 92% with two intermediate anneals and the final anneal at 760° C for 16 hr.
b All specimens were tested at a strain rate of 0.2%/min.

To study void formation in 304 stainless steel further, samples from an EBR-II control-rod shroud have been subjected to density measurement by immersion, and selected thin films have been prepared for transmission electron microscopy.[34c,36b] A comparison of the measured density changes with those predicted by transmission electron microscopy (TEM) for the different irradiation conditions showed the density decreases predicted by TEM to be consistently lower than those determined by density measurements. It appears that some of the smaller voids are not being resolved by TEM.

The French[54b] have studied the effect of irradiation to 1×10^{20} neutrons/cm^2 on the elevated-temperature ductility of various materials with face-centered cubic structures. The materials included stainless steel (17 wt.% Cr-13 wt.% Ni-0.2 wt.% Ti), pure nickel, copper, Cu-Si alloy, and Nimonic 80A. Postirradiation ductility of the stainless steel was found to be quite dependent on the carbon content, which is in agreement with the work by French investigators that was discussed earlier.[60b] The maximum postirradiation ductility was obtained for a carbon content of 0.016%, which was believed to result in ideal precipitation of carbides. The postirradiation behavior of copper at elevated temperatures was comparable to that of unirradiated copper containing

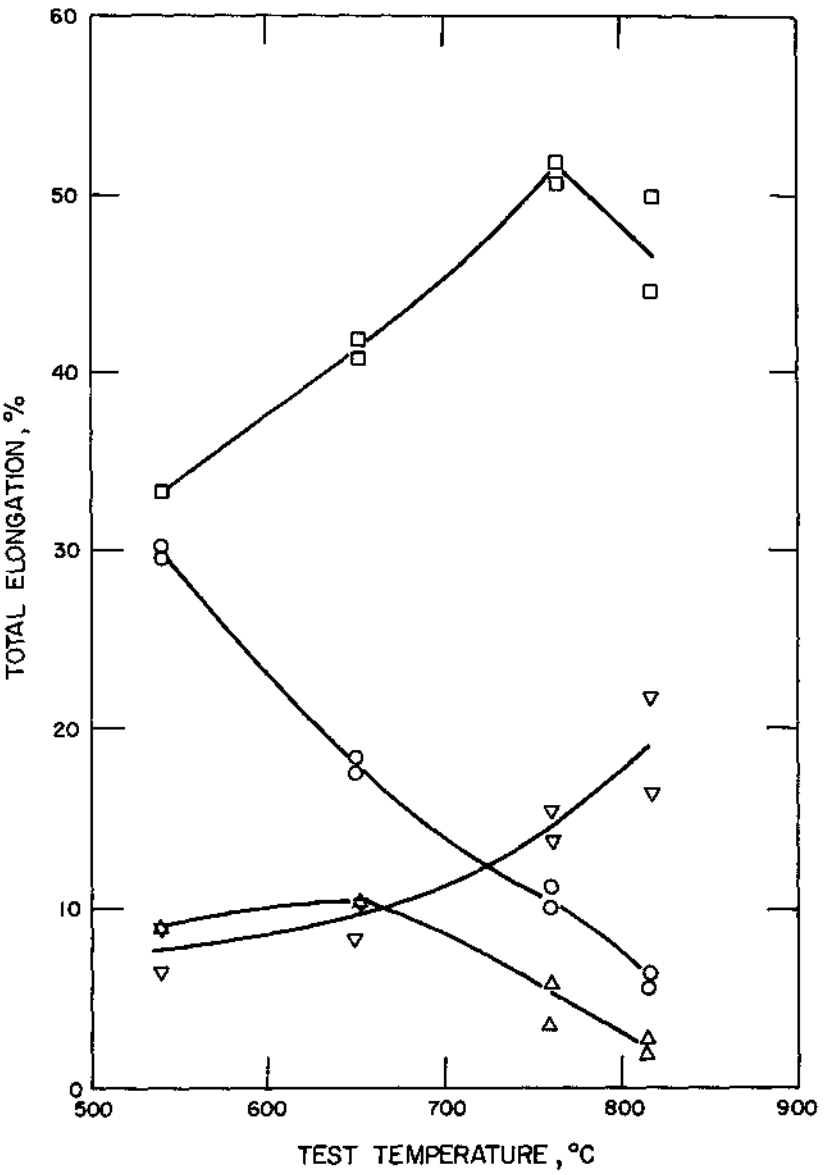

Fig. III-9 Total elongation as a function of test temperature for 316 stainless steel with no helium and with 4 x 10^{-5} atom fraction helium.[68] Carbides at grain boundaries: □ , no helium; ○ , 4 x 10^{-5} atom fraction helium. Sigma dispersed in matrix: ▽ , no helium; △ , 4 x 10^{-5} atom fraction helium. Strain rate = 0.02 min^{-1}.

silicon additions. It is postulated that the intermetallic Cu-Si particles prevent grain-boundary migration during testing and thus cause intergranular fracture with minimal strain. In irradiated copper the grain-boundary pinning is attributed to cavities that are formed during tensile testing. It was concluded from these studies that radiation-induced embrittlement at elevated temperature occurs in materials which are susceptible to intergranular fracture in the unirradiated form. The controlling mechanism was believed to be pinning of grain boundaries by cavities that are produced, or at least stabilized, by helium.

The postirradiation tensile behavior of various Fe-Cr steels at elevated temperatures was investigated by the Germans.[60c] It had been previously found that the onset of embrittlement corresponded with the $\alpha \rightarrow \gamma$ transformation. With chromium contents of 11.3, 14.6, and 17.7 wt.%, it was possible to obtain $\alpha \rightarrow \gamma$ transformation temperatures at 800, 850, and 900°C for the different alloys. These temperatures are only approximate since the transformation is fairly sluggish. After the alloys were irradiated at 50°C to a thermal fluence of 5×10^{19} neutrons/cm^2 and tested at elevated temperature, embrittlement was found to occur only after the $\alpha \rightarrow \gamma$ transition had taken place. The boron content in these alloys varied from 1 to 70 ppm; however, helium generation was not a significant factor since all of the alloys were embrittled to about the same degree. Specimens of body-centered cubic 15Mo3 steel (0.13 wt.% carbon and 0.24 wt.% molybdenum) were also irradiated for comparison since this ferritic alloy exhibits intergranular fracture when the unirradiated alloy is tested at elevated temperatures. Tensile tests on unirradiated and irradiated (5×10^{19} neutrons/cm^2) specimens showed that the ferritic alloy was significantly embrittled by irradiation before the $\alpha \rightarrow \gamma$ transformation took place. Therefore, it was concluded that the elevated-temperature embrittlement occurred in materials that were susceptible to intergranular fracture.

The effects of titanium and carbon contents and grain size on the creep properties of irradiated Incoloy 800 have been studied at Oak Ridge.[69] Specimens of Incoloy 800 were irradiated at 650 and 700°C to a fast fluence of 8×10^{20} neutrons/cm^2. Fig. III-10 shows the effects of grain size and carbon content on creep elongation of irradiated Incoloy 800 at 700°C. It appears that postirradiation creep elongation of the alloy with high carbon (0.12 wt.%) is more sensitive to grain size, with the smaller grain size favoring higher postirradiation creep elongations. Highest creep elongations are obtained with a titanium content of 0.1 wt.% regardless of the carbon content. Fig. III-11 shows that the highest rupture lives at a stress of 12,000 psi were obtained with the larger grain size, while the carbon and titanium contents appear to be secondary factors.

The effect of irradiation on the superplasticity of an Fe-28Cr-32Ni alloy at elevated temperatures has been established at Brookhaven.[67] Unirradiated and postirradiation tensile properties of the superplastic alloy were determined at 650 to 800°C. The elongation at 750°C was reduced from 175 to 17% by a fast fluence of 1.3×10^{20} neutrons/cm^2. Annealing of the irradiated superplastic alloy for 2 hr at 1000°C resulted in further reduction of the postirradiation ductility from 17 to 9%.

The effects of irradiation at 370°C to a fast fluence of 1×10^{19} neutrons/cm^2 in EBR-II on the impact properties of Inconel-X750 and 17-4PH stainless steel were determined at Argonne.[36b] The specimens irradiated in helium and sodium seemed to behave similarly and consequently it was concluded that irradiation in a sodium environment has no discernible effect on impact strength. Reductions in impact strengths of X750 and 17-4PH due to irradiation were 1.5 and 2 ft-lb, respectively, at all test temperatures.

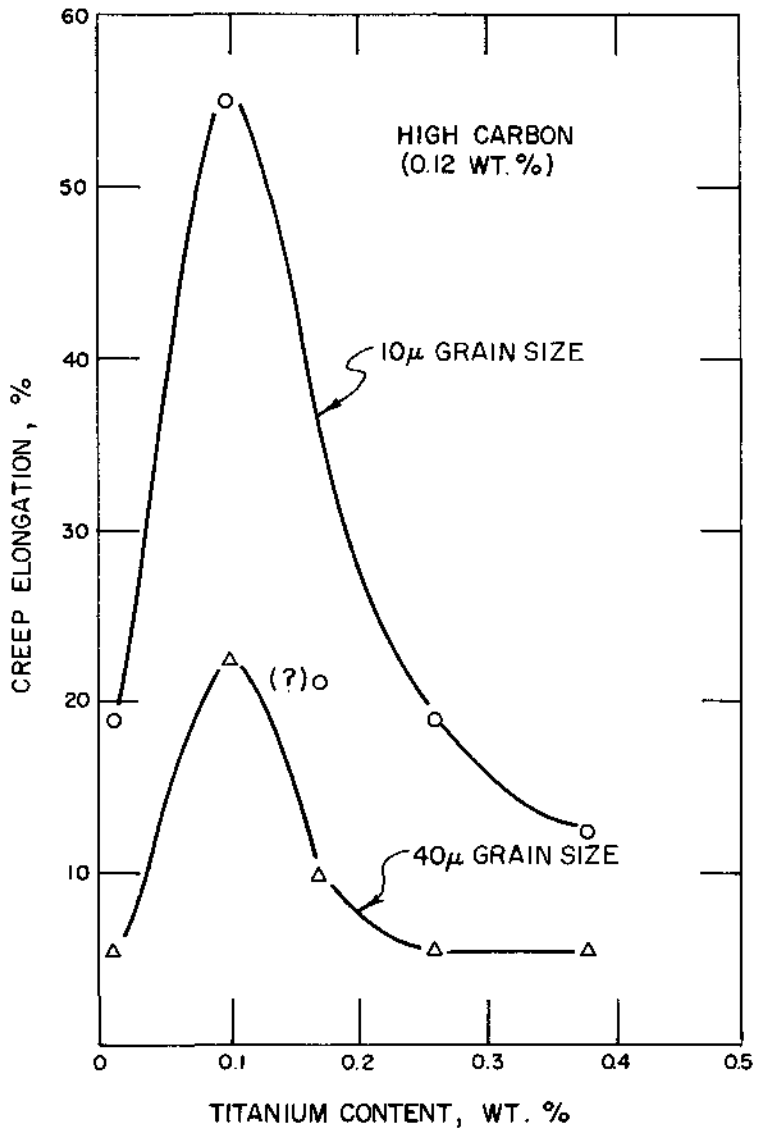

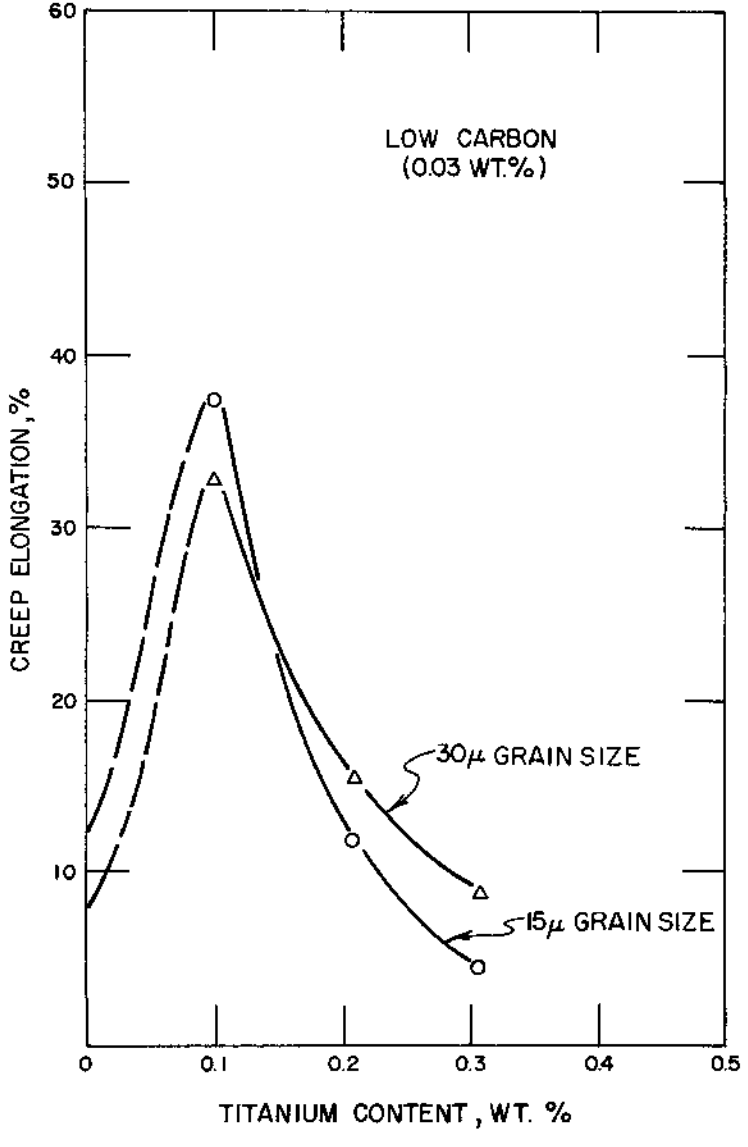

Fig. III-10 Creep elongation of Incoloy 800 at 700°C after irradiation in the ORR at 650 and 700°C to about 0.8×10^{21} neutrons/cm^2.[69]

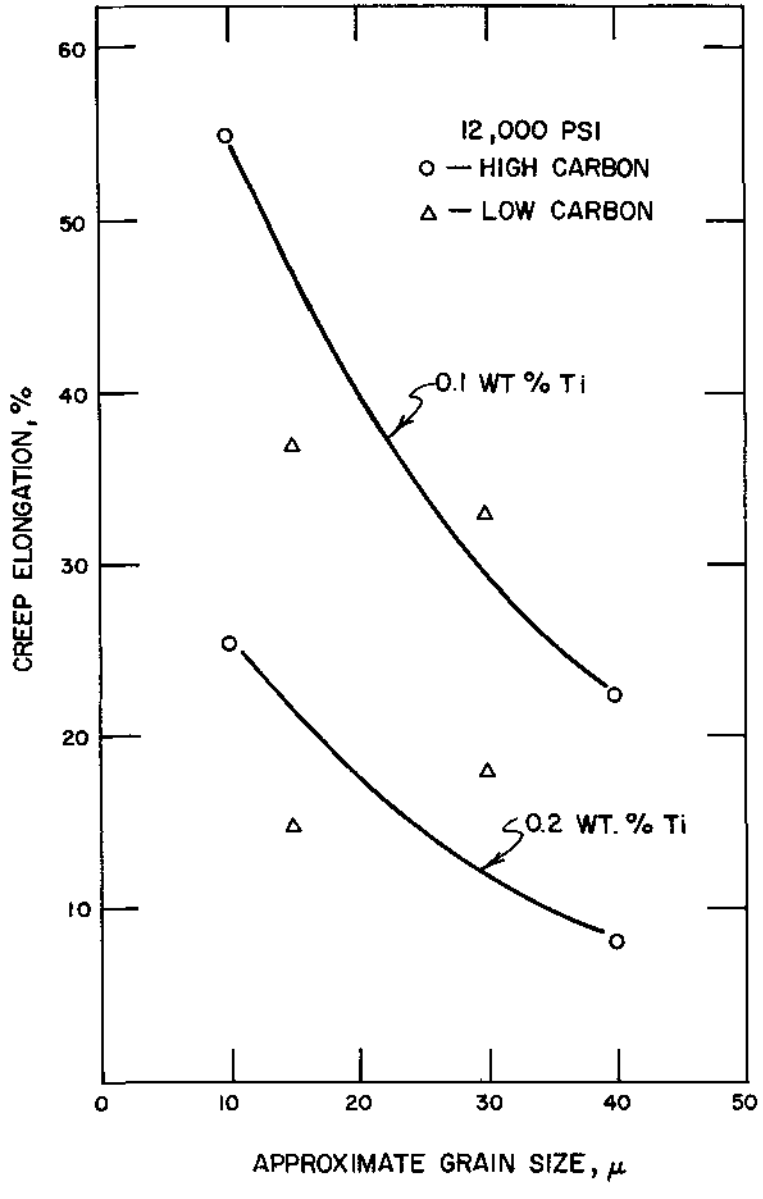

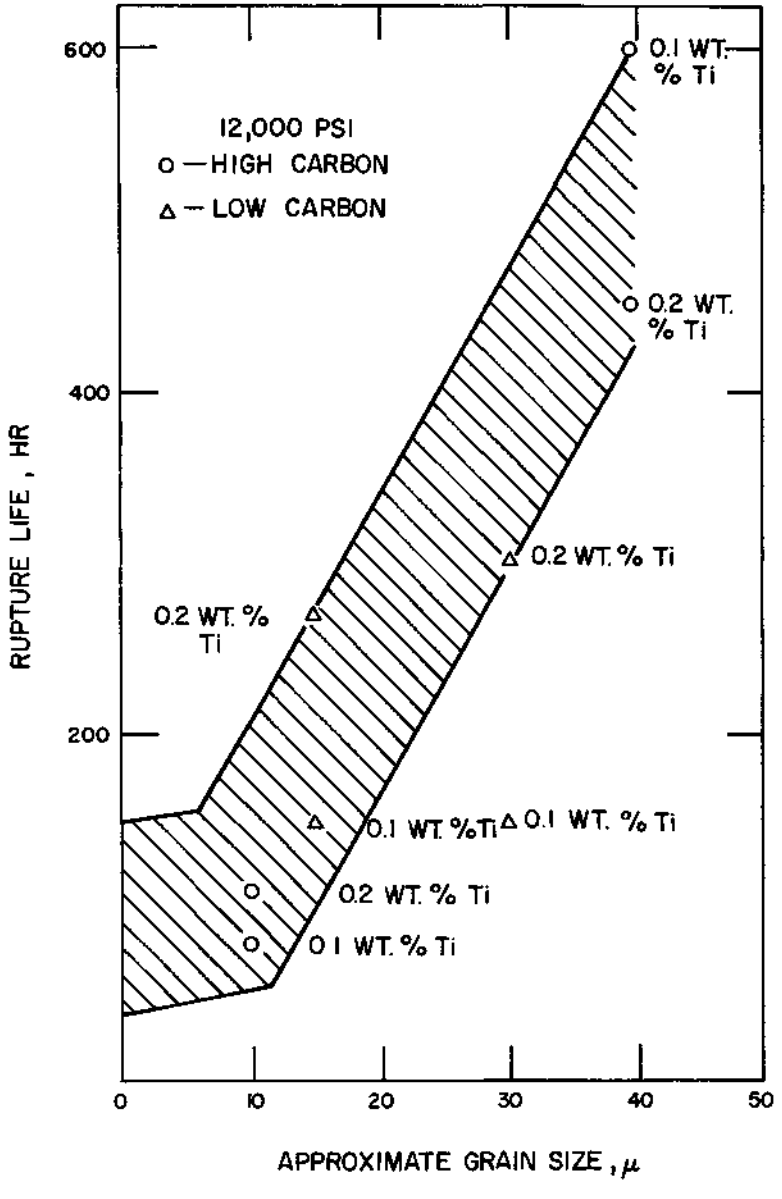

Fig. III-11 Creep properties of Incoloy 800 at 700°C after irradiation in the ORR at 650 and 760°C to about 0.8×10^{21} neutrons/cm^2.[69]

Cobalt alloys are attractive for possible application in Liquid-Metal-Cooled Fast Breeder Reactors (LMFBR) because of their high strength at elevated temperatures and their good corrosion resistance to liquid sodium. Table III-4 summarizes the postirradiation tensile properties of various commercial cobalt alloys irradiated and tested at elevated temperatures.[66,70] Experimental cobalt alloys were also tested but these exhibited postirradiation tensile properties similar to those of the commercial alloys. The commercial alloys were irradiated at about 50 to 100°C with the fast fluence ranging from 1.3×10^{20} to 1.4×10^{20} neutrons/cm^2. In one study, the irradiated specimens were annealed at 800°C for 1 hr to remove the displacement type of radiation damage so that the elevated-temperature embrittlement could be investigated.[71] Table III-4 shows that irradiation resulted in increases in strength and reductions in ductility when the specimens were tested at room temperature.[70] However, annealing of the irradiated cobalt alloys at 800°C appears to restore the preirradiation tensile properties at room temperature and 315°C. All of the irradiated cobalt alloys exhibited significant reductions in elevated-temperature ductility, even after annealing at 800°C. The elevated-temperature strength of cobalt alloys also appears to be reduced by the higher fast fluences.

The influence of nickel on the radiation-induced embrittlement at elevated temperatures has been studied[66] with a series of alloys of varying nickel content. All of the alloys had face-centered cubic crystal structures and included Nickel-200, a nonnickel manganese-stabilized austenitic stainless steel (Tenelon), and two cobalt alloys. One of the cobalt alloys contained 10 wt.% nickel (Haynes Stellite-25) while the other one did not contain any nickel (UMCo-50). These specimens were irradiated at 50°C to fast fluences ranging from 1.4×10^{21} to 1.5×10^{21} neutrons/cm^2. All of the alloys underwent reductions in ductility and strength at elevated temperatures after irradiation. Results of the tensile tests on the cobalt alloys are given in Table III-4. Metallographic examination of the fractured specimens indicated that irradiation promoted intergranular fracture at elevated temperatures in all four alloys. The fracture mode of Nickel-200 at 500°C was changed from transgranular to intergranular by irradiation.

Vanadium Alloys

The creep properties of irradiated V-20Ti alloys at 650°C were determined at Argonne.[34c] These specimens were irradiated in EBR-II at 585°C to total fluences ranging up to 2.1×10^{22} neutrons/cm^2. Irradiation apparently has no influence on the minimum creep rate of vanadium alloys at 650°C (see Fig. III-12).

Pressure-Vessel Steels

The Naval Research Laboratory has investigated[71] the contribution of minor composition differences in A302B to the radiation-induced shift in the ductile-to-brittle transition temperature. A vacuum-melted heat which was low in residual elements was found to be insensitive to irradiation at 550°F (290°C). It was established that copper and phosphorus contribute to the radiation-induced nil ductility temperature (NDT) increase while nitrogen and sulfur do not. Vanadium was found to increase the embrittlement sensitivity of steel. Long-term aging (1440 hr) at 550°F had only a minor influence on the NDT shift of the steels with the various impurity contents. Consequently, it was

Table III-4 TENSILE PROPERTIES OF IRRADIATED AND UNIRRADIATED COBALT-BASE ALLOYS

Alloy	Test temp., °C	Fast fluence, 10^{20} neutrons/cm^2	Yield strength, 1000 psi		Ultimate tensile strength, 1000 psi		Total elongation, %		Reference
			Unirr.	Irr	Unirr.	Irr.	Unirr.	Irr.	
Haynes Stellite-25	RT	1.3	67.0	139.0	152.0	142	55.0	15.0	70
	650	1.3		45.6		70.6		17	70
	750	1.3		35.0		38.2		9.2	70
	800	1.3	35.9	39.2	41.5	41.5	10.5	2.3	70
	RT[a]	14	66.3	56.2	139	133	68	55.6	66
	315[a]	14	39.7	36.0	118.5	117	86	60.2	66
	450[a]	14	36.1	29.9	96.3	70.3	42	22.8	66
	500[a]	14		31.0		66.5		17.0	66
	550[a]	14	33.9	28.5	82.3	53.5	30	8.8	66
	650[a]	14	32.3	29.8	69.3	40.5	17	4.5	66
UMCo-50	RT[a]	14	47.5		126	127	35	27.4	66
	315[a]	14	33.6	29.7	121	112.1	61	56.7	66
	450[a]	14	28.9	26.0	82.5	75.1	24.5	30.7	66
	550[a]	14	25.0	24.6	72.0	49.1	27	13.9	66
UMCo-51	25	1.3	84.7	120	171	146	36	20	70
	650	1.3	37.8	46.4	72.2	68.6	14	9	70
	750	1.3		38.7		46.6		7.5	70
	800	1.3	30.0	34.2	40.3	39.8	10	6.5	70
Multimet	25	1.3	71.0	116	121	138.0	43	31	70
	650	1.3		28.1		53.5		11	70
	800	1.3	23.6	30.0	32.9	31.3	55	6.7	70
Haynes 188	25	1.3	71.6	133	142.5	167	25	44	70
	650	1.3		46.1		60.8		10	70
	750	1.3		38.6		38.6		3	70
	800	1.3	37.5	37.4	45.5	37.4	65	1.5	70
S-1	25	1.3	47.0	114	95.2	118	18.5	4	70
	650	1.3		37.9		47.4		5	70
	750	1.3		30.5		31.7		2	70
	800	1 3	19.5	23.6	33.8	23.6	29.0	1.5	70

a Specimens were annealed for 1 hr at 800°C before testing.

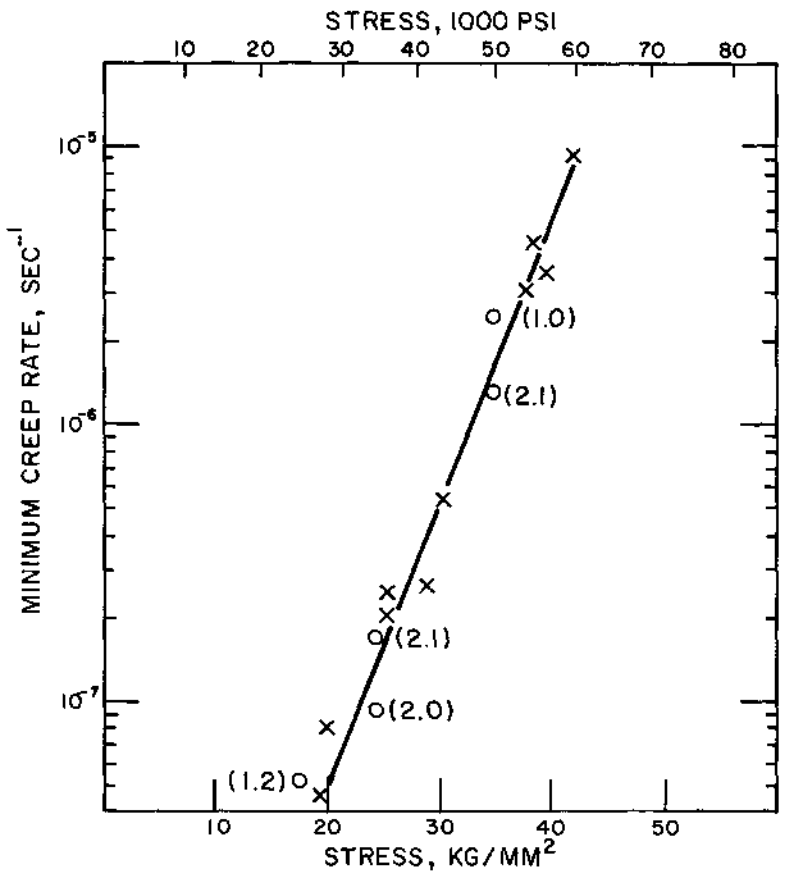

Fig. III-12 Minimum creep rate of unirradiated and irradiated V-20 wt.% Ti alloy at 650°C.[34c] ×, unirradiated; o, irradiated. Numbers in parentheses indicate the fluence in 10^{22} neutrons/cm^2.

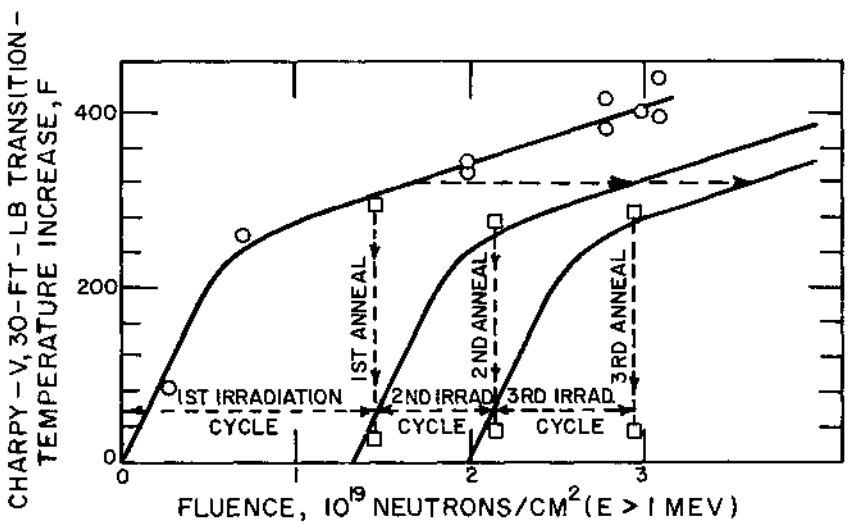

Fig. III-13 Response of the SM-1A pressure-vessel steel to cyclic irradiation and annealing.[72] Annealed at 585°F for 168 hr; irradiation temperature <240°F. o, NDT shift versus exposure for SM-1A steel (damage path); □, endpoints of irradiation and annealing cycles.

concluded that the measured NDT shifts after irradiation were independent of the thermal treatments but were dependent on the differences in composition.

If the radiation-induced shift in NDT becomes significant and perils the operation of a pressure vessel, it may be possible to alleviate this problem by in-place annealing.[72] Fig. III-13 illustrates the response of the A350-LF-1 steel to cyclic irradiation at 430°F (220°C) followed by annealing at 585°F (305°C) for 168 hr. The SM-1A reactor pressure vessel was actually annealed at 585°F to restore its NDT, which was approaching the NDT + 60°F criterion. It is suggested that NDT increases can be minimized by using more shielding, selecting insensitive steels, and utilizing in-place annealing.

Workers at Southwest Research Institute have completed the surveillance of the Elk River Reactor pressure vessel.[73] The surveillance specimens received a maximum fast fluence of 1.7×10^{19} neutrons/cm^2 at an irradiation temperature of 550°F (290°C). The maximum shift in the ductile-to-brittle transition temperature was found to be 130°F (55°C); this occurred in A302-B material originally in the strained and stress-relieved condition. The room-temperature low-cycle fatigue strengths of smooth tensile specimens of pressure-vessel and dissimilar weld-joint materials were increased by the fast-neutron exposure. The fatigue strength appears to increase with increasing fluence as shown in Fig. III-14.

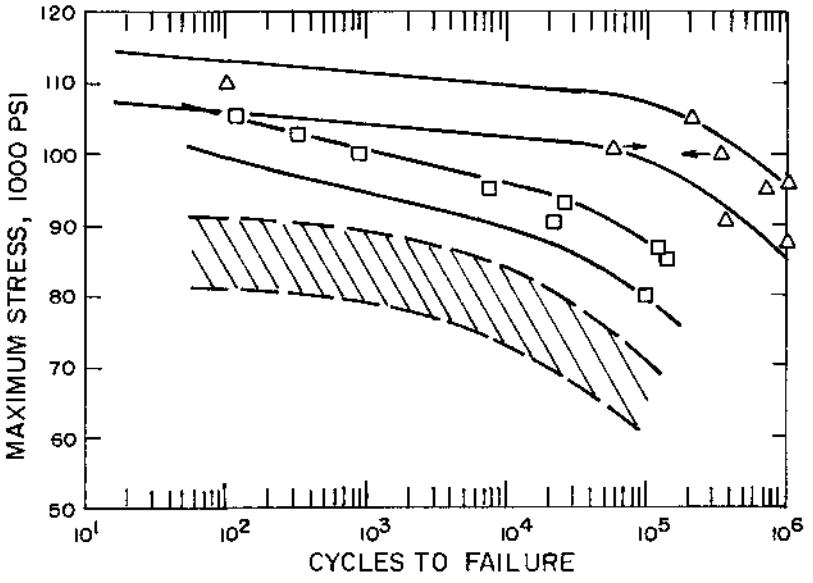

Fig. III-14 Effect of neutron irradiation on fatigue properties of A302-B.[73] ▨, unirradiated; □, irradiated to 8.3×10^{19} neutrons/cm^2 (>1 Mev); △, irradiated to 1.48×10^{19} neutrons/cm^2 (>1 Mev).

Japanese investigators[74] have compared the response of weld metal, the heat-affected zone (HAZ), and the base metal of modified HY 80 steel to irradiation at 165°F (75°C) to a fast fluence of 3.2×10^{19} neutrons/cm^2. Tests on Charpy V-notch impact specimens indicated transition-temperature shifts of 330°F (165°C) for the weld metal and 300°F (149°C) for the heat-affected zone. These changes in transition temperature were about equivalent to the change in the base metal.

Basic Studies of Radiation Effects

Chromium prepared by double melting in an inert atmosphere and irradiated at 80°C to a fast fluence of 10^{20} neutrons/cm^2 was annealed at temperatures up to 900°C to investigate thermal hardening effects.[75] The results of postirradiation annealing for 1 hr at the various temperatures indicated that a significant thermal hardening occurred in the temperature range 300 to 600°C. An annealing temperature of 900°C was required for the irradiated chromium to obtain a hardness similar to that of the unirradiated control. It was also found that irradiated chromium did not experience additional hardness increases until a total deformation of 80% was achieved. The hardness of the unirradiated control specimen increased progressively with increased deformation. Above 80% deformation, the hardness of the control and irradiated specimens increased at the same rate with increasing cold work.

Chromium containing total impurities of 0.025 wt.% (mostly oxygen and nitrogen) was irradiated to a fast fluence of 2×10^{19} neutrons/cm^2 at 85°C.[76] Examination of thin films of irradiated chromium by electron microscopy revealed dark spots, which were identified as defect clusters. These defect clusters changed to loops when the irradiated material was annealed between 600 and 800°C. It was further noted that irradiation decreased the brittle-to-ductile transition temperature 200°C. Unirradiated chromium exhibits brittle fracture in tension tests at test temperatures up to 200°C; however, the fracture mode of irradiated chromium changed from brittle to ductile above 25°C and exhibited a strain of 60% at 50°C. The improved ductility was attributed to the fact that the critical stage in fracture was changed from crack nucleation in the unirradiated material to crack propagation in the irradiated material.

The radiation-induced increase in the yield strength of most metals has been shown to depend generally on the square root of fluence. Figure III-15 illustrates that the relationship exists for irradiated niobium at lower fluences ($<10^{18}$ neutrons/cm^2), but a different behavior is evident at higher fluences.[69] The saturation in radiation-induced strength increase may be due to overlap of defect clusters, lack of nucleation of clusters after a certain fluence, or exhaustion of interstitial impurities which stabilize defect clusters. Annealing of the irradiated (2×10^{18} neutrons/cm^2) specimens at different temperatures before testing resulted in a variable strength increase as illustrated in Fig. III-16. The fact that the increase in yield strength occurs in the 200 to 400°C range suggests that it is due to the migration of mobile carbon atoms to defect clusters. Electron-transmission-microscopy observations showed that with increasing annealing temperature, large defects are formed by condensation of interstitial atoms. The areas near the grain boundaries appear to be denuded of the large defects.

Microstructural damage and subsequent recovery in molybdenum irradiated at 600°C was studied by quantitative electron microscopy.[77] After irradiation the microstructure consisted of large interstitial loops and small clusters within the grains. The area near the grain boundaries was denuded of interstitial loops but contained vacancy clusters. During annealing the interstitial loops disappeared and the vacancy loops grew at a rate equal to that of self-diffusion. Rapid annealing of small clusters within the grains occurred at a rate more nearly equal to that of vacancy migration.

Recovery of irradiated and cold-worked body-centered cubic materials has been reviewed by the Belgians.[78] The metals Fe, W, Mo, Ta, and Nb are discussed and special emphasis is given to the effect of interstitial elements on Stage III recovery.

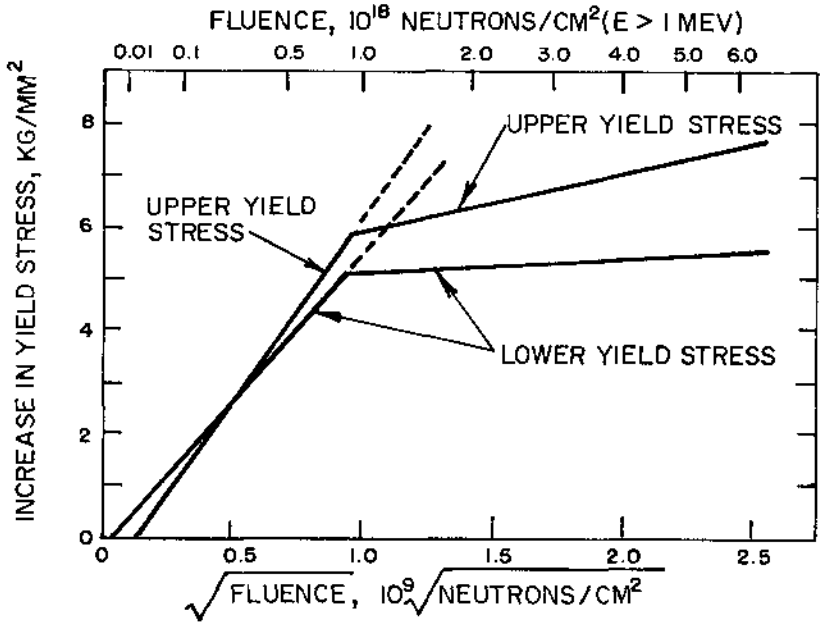

Fig. III-15 Effect of irradiation on yield stress of polycrystalline niobium.[69] (Irradiation temperature, <50°C; test temperature, 25°C).

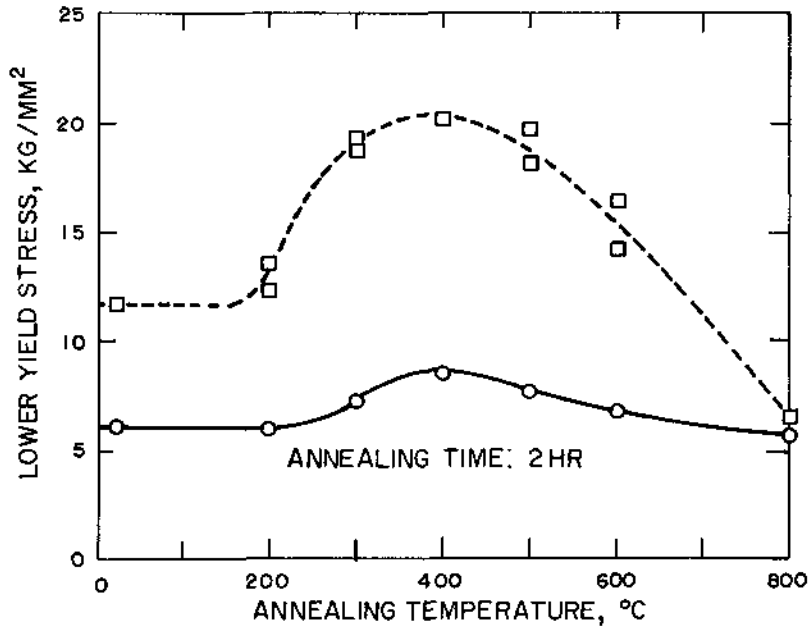

Fig. III-16 Effect of annealing on the lower yield strength of irradiated niobium.[69] □, fluence = 2 x 10^{18} neutrons/cm^2 (E > 1 Mev); ○, unirradiated.

Tungsten single crystals were irradiated[79] to fast fluences ranging from 1×10^{18} to 2.5×10^{19} neutrons/cm^2. It was found that the temperature for Stage III recovery (~350°C) shifts about 100°C when the fluence level is increased from 1×10^{18} to 2.5×10^{19} neutrons/cm^2.

It is believed that the saturation of radiation-induced yield-strength increase is dependent on the amount of carbon in solution, which governs the capture diameter. Good agreement was found[80] between the predicted and measured increases in yield stress for irradiated Ferrovac Fe and Fe-0.1C as shown in Fig. III-17. Table III-5 summarizes the expected capture diameter and the predicted fast fluence when saturation takes place in pure iron and in different steels.

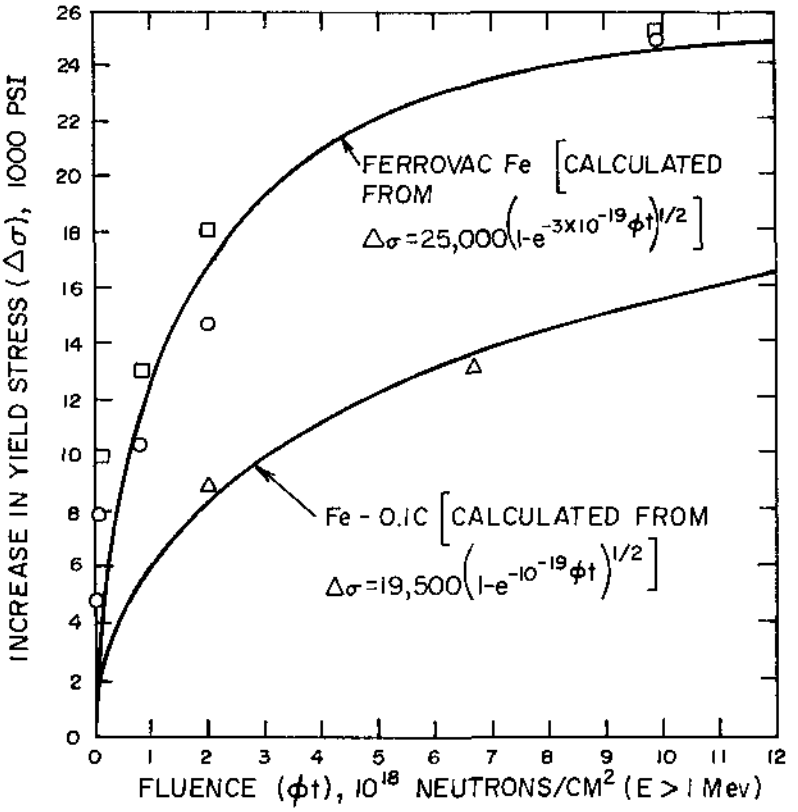

Fig. III-17 Comparison of predicted and measured irradiation-induced yield-strength changes in iron irradiated at 50 to 100°C.[80] □, △: △ ○ measured at room temperature: ○ - △ ○ measured at 145°K.

Internal-friction experiments were performed on copper of two purities (O.F.H.C. copper of 99.95% nominal purity and 99.999% pure copper)[81] after irradiation to 2×10^{11} neutrons/cm^2. It was concluded that the defect responsible for the pinning effect observed at slightly above room temperature in neutron-irradiated copper is not due to a simple vacancy mechanism, but rather is probably due to the delayed arrival of impurity-trapped vacancies at the dislocations. The activation energy of 1.03 ± 0.07 ev, which has been found to govern the pinning centered around 70°C, is in agreement with the results of other workers, but it is considered too high to be associated with the migration of free vacancies. It is also inferred that the release of vacancies from impurity traps is involved. A further pinning stage has been observed, centered around

150°C. It is believed that this pinning stage is due either to the release of further impurity-trapped vacancies or to the annealing of more complex damage such as dislocation loops.

Table III-5 ESTIMATED SATURATION FLUENCES FOR IRON AND STEELS[80]

Material	Capture diameter, A	Actual diameter (est.), A	Saturation fluence, neutrons/cm^2 (E > 1 Mev)
Ferrovac Fe	94	50	1.3×10^{19}
Fe-0.1 C	66	33	4×10^{19}
A212B	61	30	5×10^{19}
HY80	41	20	1.6×10^{19}

The effect of irradiation on the martensitic transformation in metastable beta brass has been studied at the University of Florida.[82] The brass was irradiated to fast fluences ranging from 5×10^{16} to 5×10^{18} neutrons/cm^2. Neutron irradiation decreased the martensitic-start temperature (M_s) about 8°C and increased the maximum rate of transformation. M_s was further decreased when the irradiated brass was annealed at 150°C.

(M. Kangilaski)

5. Metallurgy of Refractory Metals

The British[83] have studied the deformation of single crystals of Nb-Mo alloys as a function of composition, orientation, and temperature. Strong solid-solution hardening was observed which reached a maximum at the equiatomic composition. This hardening was attributed to the difference in atomic size between the two elements. Conjugate slip was extensive in the dilute alloy samples. At the 50 at.% composition, deformation occurred mainly by primary slip, and the onset of conjugate slip gave rise to failure by cleavage on (100). The variation of yield stress of the Nb-50 at.% Mo alloy with orientation was consistent with slip on (011) (111) slip systems. The temperature dependence of the yield stress at -196 and 250°C was similar to that of pure body-centered cubic metals, but at a much higher stress level. No evidence of twinning was found.

At NASA-Lewis, yielding, work hardening, and cleavage in Ta-Re alloy single crystals was investigated.[84] The crystals were evaluated in tension and compression as a function of solute concentration and temperature. The temperature dependence of the yield stress in tantalum was decreased by alloying with a minimum being observed at about 2 at.% rhenium. Three-stage hardening was not observed in these alloys. The alloys became more prone to cleavage with increasing rhenium content because of an increasing yield strength rather than a change in cleavage strength. Comparisons were made with other body-centered cubic alloy systems by quantitative calculations to show that the predominant hardening mechanism is due to the interaction of dislocations with misfitting solute atoms close to their slip planes.

The effects of metallic carbides and borides on the strength of Nb-W alloys and of ternary alloys with tantalum at temperatures close to 0.5 T_m have been determined by the British.[85] The alloys were room-temperature forged, solution treated, and creep tested in vacuum at high stress levels. The stable precipitates contained little or no tungsten or tantalum. Hafnium carbide at a concentration of about 2 mole % was the most effective addition. Other compounds produced effects according to their absolute melting points. A ratio of metal to nonmetal of 1.3 yielded the best properties. An empirical creep-rate equation was established which took into account the several variables and gave a hyperbolic sine stress dependence. On this basis a new equation for predicting the 100-hr rupture stress was determined.

Japanese investigators[86] found that strain-rate dependence of the flow stress of Nb-26 at.% Zr alloy was larger than that of pure niobium at all temperatures from 201 to 573°K. Above room temperature the strain-rate dependence of niobium disappears but that of the alloy is still significant. At 77°K the alloy deforms by twinning and the flow stress becomes insensitive to the strain rate. The results of this study indicate that the rate-controlling mechanism for the flow of the alloy is the same as that for pure niobium. Assuming that the double kink formation is the rate-controlling process, the kink energy of the alloy was determined to be about 1.25 ev, which is nearly three times larger than that for niobium.

Bureau of Mines researchers[87] combined niobium and tantalum with selected alloying elements to achieve solid solution and dispersion strengthening. Fifty-six alloys were evaluated to determine their formability, hardness, strength at elevated temperatures, and oxidation resistance. The following six alloys showed high-temperature strength: Nb-15Hf-5W-2Zr-4Al-4Ti-2N, Nb-15Hf-5W-5Zr, Nb-15.3Ti-4.1Zr-13.7Hf, Ta-20Hf-4Al, Ta-30Hf-4Al, and Ta-20Hf-5W-4Al. At 1200°C, the niobium alloys exhibited strength values of 40,000 psi or greather, and the tantalum alloys had strength values from 50,000 to 58,000 psi. For a 2-hr oxidation-test period at 1000°C, weight gains of only 9 and 8 mg/cm^2, respectively, were observed for Nb-15Hf-5W-2Zr-4Al-4Ti-2N and Ta-20Hf-5W-4Al.

German investigators described a kinetic model for use in interpretation of results obtained from investigations of the Nb-O system.[88] Their investigations show that tentative pressure-temperature-composition phase diagrams of the Nb-O system should be based on the assumption that the important components of the gas phase are niobium, NbO, and NbO_2 molecules; whereas the oxygen pressures measured in steady-state experiments do not affect the thermodynamic equilibrium.

The effect of oxygen content on the strain-aging behavior of electron-beam-refined niobium has been studied, using both yield-point-return and internal-friction measurements.[89] The strain-aging index, given by $\Delta\sigma_y = \Delta\sigma_f + 2\,K_y d^{-1/2}$, has been found to be proportional to the amount of oxygen migrating from free solid solution. The dislocation-locking parameter k_y attains a saturation value which increases with increasing initial oxygen content but is smaller than that for the annealed material. The results indicate that the smaller value of k_y is primarily due to the increased density of dislocations in the strain-aged material. $\Delta\sigma_f$, the increase in flow stress, commences to become greater only after the k_y parameter is almost saturated, and is associated with oxygen atoms which migrate to dislocations beyond the saturation of Cottrell atmospheres.

Resistivity measurements have been used by German researchers to determine isothermal strain aging of oxygen-doped niobium and tantalum.[90] Samples were deformed by rolling at room temperature and were then aged in silicone oil at 140 to 200°C. It was shown that an inhomogeneity of dislocation distribution influenced strain-aging kinetics and was also responsible for deviations from Matthiessen's rule in that the observed decrease in resistance was smaller when measured at 293°K than at low temperatures. Evidence for the existence of equilibrium Cottrell atmospheres was shown. Measurements on aged samples deformed a second time were in agreement with Hahn's theory of the yield point.

At the University of Pretoria,[91] dislocation-velocity measurements have been made in high-purity molybdenum single crystals as a function of stress at 77 and 300°K by the etch-pitting technique. The results were compared with data obtained from strain-rate-change experiments at 77, 180, 300, and 575°K in the macrostrain region ($\epsilon > 10^{-3}$) and at 300°K in the microstrain region ($\epsilon \leq 10^{-3}$). All the experimental observations and the calculated deformation parameters were shown to be self-consistent on the basis that dislocation mobility is controlled by the nucleation of double kinks to overcome Peierls-Nabarro hills. The results also indicate that the same rate-controlling mechanism is operative in both the micro- and macrostrain regions and that the usual assumption that the mobile dislocation density does not change during a rapid strain-rate change is valid.

Creep correlations for body-centered cubic refractory metals have been made at Lawrence Radiation Laboratory.[92] The following empirical relationship was developed:

$$\dot{\epsilon}_m = A \left(\frac{\sigma}{E} \right)^5 D$$

where $\dot{\epsilon}_m$ is the minimum creep rate, A is a constant, σ is the applied stress, E is the average elastic modulus at the test temperature, and D is the self-diffusion coefficient. This relationship is generally applicable for strain rates of less than 10^{-5}/sec and temperatures greater than about one-half the melting point in absolute units. Creep data for all six bcc refractory metals were analyzed and compared with the creep properties of fcc, hcp, and bcc metals. In general, the deformation behavior of all the refractory metals, except possibly that of tungsten, can be represented by the above relationship. This correlation is strong evidence of the similarity that exists between creep of pure close-packed metals and creep of pure bcc metals.

An investigation of the V-Tc alloy system has been conducted at Oak Ridge.[93] In addition to the terminal phases, three intermediate phases were observed. One phase is centered about 50 at.% Tc having the ordered bcc structure and two phases of higher technetium content exist above 1150°C. The structures of these phases were not determined but it was proposed that they are also related to a bcc lattice. In addition to this work, researchers at Aerojet-General have made revisions to the V-C and Nb-C binary systems.[94]

A major revision to the Ti-W phase diagram has been proposed by investigators at Aerojet-General.[95] This diagram, shown in Fig. III-18, presents a solid-solution type rather than the previous peritectic type of alloy system. No phase discontinuity could be detected and analysis of alloys quenched at solidus temperatures revealed only a single phase. The discrepancy between this work and the results of previous investigations

concerning the high-temperature phase equilibrium of this system was attributed to insufficient homogenization of the alloys after arc melting.

(J. H. Peterson)

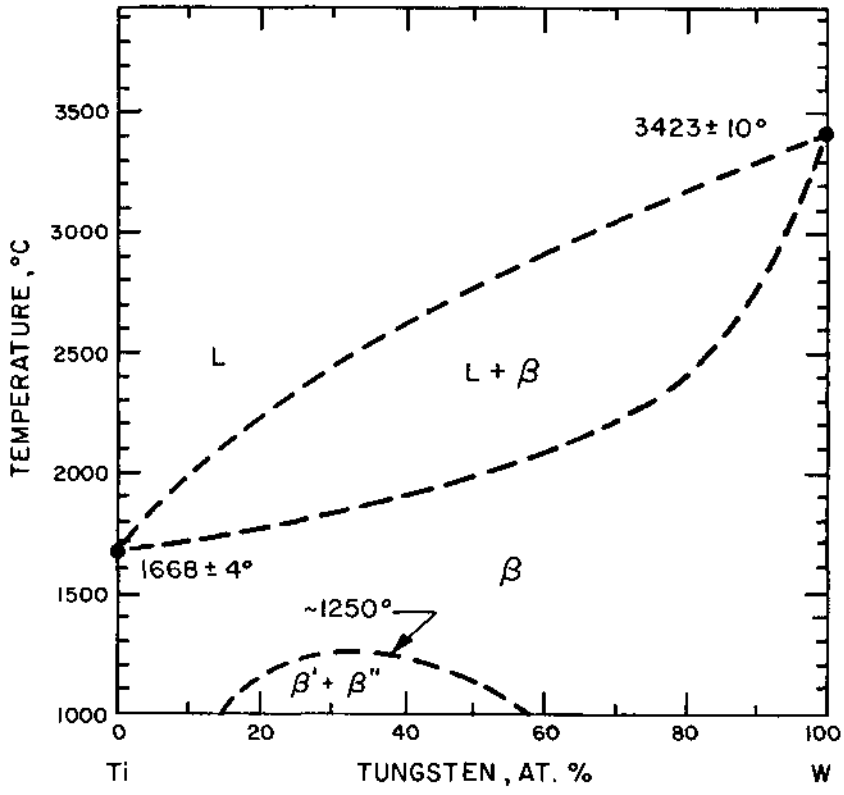

Fig. III-18 Ti-W phase diagram as determined at Aerojet-General.[95]

6. Metallurgy of Common Cladding and Structural Materials

Aluminum and Magnesium Alloys

The minimum creep rate of compacted magnesium powder containing 1 wt.% oxygen was found to be significantly lower at 450°C than that of magnesium alloys containing aluminum, manganese, or zirconium, as shown in Fig. III-19.[96] The low creep rate of the oxygen-containing compacts was attributed to the presence of MgO particles at the grain boundaries. These particles reduced grain-boundary migration processes, restricting both intergranular slide and intergranular shear. Diffusion creep was found to be inoperative in the compacted material.

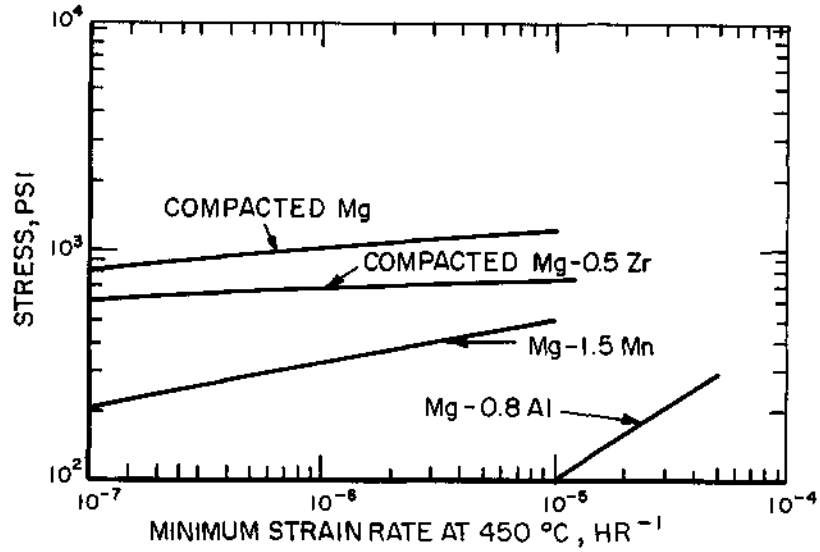

Fig. III-19 Comparative creep strengths of AL80 (Mg-0.8Al), AM-503 (Mg-1.5Mn), compacted Mg-0.5Zr, and compacted magnesium at 450°C.[97]

The primary creep of magnox AL80 at 450 to 620°C can be described by[97]

$$\epsilon = 3.2 \times 10^5 \, \sigma^{4/3} \, t^{0.7} \, e^{-32,000/RT}$$

and it is suggested that a function of grain size may be incorporated such that

$$\epsilon = 1.2 \times 10^3 \, d^{-3/2} \, \sigma^{4/3} \, t^{0.7} \, e^{-32,000/RT}$$

where

ϵ = primary creep strain, %

d = mean grain diameter at end of primary creep stage, in.

σ = stress, psi

t = time, hr

R = gas constant = 1.98 cal/(mole)(°K)

T = temperature, °K.

The primary creep strain at a particular time is related to the secondary creep rate. Approximate values of the secondary creep rate of magnox AL80 may be derived from short-term primary creep tests by application of the equation

$$\dot{\epsilon} \approx 0.23\, \epsilon^{4/3}/t$$

where $\dot{\epsilon}$ = secondary creep rate, %/hr.

Zirconium Alloys

Hot-rolling experiments were conducted[98] to define the causes of surface cracking in Zircaloy-4 during rolling at 795°C. To prevent surface oxidation during rolling, specimens were jacketed in mild steel, which was removed mechanically after rolling. It was found that strips that had been rolled by a 20-pass schedule exhibited inhomogeneous deformation with transverse corrugations. Strips that had been reduced by 5 passes did not have such corrugations. Those rolled at 20 passes contained bands of material with a crystallographic orientation different from that of the rest of the strip. Local thinning was also noticeable where the bands intercepted the surface. It is postulated that the positions at which banding occurs may depend upon localized differences in composition, crystallographic orientation, residual-stress distribution, dislocation densities, and grain size.

Empirical kinetic equations have been derived to describe the recovery of cold-worked Zircaloy-4 plate and tubing at 550 to 1020°F (288 to 549°C).[99] Samples which contained from 15 to 78% cold work were heated at temperature for up to 4000 hr. Figure III-20 illustrates the recrystallization of 78% cold-worked tubing in three directions as a function of temperature. The annealing process was found to take place as follows: (1) a dislocation climb and annihilation process to the limit allowed by the size of the deformation subcells, (2) a reorientation of the subgrain material into a recrystallization texture, (3) a growth of reoriented cells located in the most highly worked bands, and (4) a consumption of less favorably strained and/or oriented cells by the high-angle boundaries of the reoriented cells. Comparison of 15 and 73% cold-worked tubing showed the activation energy to be less (21 kcal/mole compared with 60 kcal/mole) and the subcell greater (8000 A compared with 1000 A) for the 15% cold-worked material.

Theoretical predictions have been derived to explain the supersaturation of hydrogen in Zircaloy.[100] It was shown that precipitation of hydride platelets was inhibited by the stresses which would result from the volume increase due to formation of hydride platelets. An equation derived from a thermal-cycling model predicts values of hydrogen concentration as a function of the number of cycles. These results agreed well with the data of Westerman.[101] The dissolution of ZrH platelets in Zircaloy-4 was found to be very rapid at high temperatures.[102] It was observed that for hydrogen contents of up to 200 ppm, the dissolution time at a temperature sufficiently above the phase boundary was given by:

$$t \approx 1.65\, h^2 \exp(24,900/RT) \text{ sec}$$

where h is the thickness of the ZrH platelet.

Soviet investigators[103] have found that the maximum amount of hydrogen precipitation in zirconium held under a thermal gradient occurs at about 245°C as illustrated in Fig. III-21. A zirconium specimen with a uniform hydrogen concentration was used to initiate the experiment and the changes in hydrogen concentration after exposure to a thermal gradient were established by metallographic and chemical analyses.

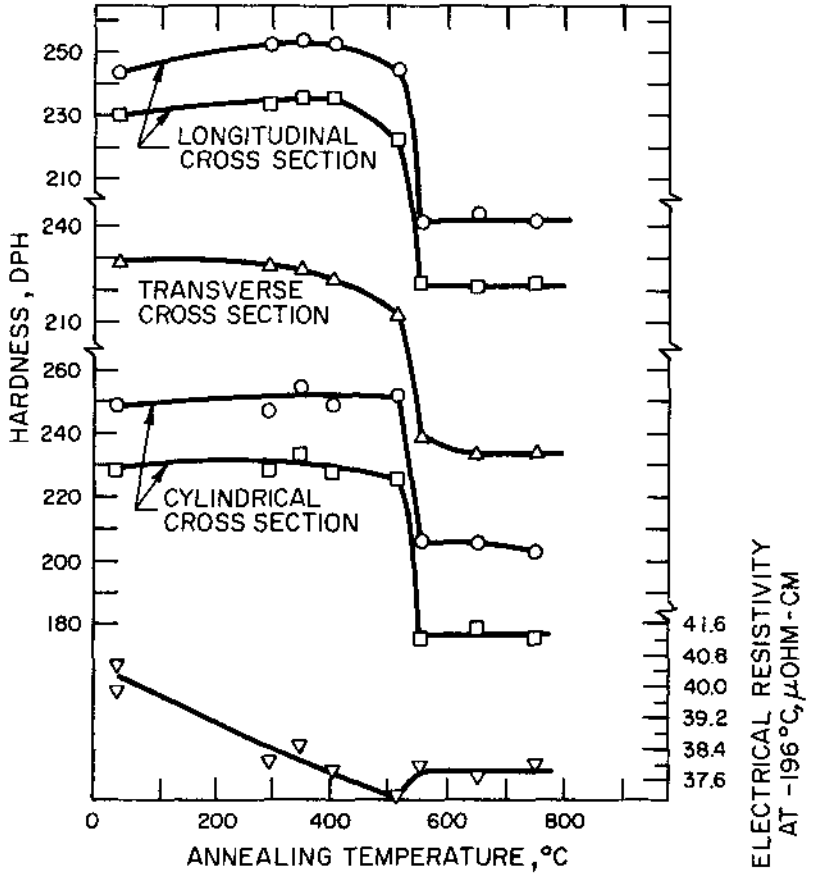

Fig. III-20 The effects of annealing for 4 hr on the microhardness of 78% cold-worked Zircaloy-4 tubing.[99] ○, perpendicular to tube axis; □, parallel to tube axis; △, random; ▽, electrical-resistivity data.

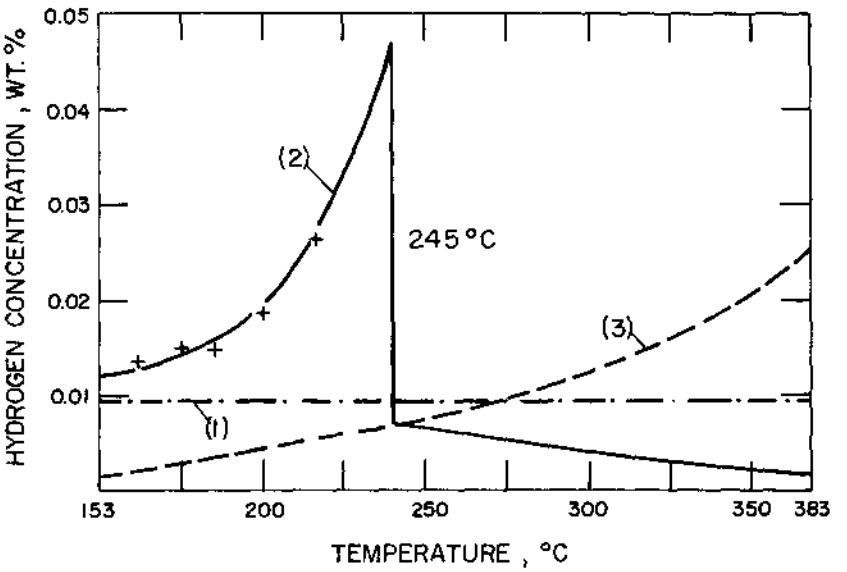

Fig. III-21 Hydrogen migration in zirconium resulting from a thermal gradient.[103] (1) Initial hydrogen concentration; (2) final hydrogen concentration; (3) limiting solubility of hydrogen in α-zirconium.

Research is continuing at General Electric[104] to develop a zirconium-base alloy having nuclear properties better than those of Zircaloy-2. Extensive tests are being carried out on Zr-2Cr-0.15Fe, which has shown excellent corrosion resistance to pure water at 300°C. Burst- and tensile-test results at room temperature indicate that the alloy is stronger but less ductile than Zircaloy-2. However, the stress-rupture performance of the alloy at 400 to 600°C is poorer than that of Zircaloy-2. The small grain size (ASTM 10 compared with ASTM 7 for Zircaloy-2) of the Zr-Cr-Fe alloy may reflect its performance relative to Zircaloy-2.

Zirconium-alloy development is also being conducted by the Indians.[105] Additions of chromium to zirconium have resulted in strengthening, while niobium additions improved work hardening. The highest strength was obtained by adding both niobium and chromium to zirconium. The strength increase was not evident in the annealed material but was obtained by quenching and tempering as shown in Table III-6. The strength increase was attributed to the martensite which formed on quenching. Annealing temperatures higher than 500°C resulted in precipitation of $ZrCr_2$ and destruction of the martensite.

Creep tests have also been performed on Zr-0.5Nb-1.0Cr in air[106] at 300 to 470°C with stresses of 30,000 to 75,000 psi. It was found that in this temperature range, the alloy exhibited creep properties superior to those of Zircaloy-2 and comparable to those of Zr-2.5Nb. The effects of oxygen content and quenching temperature on the amount of prior alpha in Zr-2.5Nb have been determined.[57b] The percentage of prior alpha phase was observed to increase with both decreasing quenching temperature and increasing oxygen content.

Table III-6 EFFECT OF HEAT TREATMENT ON THE ROOM-TEMPERATURE TENSILE PROPERTIES OF THE ZIRCONIUM ALLOYS[105]

Alloy composition (balance zirconium), wt.%	Heat treatment	Yield strength, 1000 psi		Ultimate tensile strength, 1000 psi
		0.1% offset	0.2% offset	
3.5Nb	Annealed at 850°C for 1 hr and furnace cooled	40.2	42.1	60.5
1.0Cr	Ditto	37.4	40.2	60.5
1.0Cr-0.5Nb	"	37.4	42.3	59.0
Zirconium (sponge)	"	--	32.4	43.1
0.5Nb	β-quenched from 900°C	45.0	50.9	71.9
1.0Cr	Ditto	68.0	74.3	104
0.5Nb-1.0Cr	"	64.2	75.3	146
0.5Nb-1.0Cr	β-quenched from 900°C and tempered at 300°C for 24 hr	56.7	66.7	130
	Tempered at 400°C	84.4	97.8	138
	Tempered at 500°C	70.0	86.8	144
	Tempered at 600°C	60.6	72.1	106
	Tempered at 700°C	49.1	52.7	73.7

Transformation characteristics of Zr-Cu alloys upon quenching from the beta phase have been studied by the French.[107] Figure III-22 illustrates the TTT curve for Zr-2.4Cu quenched from 960°C. Fast quenching rates result in martensitic transformation of an omega phase which has a hexagonal structure, whereas intermediate quenching rates result in omega-phase zirconium, alpha-phase zirconium supersaturated with copper and possibly Zr_2Cu. Slow cooling rates result in alpha zirconium and particles of Zr_2Cu. Decomposition of the omega phase occurs at 418 to 455°C.

In a Zr-3 vol.% Y_2O_3 dispersion, chemical reactions were found to increase with increasing sintering times and temperatures.[108] The reaction was not predicted thermodynamically for the Zr-Y-O system. The yttria particles tended to minimize grain growth and inhibit recovery and recrystallization of worked material. Additions of greater than 2 vol.% Y_2O_3 resulted in significant improvements in rupture times and reductions in minimum creep rate[109] as shown in Fig. III-23. The dispersed particles are believed to affect the rupture properties by restricting the shear and migration of grain boundaries.

Stainless Steels and Nickel-Base Alloys

An evaluation of Hastelloy X as a nuclear cladding has been summarized by researchers at Aerojet-General.[9] Their main conclusion was that the microstructure of Hastelloy X was not stable if annealed for long times at temperatures above 1300°F

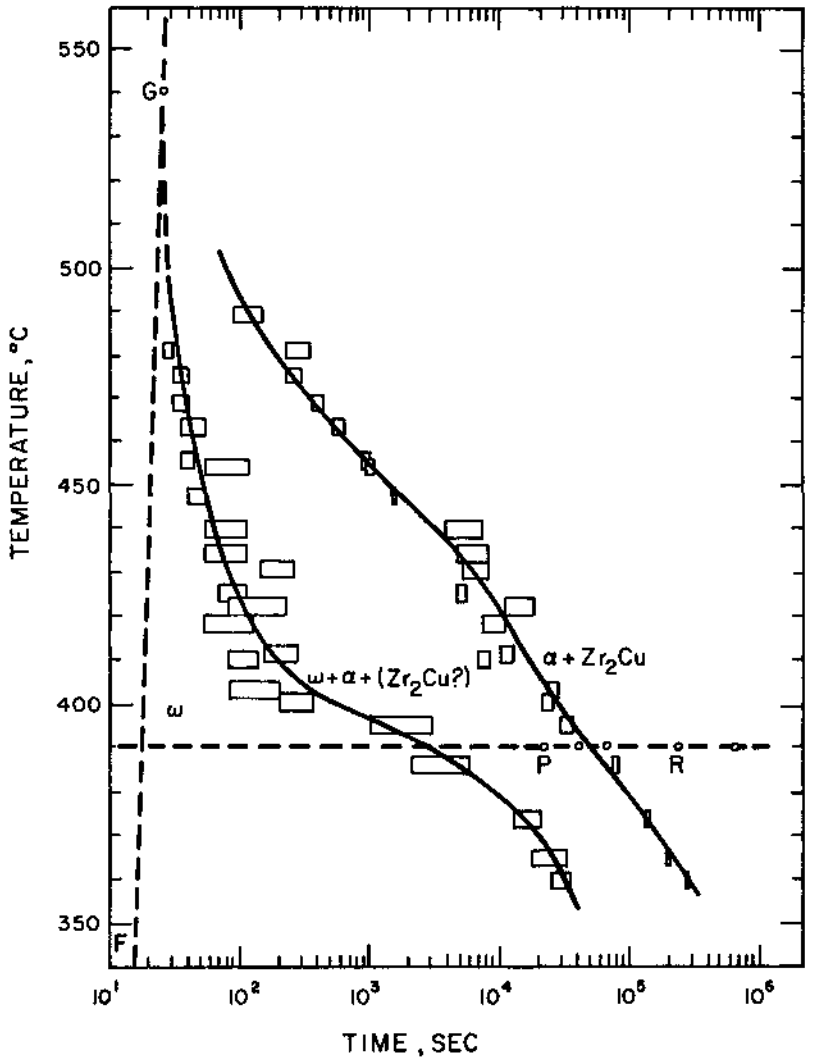

Fig. III-22 Transformation curves for Zr-2.4Cu quenched from 960°C.[107]

(705 °C). A uniform carbide precipitate, with a composition varying from M_4C to $M_{12}C$, resulted from long thermal treatments at 1300 to 1600 °F (705 to 870 °C). At annealing temperatures above 1600 °F, these particles had a tendency to coalesce and reorient at the grain boundaries. The presence of sigma phase was detected in specimens at 1300 to 1450 °F (705 to 790 °C) and mu phase (Ni_7Mo_6) was found in specimens annealed at 1600 to 1750 °F (870 to 955 °C). The long heat treatments resulted in decreased strength and ductility at most of the testing temperatures.

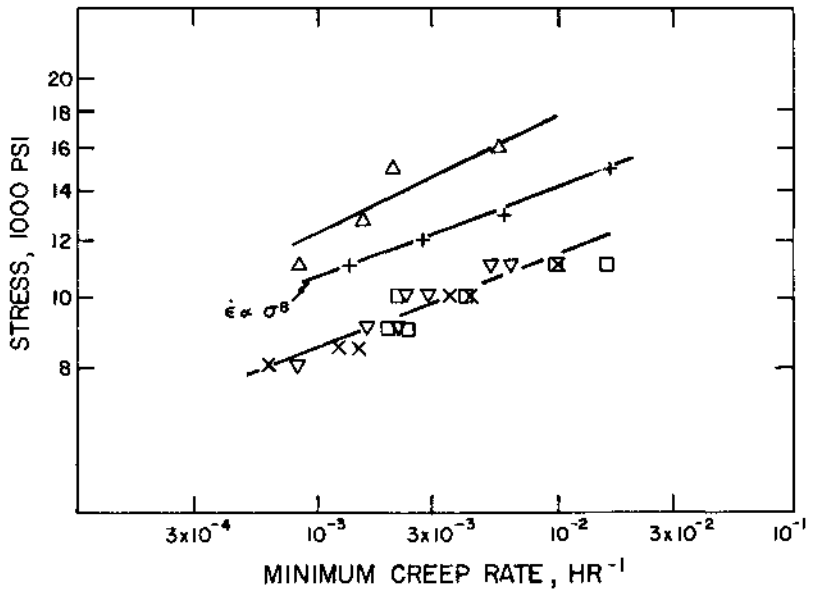

Fig. III-23 Minimum creep rates for sintered Zr-Y_2O_3 dispersions.[109] Y_2O_3 additions: △, 5 vol.%; +, 3 vol.%; □, 2 vol.%; ×, 1 vol.%; ▽, 0 vol.%.

Improvement of the creep strength of Hastelloy N for pressure-vessel application in the Molten Salt Reactor Experiment (MSRE) by modifying the composition is still being investigated.[10b] It was previously observed that an addition of 0.5 wt.% titanium improved the creep strength at 650 °C. Figure III-24 illustrates the improvement of stress-rupture properties of titanium-modified Hastelloy N at 650 °C with increasing carbon content. High-temperature annealing of Hastelloy N results in the precipitation of M_6C phases as Ni_3Mo_3C in the matrix and Ni_2Mo_4C at the grain boundaries. Increase of silicon content in the alloy caused large increases in the silicon content of the carbide precipitates.

Pressure-Vessel Steels

Long-time stress-rupture tests were conducted on 10 different steels in both the quenched-and-tempered and the normalized condition.[110] It was found that the rupture life was longest for quenched-and-tempered specimens at lower testing temperatures, while normalized steels exhibited longer rupture lives at higher testing temperatures.

Welding was found to reduce the strength of AS17E, AS17F, AS17A, and A542, while the strength of the other steels was unaffected by welding. It was not possible to correlate the response of notched specimens to composition, microstructure, or smooth-bar properties

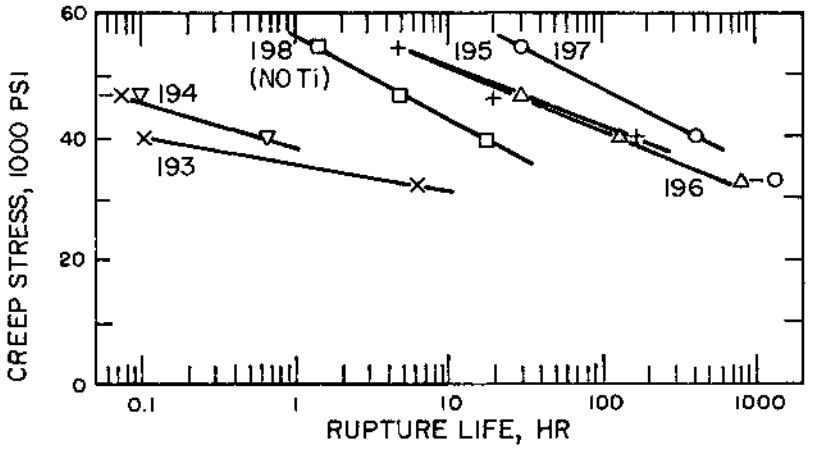

Fig. III-24 Effect of carbon on the rupture life of modified Hastelloy N at 650°C.[10b]

Heat	Carbon content, %
× 193	0.003
▽ 194	0.007
+ 195	0.037
△ 196	0.05
○ 197	0.27
□ 198	0.04 (without titanium)

Long-time (up to 20,000 hr) creep-rupture properties of 12 wt.% Cr-Mo-V-Nb steel at 500 and 550°C were found to depend on the initial tempering temperature and carbon and boron contents.[111] The properties were changed by dissolution of precipitates (fine M_2X) and their subsequent agglomeration as $M_{23}C_6$ during the long time at temperature. It was observed that a high tempering temperature (700°C or above), a low carbon content (<0.10 wt.%), and a high boron content (0.006 wt.%) resulted in improved creep properties.

(M. Kangilaski)

7. Diffusion

The Diffusion Information Center in Cleveland, Ohio, has been publishing Diffusion Data,[112] a periodical that gives a continuous compilation of references on diffusion since 1967. The compilations include references on diffusion in solid and liquid metal and alloy systems, diffusion in intermetallic compounds, ceramics, glasses, and miscellaneous systems, and permeation of gases into and through solids and liquids. A compilation of all diffusion data published prior to 1967 is planned for publication as a special volume.

A number of bibliographies have appeared in the literature which will further assist those involved in investigations of diffusion behavior. A selected bibliography of ionic self-diffusion in simple oxides has been compiled by P. J. Harrop.[113] Activation energies, frequency factors, and temperature ranges are tabulated for specific elements diffusing into the oxide. A similar bibliography by Askill[114] also contains a number of systems and references, specifically impurity diffusion in oxides. Along with Harrop's and Cumming's earlier bibliography,[115] these listings offer a fairly complete reference of currently available data on the diffusion in oxides. In addition, the National Bureau of Standards[116] has tabulated diffusion constants for various systems. Frequency factors and activation energies are given for the diffusion in the borides, carbides, and oxides of Be, Hf, Mo, Nb, Ta, Th, Ti, and Zr and for diffusion of carbon, nitrogen, and oxygen in these metals and some of their compounds. A similar list of data is being compiled for uranium compounds.

Kelly[117] has developed a correction for Fick's second law of diffusion which was considered unsatisfactory since it permits some of the diffusing particles to travel at speeds relatively faster than the free-space speed of light. An analysis was based on the covariant form of the Boltzmann equation which produced a more satisfactory relativistic diffusion equation to describe the required casual behavior.

The concept of an effective binary diffusion coefficient (EBDC) was evaluated[118] to describe diffusion of a species in systems containing three or more components, two of which are independently variable. The use and limitations of the EBDC were considered in the cases of steady-state diffusion, the unsteady state with infinite and semi-infinite couples, and a unidirectional unsteady state with finite diffusion lengths.

Correlation of the activation energy of self-diffusion in metals with the atomic-bond parameter and the activation volume for self-diffusion have been evaluated.[119] It was suggested that differences in activation-energy values for solute diffusion and self-diffusion can be attributed to the differences in cohesive-bond parameters if a depletion or contribution of valence electrons by solutes occurs and changes the Fermi energy of the solvent. In the case of diffusion of nontransition elements in noble metals, an increase in the Fermi energy of the solvent reduces the binding energy which thereby decreases the activation energy for diffusion. The converse is postulated for transition-element diffusion in noble metals. However, this model does not appear to give good correlation when compared with existing diffusion data for self-diffusion and tracer diffusion of transition elements in noble metals.

Anomalous values for the activation energy and frequency factor for surface self-diffusion were analyzed[120] and a theory was developed to explain these discrepancies. Two mechanisms for surface diffusion in face-centered cubic metals were indicated using a terrace-ledge-kink model. At high temperatures, the resulting diffusion constants agreed well with the adatom mechanism in that diffusion occurs over terraces in the surface. At low temperatures, diffusion is associated with the migration of surface vacancies. The high- and low-temperature diffusion constants in these metals were related to the absolute melting point: for $T/T_m > 0.75$, $Q_s = 30\ T_m$ kcal/mole and $D_o = 740\ cm^2/sec$; for $T/T_m < 0.75$, $Q_s = 13\ T_m$ kcal/mole and $D_o = 0.014\ cm^2/sec$. Q_s is the activation energy for surface diffusion and D_o is the frequency factor. Only one mechanism was observed operating for surface diffusion in body-centered cubic metals which is characterized by the diffusion constants $Q_s = 19\ T_m$ and $D_o = 3.6\ cm^2/sec$, at least for

diffusion at low temperatures. These constants suggest that a surface-vacancy mechanism is at work in these metals. The identification of impurity effects by correlating values of the surface diffusion coefficient with relative temperatures of diffusion were discussed, along with mechanisms by which diffusion is either enhanced or suppressed by these impurities.

Diffusion in zirconium, its alloys, and its oxides has been the subject of several investigations. Oxygen diffusion in zirconium, making use of the $^{16}O(d,p)^{17}O$ nuclear reaction, was described by French investigators.[121] Energy spectra of protons obtained experimentally were compared with spectra calculated on a theoretical basis. The oxygen-concentration profile in zirconium and in a Zr-Cu alloy after an oxidizing treatment at 750°C was measured. The results showed that the relation of microhardness to oxygen content is not linear and that the diffusion coefficient of oxygen in zirconium is dependent on concentration. A Cu-Mo-Zr alloy was subjected[122] to diffusion annealing in close contact with magnesium at 510°C for 1000 hr. Diffusion penetration of magnesium led to total embrittlement of the alloy, while the tensile strength and the yield point were decreased by 25 and 11%, respectively.

A study of the electromigration of oxygen, carbon, and nitrogen in zirconium is being conducted by Ames Laboratory.[42] The movement of the interface between sections of a rod with high and low oxygen and carbon contents was traced at different temperatures, and the migration velocities of the solutes were determined. Oxygen was added to the zirconium as ZrO_2 and the concentration profile was determined by vacuum-fusion analysis. The migration velocity of oxygen in zirconium was found to be 1.0, 1.1, and 2.7 mm/hr at 1625, 1700, and 1800°C, respectively. The migration of carbon was traced by doping the zirconium rod with ^{14}C and determining the beta activity with a low-beta radiation counter. At 1800°C a migration velocity of 0.25 mm/hr was found for carbon. Additional experiments are being conducted to measure the movement of carbon at 1625 and 1700°C.

Oxygen-ion diffusion in ZrO_{2-x} was determined[123] by measurements of the oxide growth rate on zirconium samples exposed to oxygen at 700, 750, 800, and 850°C up to 250 hr. It was assumed that the diffusion coefficient for oxygen in alpha zirconium was $5.4 \exp(-50,800/RT)$ cm^2/sec as previously observed by Kearns and Chirigos.[124] The oxygen concentration at the surface of zirconium oxide was also assumed to correspond to that in ZrO_2. The oxygen concentration initially was 9.3×10^{-4} g/cm^3 in zirconium. A least-squares analysis of the data, including independent measurements at 600°C by Hussey and Smeltzer[125] resulted in the Arrhenius-type equation $D = 2.88 \times 10^{-4} \exp(-28,400/RT)$ cm^2/sec for the temperature range 600 to 850°C.

Self-diffusion in zirconium and hafnium and diffusion of ^{95}Nb in alpha zirconium were investigated by Argentine researchers.[126] They also determined new data for self-diffusion in titanium. The temperature dependence of diffusion of the various isotopes in alpha zirconium is shown in Fig. III-25, and similar results for self-diffusion in alpha hafnium are given in Fig. III-26. Diffusion constants determined for ^{44}Ti in 99.99 wt.% titanium between 700 and 850°C were established as 8.6×10^{-6} cm^2/sec for the frequency factor and 35,900 cal/mole for the activation energy. Previous experiments and explanations concerned with the anomalous diffusion behavior in these metals were reviewed, and it was suggested that the same mechanism producing anomalous behavior in the beta phases (body-centered cubic) of these metals also operates in alpha

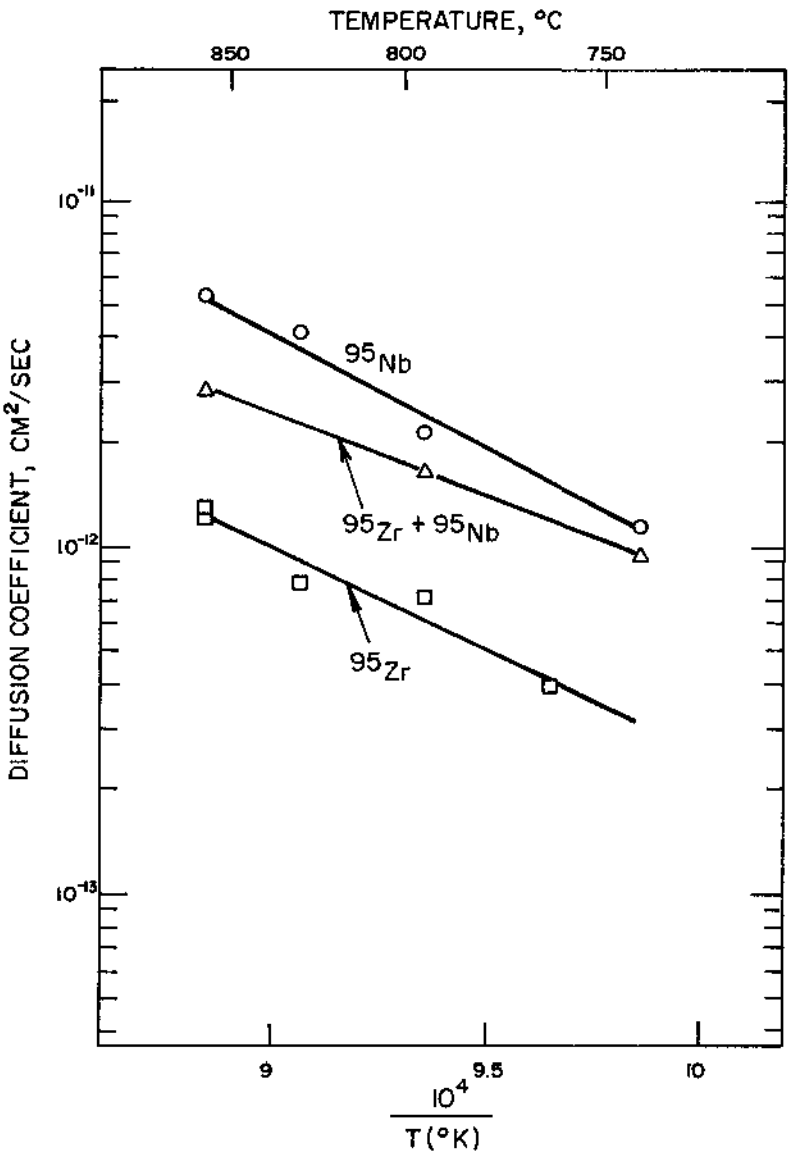

Fig. III-25 Temperature dependence of diffusion of ^{95}Zr, $^{95}Zr + ^{95}Nb$, and ^{95}Nb in hcp zirconium.[124]

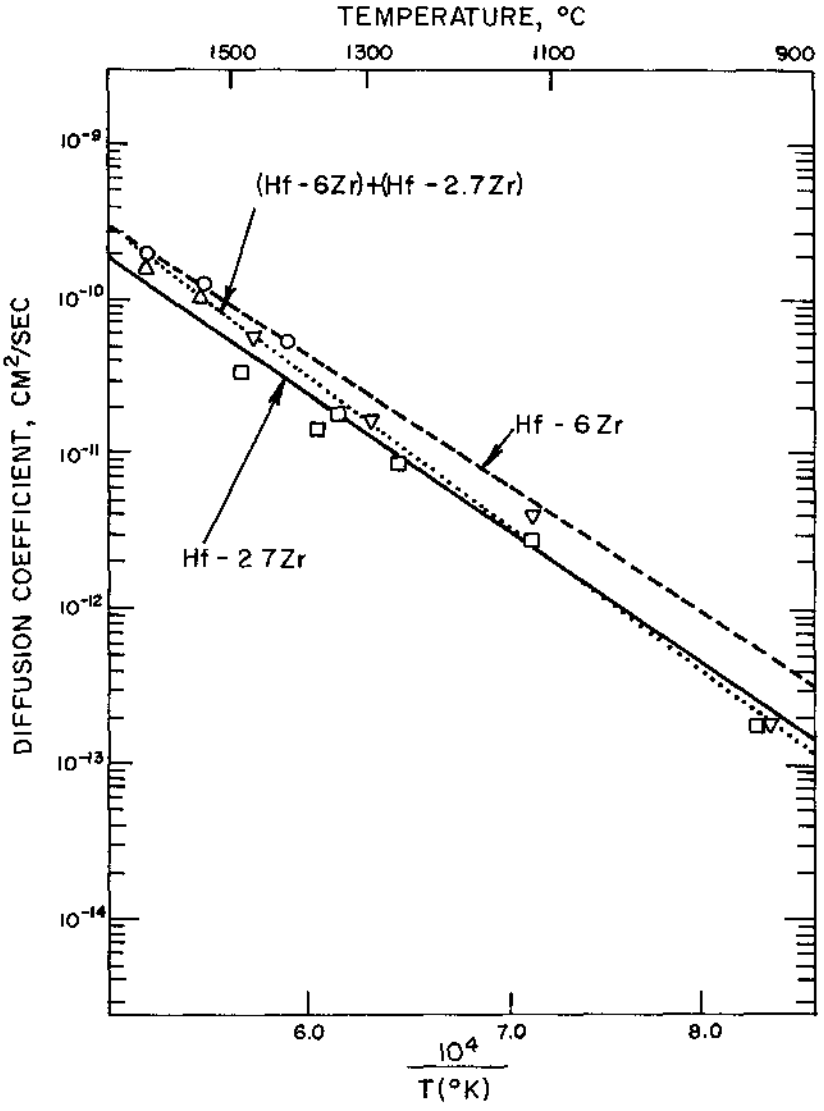

Fig. III-26 Temperature dependence of diffusion of $^{175}Hf + {}^{181}Hf$ in hcp hafnium.[124]

phases (hexagonal close packed). This mechanism occurs either by itself or in combination with a second mechanism operating in the higher temperature region.

A number of diffusion studies conducted by Ames Laboratory during the past year were summarized.[42] The diffusion of carbon, oxygen, and nitrogen in beta thorium was determined[42b] between 1440 and 1715°C. The results were given by the following temperature-dependent equations:

$$D_{C \text{ in } \beta\text{-Th}} = 2.2 \times 10^{-2} \exp(-27,000/RT) \text{ cm}^2/\text{sec}$$

$$D_{N \text{ in } \beta\text{-Th}} = 3.2 \times 10^{-3} \exp(-17,000/RT) \text{ cm}^2/\text{sec}$$

$$D_{O \text{ in } \beta\text{-Th}} = 1.3 \times 10^{-3} \exp(-11,000/RT) \text{ cm}^2/\text{sec}.$$

The mobility and diffusion coefficients for carbon, nitrogen, and oxygen in lutecium at 1330, 1450, and 1700°C were also measured[42c] by chemical analyses (for nitrogen and oxygen) and by ^{14}C tracer techniques (for carbon). The interstitials moved in the direction of electron flow when a d-c current was applied to the lutecium rod. Diffusion of oxygen in rare-earth oxides was studied[42d] by a thermobalance technique by which the rates of weight gains of substoichiometric oxides were determined. Results of cation diffusion in the rare earth oxides are also determined.[42e] Radioactive-trace techniques established that ^{91}Y diffuses into Y_2O_3 according to relation $D = 1.65 \times 10^{-2} \exp(-69,200/RT)$ cm^2/sec, while for ^{169}Er in Er_2O_3, the relation was found to be $D = 1.48 \exp(-102,200/RT)$ cm^2/sec.

A bibliography on the permeation and diffusion of nitrogen, oxygen, and rare gases through stainless steel has been prepared by Los Alamos.[127] Some 24 pertinent abstracts were found in a search of Chemical Abstracts, Nuclear Science Abstracts, and the Review of Metal Literature from 1947 to date.

Uranium diffusion in ThO_2 and in a ThO_2-UO_2 solid solution was investigated by ^{237}U tracer techniques.[128] Diffusion of ^{237}U in ThO_2 was determined between 1800 and 2000°C, and diffusion of ^{237}U in a ThO_2 - UO_2 solid solution was examined at temperatures of 1800 to 2300°C. Penetration data were obtained by serial sectioning and measuring residual activity of the gamma spectrum of ^{237}U by X-ray spectrometry. Lattice-diffusion contributions near the surface were separated from the grain-boundary-diffusion effects by extrapolating the linear slope of the grain boundary penetration-activity curve from the regions unaffected by lattice diffusion to regions near the surface. Lattice-diffusion coefficients derived by this technique were expressed by the following equations:

$$D_{U \text{ in } ThO_2} = 1.10 \times 10^{-4} \exp(-76,400/RT) \text{ cm}^2/\text{sec}$$

$$D_{U \text{ in } ThO_2 - UO_2} = 7.59 \times 10^{-4} \exp(-85,900/RT) \text{ cm}^2/\text{sec}.$$

Grain-boundary-diffusion coefficients were obtained using the equation of LeClaire[129] and resulted in the following expressions:

$$D' \times 2a_{U \text{ in } ThO_2} = 2.35 \times 10^{-9} \exp(-47,900/RT) \text{ cm}^3/\text{sec}$$

and

$$D' \times 2a_{U \text{ in } ThO_2 - UO_2} = 1.04 \times 10^{-7} \exp(-64,200/RT) \text{ cm}^3/\text{sec}$$

where D' is the coefficient associated with grain-boundary diffusion and 2a is the grain-boundary width.

Lattice and grain-boundary diffusion at 600 and 1300°C have also been studied[130] with ^{59}Fe in stainless steels having grain sizes of about 50 μ or ranging from 2000 to 4000 μ. Lattice diffusion predominated in the coarse-grained material, especially above 900°C where grain-boundary diffusion effects were nil. Lattice diffusion above 900°C was expressed by the equation $D = 1.74 \exp(-67,900/RT)$ cm^2/sec. Below 900°C, evidence existed that dislocation pipes contributed short-circuit paths for diffusion. In the fine-grained material, grain-boundary diffusion predominated between 600 and 900°C and was described by the relation $D' \times 2a = 8.3 \times 10^{-7} \exp(-43,000/RT)$ cm^3/sec.

(A. N. Ashurst)

8. Concrete

A study of the time-dependent strains in stressed and unstressed concrete heated at temperatures up to 290°F (140°C) was conducted by the U. S. Bureau of Reclamation.[131] Concrete prepared using Type V cement and amphibole schist aggregate (1-1/2-in. max) was molded into cylinders 6 in. in diameter by 16 in. long which were fog-room cured for 1 month, then cured in air (50% relative humidity) at 73°F (23°C) for an additional month before testing. These specimens were loaded in uniaxial compresssion to 800 psi at room temperature and heated to 130, 180, 230, and 290°F (55, 80, 110, and 145°C); strains were then measured as a function of time up to 180 days. Similar strains were measured in stressed specimens (800 psi) maintained at room temperature and in unstressed specimens maintained at room temperature and 130, 180, 230, and 290°F. Results of this study are given in Fig. III-27.

The magnitude and even the sign of the deformations occurring in heated concrete were dependent on the temperature level, heating rate, external stress level, and time. The complex nature of the situation was underscored by the fact that there are as many as six factors that can contribute to the overall deformation observed, including: (1) drying shrinkage related to the loss of evaporable water, (2) reversible elastic deformations associated with normal thermal expansion of the aggregate, (3) irreversible deformations associated with thermal expansion of the hydrated-cement phase, (4) reversible elastic deformations associated with the instantaneous application of external stress, (5) time-dependent deformations associated with the presence of an external stress, and (6) time-dependent deformations associated with the change in mineralogical makeup of the hydrated-cement phase during heating.

(D. R. Lankard)

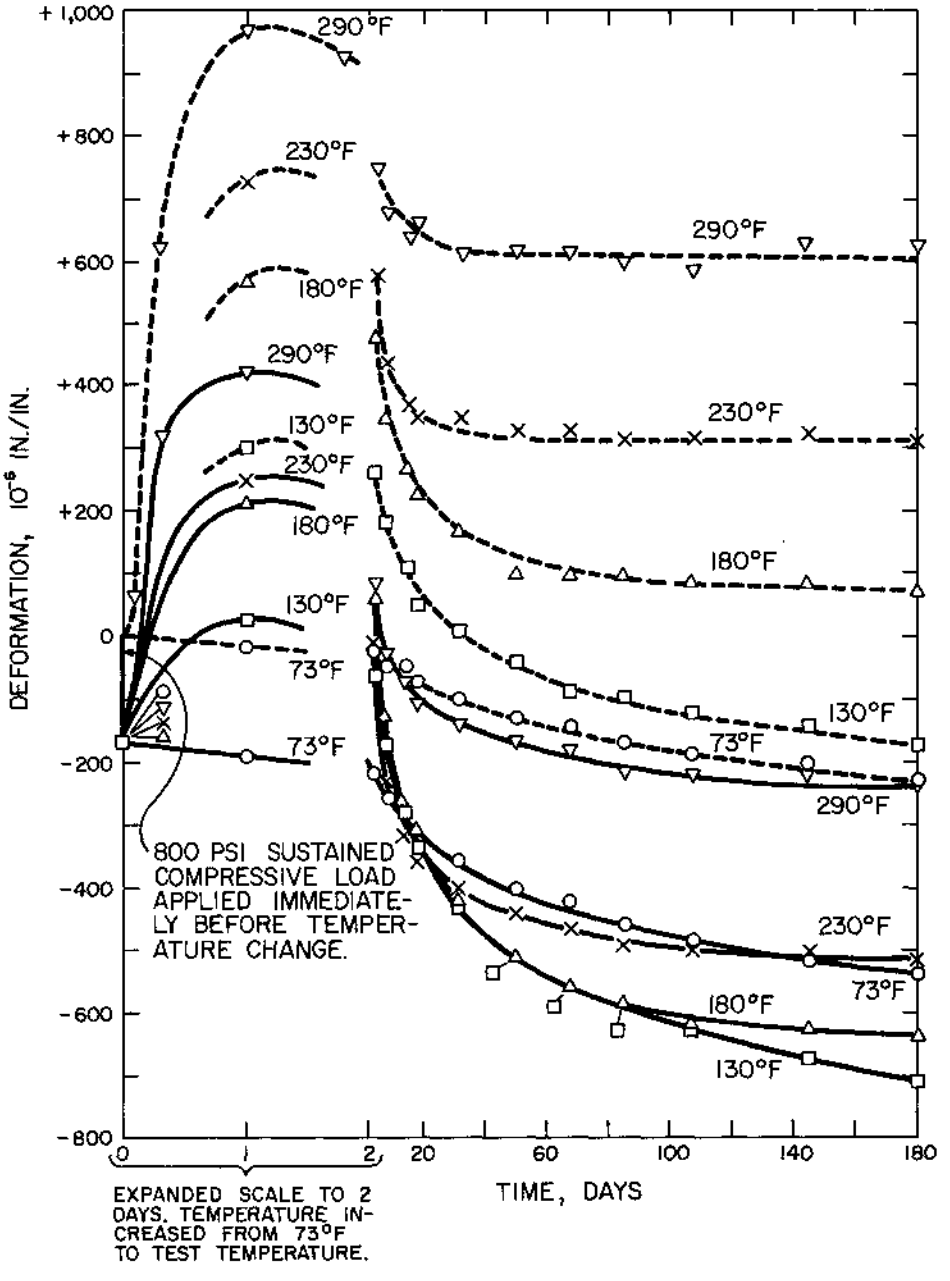

Fig. III-27 Deformations of concrete with and without sustained loads.[131] Dashed lines denote concrete not under load; solid lines denote loaded concrete.

[redacted]

9. Ceramic Technology

The mechanisms by which fibrous insulations attenuate the transfer of thermal energy were investigated by the Air Force Materials Laboratory.[132] Dynaquartz (heat-stabilized silica material), sapphire wool, and Dyanflex (alumina-silica fiber with chromia additive) were evaluated for their usefulness in the high-temperature environment. Effective thermal conductivities were measured in air, argon, and vacuum up to 2500°F (1371°C). Transmission experiments were carried out to evaluate the relative contribution of radiation-attenuation parameters for Dynaquartz.

It was found that measurement of the effective thermal conductivity of the three materials in air up to 2500°F could be carried out in a one-dimensional, guarded hot-plate apparatus with an accuracy of ±15 percent. At temperatures above 1500°F, radiation was the principal contributor to heat transfer in fibrous insulating materials. Gas conduction was the second largest contributor, but it can be effectively reduced by evacuation to moderate pressures. Solid conduction was of lesser importance in low-density fibrous insulations. The effective thermal conductivity of Dynaquartz may be predicted from estimates of the solid-conduction contribution, gas-conductivity data, and estimates of the absorption-scattering cross sections of the insulation. Measurements of the absorption and scattering cross sections can be used to guide the choice of insulation components at high temperatures where radiation is the principal heat-transfer mechanism. Because of the high contribution of radiation to effective thermal conductivity, temperature gradients in the insulation will not be linear under steady-state heat-transfer conditions.

Wirth[133] has studied the sintering kinetics in the initial, intermediate, and final stages of sintering of ultrafine calcia-stabilized zirconia. Initial stage kinetics, as determined by isothermal-shrinkage studies, indicated that grain-boundary diffusion was operative. Since the activation energy in this stage agreed closely with that for oxygen-ion diffusion, this species apparently is rate controlling. Intermediate stage kinetics, observed by isothermal-porosity determination, indicated that oxygen-ion diffusion was still the rate-controlling mechanism. Material transport was postulated still to occur by grain-boundary diffusion, on the basis of the high ratio of grain-boundary volume to bulk volume. In the final stage, as observed by isothermal grain-growth studies, rate control apparently had changed to cation diffusion, on the basis of agreement of the activation energy for sintering and that for cation bulk diffusion.

Bennett, et al.,[134] examined the application of a microwave-stimulated electrodeless gas discharge to the sintering of Al_2O_3, BeO, HfO_2, MgO, and ThO_2. The apparatus is described, together with its method of operation. For Al_2O_3 and HfO_2, improved sinterability was attained. Specimens sintered by this method were mechanically better than conventionally sintered pieces from the same raw material. This effect resulted from easier attainment of the combination of small grain size and low porosity.

Young's modulus, fracture stress, and fracture strain of commercial alumina ceramics were determined at temperatures from -200 to 1200°C from bend tests by the Germans.[135] The influence of porosity, grain size, specimen diameter, and length on these properties was investigated. Bend tests were also made on commercially obtained magnesia, zirconia, and spinel ceramics in the same temperature range. Porosity

ranged from about 4 to 20% and grain size varied from 5 to 60 μ. Efforts to describe the combined effects analytically were limited to assuming the effect grain size had on strength and treatment of the observed porosity effect. On this basis, the weakening influence of porosity was found to diminish with increasing temperature. As has been found by other investigators, no effect of grain size on Young's modulus was noted. The reduction in Young's modulus with increasing porosity was approximately independent of temperature. Refined bend tests of alumina-ceramic specimens indicated that Young's moduli in tension and compression are equal.

Diffusion mechanisms in ceramic oxides were reviewed by the Australians.[136] Methods of measurement also were discussed, and it was concluded that a simple correlation for cation self-diffusion based on structures does not exist.

Russian investigators have investigated phase relationships in the Cr_2O_3-TiO_2 and Cr_2O_3-ZrO_2 systems.[137] Two eutectics (2153°K, 50 mole % TiO_2, and 2033°K, 96 mole % TiO_2) were found in the Cr_2O_3-TiO_2 system. The phase $Cr_2Ti_2O_7$ melts congruently at 2253°K. There are two high-temperature series of solid solutions, between 80 and 94 and 96 and 100 mole % TiO_2. In the system Cr_2O_3-ZrO_2, one eutectic at 39 mole % ZrO_2, melting at 2360°K, was found in accordance with Wartenburg's data.

(H. D. Sheets)

III. CLADDING AND STRUCTURAL MATERIALS

REFERENCES

1. E. N. Aqua, R. J. Allio, and K. C. Thomas, Corrosion and Hydriding of Zircaloy Under Heat Transfer Conditions, USAEC Report WCAP-3269-56, Westinghouse Electric Corp., Atomic Power Division, August 1967.

2. E. J. Callahan and J. F. Kabat, The Effects of Silica in Autoclave Test Water on the Steam Corrosion of Zircaloy, USAEC Report KAPL-M-6748, Knolls Atomic Power Laboratory. Jan. 30. 1968.

13. R. B. Richman and C. W. Pollock, Corrosion and Wear Surveillance in the Plutonium Recycle Test Reactor Through December 1967, USAEC Report BNWL-726, Battelle-Northwest, July 1968.

14. D. A. Kubose and H. I. Cordova, Electrochemical Corrosion Studies of Galvanically Coupled SNAP-21 Materials, Report USNRDL-TR-68-26, U.S. Naval Radiological Defense Laboratory, Jan. 15, 1968.

15. J. C. Griess, Jr., Crevice Corrosion of Titanium in Aqueous Salt Solution, Corrosion, 24 (4): 96-109 (April 1968).

16. A. Cassuto and J. Mihe, Oxidation of Tungsten and Rhenium Under Low Pressure, Compt. Rend., Ser. C, 266: 863-866 (Mar. 18, 1968).

17. W. W. Smeltzer and A. E. Jenkins, Diffusional Properties of Oxygen in Niobium Pentoxide Crystals and Scales Formed on Niobium, J. Electrochem. Soc., 115: 338-343 (April 1968).

18. I. I. Korobkov, V. V. Osipov, and N. N. Zapleshko, Investigation of the Oxidation Processes of Alloys of the Niobium-Tantalum System at 550 to 1050°, Fiz. Metal. Metalloved, 25: 85-93 (January 1968).

19. J. Van Landuyt and C. M. Wayman, A Study of Oxide Plate Formation in Tantalum. I Growth Characteristics and Morphology, Acta Met., 16: 803-814 (June 1968).

20. C. M. Wayman and J. Van Landuyt, A Study of Oxide Plate Formation in Tantalum. II Crystallographic Analysis, Acta Met., 16: 812-822 (June 1968).

21. J. Stringer, The Oxidation of Tantalum at High Temperatures: Geometrical Effects, J. Less-Common Metals, 16: 55-64 (1968).

22. V. I. Khitrova, V V. Klechkovskaya, and Z. G. Pinsker, Electron-Diffraction Study of Tantalum Dioxide in Thin Films, Sov. Phys.-Cryst. (Engl. Trans.), 12· 907-912 (May-June 1968).

23. J. W. May, R. T. Szostak, and L. H. Germer, Ammonia Adsorption and Decomposition on a Tungsten (211) Surface, Report NASA-CR-95706, Cornell University, 1968.

24. C. C. Chang, LEED Studies, Adsorption of Carbon Monoxide on the Tungsten (112) Face, J. Electrochem. Soc., 115: 354-358 (April 1968).

25. R.P.H. Gasser and C. P. Lawrence, Chemisorption of Nitrous Oxide by Tungsten, Surface Sci., 10: 91-101 (April 1968).

26. A. E. Bell, L. W. Swanson, and L. C. Crouser, A Field Emission Study of Oxygen Adsorption on the (110), (211), (111), and (100) Planes of Tungsten, Surface Sci., 10:254-274 (1968).

27. H. V. Borgstedt and W. Heim, Mass Transfer Phenomena Caused by Liquid Sodium with Nickel and Molybdenum Alloys (In German), Werkst. Korros., 18: 311-316 (April 1967).

28. E. M. Simons, Corrosion by Nonaqueous Liquids and Vapors, Reactor Materials, 11 (2): 106-109 (Summer 1968).

29. J. W. Moberly, M. Barlow, M. C. Garrison, and P. J. Planting, Interaction of Liquid Sodium with 304 Stainless Steel, USAEC Report TID-24602, Stanford Research Institute, Jan. 31, 1968.

30. J. R. Weeks (Comp.), Quarterly Progress Report of Work Sponsored by the Fuels and Materials Branch, Division of Reactor Development and Technology, U.S. Atomic Energy Commission, January 1 – March 31, 1968, USAEC Report BNL-50111 (T-494), pp. 10-20, Brookhaven National Laboratory. (Official Use Only)

31. W. T. Lee, Biaxial Stress-Rupture Properties of Austenitic Stainless Steels in Static Sodium, USAEC Report AI-AEC-12694, Atomics International, June 30, 1968.

32. J. G. Conner and S. W. Porembka (Eds.), A Compendium of Properties and Characteristics for Selected LMFBR Cladding Materials, USAEC Report BMI-1900, Battelle-Columbus, May 15, 1968.

33. R. L. Eichelberger and R. L. McKisson, Solubility of Copper in Sodium, USAEC Report AI-AEC-12671, Atomics International, May 31, 1968.

34. Argonne National Laboratory, Reactor Development Program Progress Report, May 1968, USAEC Report ANL-7457, (a) p. 128, (b) pp. 143-146, (c) pp. 108-109, July 2, 1968.

35. Argonne National Laboratory, Reactor Development Program Progress Report, August 1968, USAEC Report ANL-7487, p. 101, Sept. 26, 1968.

36. Argonne National Laboratory, Reactor Development Program Progress Report, June 1968, USAEC Report ANL-7460, (a) pp. 93-96, (b) pp. 98-100, July 29, 1968.

37. J. H. Sinclair, Compatibility of Several Iron-, Cobalt-, and Nickel-Base Alloys with Refluxing Potassium at 1800°F, Report NASA-TM-X-1617 (N68-30065), National Aeronautics and Space Administration, Lewis Research Center, Mar. 11, 1968.

38. R. C. McRae, L. Reed, J. Toth, and R. Lindberg, Compatibility of Alumina and Beryllia Ceramics with Potassium Vapor, Amer. Ceram. Soc. Bull., 47: 484-487 (May 1968).

39. A. P. Fraas, H. C. Young, and A. G. Grindell, Survey of Information on Turbine Bucket Erosion, USAEC Report ORNL-TM-2088, Oak Ridge National Laboratory, July 1968.

40. R. J. Ziobro and A. E. Koestel, Mercury Boiler Development on the SNAP 2/MRPC Program, Topical Report No. 34, USAEC Report TRW-690-32, TRW Equipment Laboratories, June 3, 1968.

41. R. C. Schulze and E. J. Vargo, Corrosion Products in the SNAP 2/MRPCP CRU V Test System, Topical Report No. 35, USAEC Report TRW-690-33, TRW Equipment Laboratories, June 1968.

42. Ames Laboratory, Ceramic and Mechanical Engineering, Chemical Engineering, Chemistry, Mathematics and Computer Science, Metallurgy, Physics, and Reactor Divisions Annual Summary Research Report, July 1, 1967 – June 30, 1968, USAEC Report IS-1900, (a) pp. C&ME 13-18, (b) p. M 81, (c) p. M 82, (d) pp. C&ME 1-4, (e) pp. C&ME 7-8, July 1968.

43. R. R. Eggleston (Ed.), Piqua Nuclear Power Facility Surveillance and Recovery Program Final Report, USAEC Report AI-AEC-12696, Atomics International, June 15, 1968.

44. R. G. Hart, I. E. Oldaker, H. E. Thexton, and J. F. Walker, Uranium Dioxide Fuels in Organic-Cooled Reactors, Canadian Report AECL-2758, December 1967.

45. E. D. Falk, R. E. Forrester, W. B. Wolfe, and R J. Sullivan, Heavy Water Organic Cooled Reactor Fuel Irradiation Experiment EXP-NRU-305 Alternate 1, USAEC Report AI-CE-75, Atomics International and Combustion Engineering, June 15, 1968.

46. G. DeBeni, Method of Protecting Magnesium or Its Alloys From Corrosion in Organic Liquids, British Patent 1,113,572, May 15, 1968.

47. G. E. Metzger, Survey of Structural Materials for the Molten Salt Experimental (MOSEL) Reactor, Nucl. Eng. Design, 7: 29-39 (1968).

48. H. A. McLain, Potential Metal-Water Reactions in Light-Water-Cooled Power Reactors, USAEC Report ORNL-NSIC-23, Oak Ridge National Laboratory, August 1968.

49. H. C. Brassfield, J. F. White, L. Sjodahl, and J. T. Bittel, Recommended Property and Reaction Kinetics Data for Use in Evaluating a Light-Water-Cooled Reactor Loss-of-Coolant Incident Involving Zircaloy-4 or 304-SS-Clad UO_2, USAEC Report GEMP-482, General Electric Co., Nuclear Materials and Propulsion Operation, April 1968.

50. W. F. Sheeley, Radiation Effects Symposium held at Ashville, N.C., September, 1965, Metallurgical Society Conferences, Vol. 37, Gordon and Breach, Science Publishers, Inc., New York, 1967.

51. Brittleness and Irradiation Effects, 10th Colloqium of Metallurgy, Saclay, June 23-24, 1966, Report CONF-660656, 1967.

52. E. R. Gilbert and N. E. Harding, In-Reactor Creep of Structural Materials for Nuclear Applications, USAEC Report BNWL-SA-1458, Battelle-Northwest, 1968.

53. Conference on the Use of Zirconium Alloys in Nuclear Reactors, Marianske Lazne, Czechoslovakia, October 20-21, 1966, General Proceedings, Vol. I and II.

54. Papers presented at American Nuclear Society meeting on Fundamental Properties of Materials in Nuclear Fuel Assemblies, Schenectady, N. Y., August 22-23, 1968.

a. F. J. Azzarto, E. E. Baldwin, F. W. Wiesinger, and D. M. Lewis, Unirradiated, In-Pile, and Postirradiation Low Strain Rate Tensile Properties of Zircaloy-4.

b. G. Sainfort, J. Gregoire, P. Morgand, A. Silvent, and G. Cabane, Effects of Irradiation on the Deformation and Rupture Characteristics of Some Metals and Alloys With a Face-Centered Cubic Structure.

55. P. H. Kreyns and M. W. Burkart, Radiation-Enhanced Relaxation in Zircaloy-4 and in a Zirconium + 2.5 Wt.% Niobium + 0.5 Wt.% Copper Alloy, USAEC Report WAPD-TM-746, Westinghouse Electric Corp., Bettis Atomic Power Laboratory, May 1968.

56. S. Ray and B. D. Sharma, Radiation Damage Studies on Zr-0.5 Percent Nb-1 Percent Cr Alloy, Indian Report BARC-300, 1967.

57. Atomic Energy of Canada Limited, Fuels and Materials Division Progress Report, January 1 – March 31, 1968, Canadian Report PR-FM-4, (a) pp. 97-99, (b) p. 75, 1968.

58. J. J. Holmes, R. E. Robbins, and A. J. Lovell, Postirradiation Tensile Behavior of 300 Series Stainless Steels, USAEC Report BNWL-SA-1455, Battelle-Northwest, June 1968.

59. D. L. Keller, Progress Relating to Civilian Applications During July 1967 – June 1968, USAEC Report BMI-1845, Battelle-Columbus, July 1, 1968.

60. Papers presented at the 71st Annual Meeting of ASTM, San Francisco, California, June 23-28, 1968.

a. M. Kangilaski, J. S. Perrin, and R. A. Wullaert, Irradiation Induced Embrittlement in Stainless Steel at Elevated Temperature.

b. M. Weisz, J. Malkin, J. Erler, and J. P. Andre, Contribution to the Studies Concerning the High Temperature Embrittlement of AISI 316 Austenitic Stainless Steels After Irradiation.

c. H. Böhm and H. Hauck, Investigation of Radiation Induced High Temperature Embrittlement of Ferritic Steels in the Temperature Range of the $\alpha \longrightarrow \gamma$ Transformation.

61. F. N. Rhines and P. J. Wray, Investigation of the Intermediate Temperature Ductility Minimum in Metals, Trans. Amer. Soc. Metals, 54: 117-128 (1961).

62. W. R. Martin and J. R. Weir, Jr., Irradiation Embrittlement of Low- and High-Carbon Stainless Steels at 700, 800, and 900°C, USAEC Report ORNL-TM-1516, Oak Ridge National Laboratory, June 1966.

64. H. Böhm, H. Hauck, and G. Hess, Investigation of the High-Temperature Embrittlement After Neutron Irradiation of 16/13-CrNi-Steels, J. Nucl. Mater., 24(2): 198-209 (November 1967).

65. W. R. Martin and J. R. Weir, Jr., Influence of Grain Size on the Irradiation Embrittlement of Stainless Steel at Elevated Temperatures, USAEC Report ORNL-TM-1043, Oak Ridge National Laboratory, March 1965.

66. D. L. Keller, Progress Relating to Civilian Applications During July – September, 1968, USAEC Report BMI-1851, Battelle-Columbus, Oct. 1, 1968.

67. J. R. Weeks (Comp.), Quarterly Progress Report on Work Sponsored by the Fuels and Materials Branch, Division of Reactor Development and Technology, U. S. Atomic Energy Commission, April 1 – June 30, 1968, USAEC Report BNL-50123 (T-501), pp. 31-33, Brookhaven National Laboratory, 1968. (Official Use Only)

68. D. Kramer, K. R. Garr, C. G. Rhodes, and A. G. Pard, Helium Embrittlement of Type 316 Stainless Steel, USAEC Report AI-AEC-12670, Atomics International, Apr. 30, 1968.

69. P. Patriarca (Comp.), Fuels and Materials Development Program Quarterly Progress Report for Period Ending March 31, 1968, USAEC Report ORNL-TM-2217, pp. 56-62, Oak Ridge National Laboratory, June 1968. (Official Use Only)

70. J. G. Y. Chow, Effect of Irradiation on Mechanical Properties of Cobalt Base Alloys, USAEC Report BNL-12438, Brookhaven National Laboratory, 1968.

71. J. R. Hawthorne, U. Potapovs, and C. Z. Serpan, Jr., Irradiation Effects on Reactor Structural Materials, Quarterly Progress Report, November 1967 – January 31, 1968, USAEC Report NRL-Memo-1853, Naval Research Laboratory, Feb. 15, 1968.

72. L. E. Steele, G. W. Knighton, and U. Potapovs, Radiation Embrittlement of Pressure Vessels and Procedures for Limiting This Effect in Power Reactors, Nucl. Appl., 4: 230-44, Naval Research Laboratory (April 1968).

73. D. R. Ireland and E. B. Norris, Influence of Neutron Irradiation on the Properties of Steels and Welds Typical of the ERR Pressure Vessel After Two Power Years Operation, USAEC Report SWRO-1228P9-15, Southwest Research Institute, March 1968.

74. H. Susukida and T. Ando, Effects of Neutron Irradiation on the Impact Properties of Welded Joints of Ni-Cr-Mo High Strength Steel Plate for Nuclear Reactor Vessels, Mitsubishi Juko Giho, 5: 115-20 (March 1968).

75. V. K. Kritskaya, A. P. Kuznetsova, B. V. Sharov, and M. N. Sparsky, Some Peculiarities in the Behavior of the Microhardness of Neutron Bombarded Chromium on Annealing and Deformation, Fiz. Metal. Metalloved., 23(2): 96-99 (February 1967).

76. C. W. Weaver, Irradiation and the Ductility of Chromium, Scripta Met., 2: 463-466 (August 1968).

77. J. L. Brimhall, B. Hastel, and T. K. Bierlein, Thermal Stability of Radiation Produced Defects in Molybdenum, Acta Met., 16: 781-788 (June 1968).

78. J. Nihoul and L. Stals, The Recovery of Structural Defects in Refractory BCC Metals After Irradiation and After Cold Work, Belgian Report BLG-424, August 1967.

79. R. H. Chambers, T. E. Firle, T. Trozera, and G. Buzzelli, A Program of Basic Research on Mechanical Properties of Reactor Materials, USAEC Report GA-7978, General Dynamics Corp., General Atomic Division, July 28, 1967.

80. W. E. Winsche and F. T. Miles, Nuclear Engineering Department, Annual Report, USAEC Report BNL-50082, pp. 114-115, Brookhaven National Laboratory, Dec. 31, 1967.

81. T. J. Queen, Dislocation Pinning in Neutron Irradiated O.F.H.C. and 99.999% Copper, Phil. Mag., 16: 297-302 (August 1967).

82. R. E. Hummel and J. W. Koger, The Influence of Neutron Irradiation, Heat Treatment and Deformation on the Martensitic Transformations in Metastable B_1-Brass, Scripta Met., 2: 403-404 (July 1968).

83. I. Milne and R. E. Smallman, Plastic Deformation of Niobium (Columbium)-Molybdenum Alloy Single Crystals, Trans. Met. Soc. AIME, 242: 120-126 (January 1968).

84. P. L. Raffo and T. E. Mitchell, Yielding, Work Hardening, and Cleavage in Tantalum-Rhenium Alloy Single Crystals, Trans. Met. Soc. AIME, 242: 907-917 (May 1968).

85. G. D. McAdam, Influence of Carbide and Boride Additions on the Creep Strength of Niobium Alloys, J. Inst. Metals, 96: 13-16 (January 1968).

86. M. Yajima and M. Ishii, Strain Rate Dependence of the Tensile Flow Stress of a Nb-Zr Solid Solution Alloy, Nippon Kinzoku Gakkaishi, 32: 160-163 (1968).

87. H. R. Babitzke and J. G. Croeni, Study of Columbium and Tantalum Alloys, USAEC Report BM-RI-7116, Bureau of Mines, Albany Metallurgy Research Center, April 1968.

88. E. Fromm and H. Jehn, On The Phase Diagram of the Niobium-Oxygen System, J. Less-Common Metals, 15: 242-243 (June 1968).

89. Z. C. Szkopiak, Oxygen Dependence of Strain-Aging in Niobium, Acta Met., 16: 381-391 (March 1968).

90. A. Koethe, Resistivity Study of Strain-Aging in Ta-O and Nb-O, Acta Met., 16: 357-367 (March 1968).

91. H. L. Prekel, A. Lawley, and H. Conrad, Dislocation Velocity Measurements in High Purity Molybdenum, Acta Met., 16: 337-345 (March 1968).

92. R. Vandervoort, Creep Correlations for Bcc Refractory Metals, USAEC Report UCRL-70618; also Trans. Met. Soc. AIME, 242: 345-347 (February 1968).

93. C. C. Koch and G. Love, Investigation of the Vanadium-Technetium Alloy System, J. Less-Common Metals, 15: 43-58 (May 1968).

94. E. Rudy, St. Windisch, and C. E. Brukl, Revision of the Vanadium-Carbon and Niobium-Carbon Systems, Planseeber. Pulvermet., 16(1): 3-33 (April 1968).

95. E. Rudy and St. Windisch, Revision of the Titanium-Tungsten System, Trans. Met. Soc. AIME, 242: 953-954 (May 1968).

96. W. Vickers and P. Greenfield, The High Temperature Creep Properties of Compacted Magnesium Powder, J. Nucl. Mat., 27: 73-79 (July 1968).

97. J. D. Noden and G. Willoughby, The Primary Creep of Magnox AL80 from 450 C to 620 C, Metallurgia, 77: 111-115 (March 1968).

98. J. L. Jellison, A. Nugent, and R. F. Lupi, Inhomogeneous Deformation Effects in Zircaloy-4 Rolled Plate, USAEC Report KAPL-P-3406, Knolls Atomic Power Laboratory, Feb. 8, 1968.

99. O. M. Katz, Recovery and Recrystallization Kinetics of Cold-Worked Zircaloy-4 Plate and Tubing, USAEC Report WAPD-TM-590, Westinghouse Electric Corp., Bettis Atomic Power Laboratory, February 1968.

100. G. P. Marino, Hydrogen Behavior in Zirconium-Based Alloys, USAEC Report WAPD-TM-759, Westinghouse Electric Corp., Bettis Atomic Power Laboratory, June 1968.

101. R. Westerman, Charging Zircaloy-2 With Hydrogen Beyond the Solubility Limit, J. Nucl. Mat., 18: 31-38, Battelle-Northwest, January 1966.

102. J. J. Kearns, Dissolution Kinetics of Hydride Platelets in Zircaloy-4, J. Nucl. Mat., 27: 64-72 (July 1968).

103. V. S. Emel'yanov, N. V. Borkov, A. I. Evstyukhin, and A. T. Kazakevich, Experimental Study of the Effect of Temperature Gradient on the Distribution of Hydrogen in Zirconium, in High Purity Metals and Alloys, pp. 7-13, Consultants Bureau, New York, 1967.

104. R. N. Duncan, H. H. Klepfer, E. A. Pickett, R. E. Blood, and G. F. Rieger, Specific Zirconium Alloy Design Program, Quarterly Progress Report Nos. 18 and 19, USAEC Report GEAP-5603, General Electric Co., Nuclear Fuels Dept., January 1968.

105. S. Ray and M. L. Mehta, Effect of Heat Treatment on the Mechanical Properties of Zr-1 Percent Cr, Zr-0.5 Percent Nb, and Zr-0.5 Percent Nb-1 Percent Cr Alloys, Indian Report BARC-306, 1967.

106. S. Ray and M. L. Mehta, The Creep Behavior of Zr-0.5 Wt. Percent Nb-1.0 Wt. Percent Cr Alloy, Indian Report BARC-308, 1967.

107. A. Couterne, G. Cizeron, and P. Lacombe, Structural Changes During Tempering or Annealing of Zr-Cu Alloys Containing Less Than 5 Wt.% Copper, J. Nucl. Mat., 27: 121-136 (August 1968).

108. B. G. Childs, Microstructures and Dispersoid Morphology in Yttria-Zirconium Dispersion, Canadian Report AECL-2798, October 1967.

109. J. Rezek and B. G. Childs, Structure and Properties of Yttria-Zirconium Dispersions, J. Nucl. Mat., 26: 285-299 (June 1968).

110. J. P. Steiner, J. J. de Barbadillo, A. W. Pense, and R. D. Stout, The Creep Rupture Properties of Pressure Vessel Steels-Part III, Weld. J. (N.Y.), 47: 144s-154s (April 1968).

111. M. C. Murphy and G. D. Branch, Properties and Microstructures of 12%Cr-Mo-V-Nb Creep Resisting Steel, J. Iron Steel Inst., 206: 266-274 (March 1968).

112. Continuous Compilation of New Reference Data on Diffusion Processes in Inorganic Solids and Their Melts, May, 1967, to August, 1968, Diffusion Data, Vols. 1 and 2.

113. P. J. Harrop, Self-Diffusion in Simple Oxides – A Bibliography, J. Mater. Sci., 3: 206-222 (March 1968).

114. J. Askill (Comp.), A Bibliography on Tracer Diffusion in Metals: Part V – Self- and Impurity Diffusion in Simple Metal Oxides, USAEC Report ORNL-3795, Part V, Oak Ridge National Laboratory, January 1968.

115. P. A. Cumming and P. J. Harrop, Bibliographic Review of Self-Diffusion in Metal Oxides, British Report AERE-Bib-143, October 1965.

116. A. L. Dragoo, Diffusion Rates in Inorganic Nuclear Materials, J. Res. Nat. Bur. Stand., A, 72: 157-173 (March-April 1968).

117. D. Kelly, Diffusion: A Relativistic Appraisal, Report AD-662908, Yale University, 1967.

118. Case Western Reserve University, The Use and Limitations of the Concept of An Effective Binary Diffusion Coefficient for Multi-Component Diffusion, Report NASA-CR-95400 (N68-28918).

119. S. P. Ray, B. D. Sharma, and G. P. Tiwari, Correlation of Diffusion Data with an Atomic Bond Parameter, Indian Report BARC-302, 1967.

120. N. A. Gjostein, Surface Self-Diffusion in FCC and BCC Metals: A Comparison of Theory and Experiment, Report CONF-660836, Ford Motor Co., 1967.

121. G. Beranger, B. de Gelas, and P. Lacombe, Use of the Nuclear Reactor $^{16}O(d,p)^{17}O$ to Study Oxygen Diffusion in Solids and Its Application to Zirconium, J. Appl. Phys., 39: 2246-2255 (April 1968).

122. K. Splichal and V. Kraus, Diffusion Annealing of Zirconium With Its Alloys (in Czechoslovakian), Report CONF-661059, Institute of Nuclear Research, Czechoslovak Academy of Sciences, October 1966.

123. C. J. Rosa and W. C. Hagel, Oxygen-Ion Diffusivity in Hypostoichiometric Zirconium Dioxide, J. Nucl. Mater., 27: 12-20 (1968).

124. J. J. Kearns and J. N. Chirigos, The Use of Microhardness in the Determination of the Diffusitivity of Oxygen in Alpha Zirconium, USAEC Report WAPD-TM-306, Westinghouse Electric Corp., Bettis Atomic Power Laboratory, February 1962.

125. R. J. Hussey and W. W. Smeltzer, The Mechanism of Oxidation of Zirconium in the Temperature Range 400°-800°C, J. Electrochem. Soc., III: 1221-1224 (1964).

126. F. Dymert and C. M. Libanati, Self-Diffusion of Ti, Zr, and Hf in Their HCP Phases and Diffusion of Nb^{95} in HCP Zr, J. Mater. Sci., 3: 349-359 (1968).

127. J. Furnish (Comp.), Permeation and Diffusion of Nitrogen, Oxygen, and Rare Gases Through Stainless Steel: A Bibliography, USAEC Report LA-3909-MS, Los Alamos Scientific Laboratory, January 1968.

128. H. Furuya, Lattice and Grain-Boundary Diffusion of Uranium in ThO_2 and ThO_2-UO_2 Solid Solution, J. Nucl. Mater., 26: 126-128 (1968).

129. A. D. LeClaire, The Analysis of Grain Boundary Diffusion Measurements, Brit. J. Appl. Phys., 14: 351-356 (1963).

130. A. F. Smith and G. B. Gibbs, Volume and Grain-Boundary Diffusion of Iron in 20 Cr/25 Ni/Nb Stainless Steel, Metal Sci. J., 2: 47-50 (March 1968).

131. K. B. Hickey, Creep, Strength, and Elasticity of Concrete at Elevated Temperatures, Report C-1257, U.S. Dept. of the Interior, Bureau of Reclamation, Concrete and Structural Branch, Division of Research, December 1967.

132. E. J. Rolinski and G. V. Purcell, Investigation of Radiation and Conduction Heat Transfer in Fibrous High Temperature Insulations, Report AFML-TR-67-251, Air Force Materials Laboratory, December 1967.

133. D. G. Wirth, Jr., Sintering Kinetics of Ultra-Fine Calcia Stabilized Zirconia, Thesis, University of Illinois, 1967.

134. C.E.G. Bennett, N. A. McKinuon, and L. S. Williams, Sintering In Gas Discharge, Nature, 217: 1287-1288 (Mar. 30, 1968).

135. H. Neuber and A. Wimmer, Experimental Investigations of the Behavior of Brittle Materials at Various Ranges of Temperature, Report AFML-TR-68-23, Institute Mechanik, March 1968.

136. H. J. de Briun, D. H. Bradhurst and D. G. Walker, Atomic Diffusion in Ceramic Oxides, Australian Report AAEC/E-188, December 1967.

137. A. S. Berezhnoi and N. V. Gul'ko, Phase Diagrams of the Cr_2O_3-TiO_2 and Cr_2O_3-ZrO_2, Dopov. Akad. Nauk. Ukr. RSR, Ser. B, No. 3: 250-253 (March 1968).

IV. SPECIAL FABRICATION TECHNIQUES

1. Cast and Wrought Materials

Melting and Casting Processes

The French[1] have patented an apparatus for the electron-beam melting and continuous casting of refractory materials such as UC. The apparatus consists of an electron gun mounted axially above the crucible, a device for supplying the material to be melted, rotating members for continuously replacing the crucible side wall, and a means for rotating the complete crucible assembly to achieve better particle distribution at the surface of the melt.

Longitudinal and transverse sections of electron-beam melted and continuous-cast UC rods have been studied by microscopic methods.[2] A critical casting rate was identified which was due to the competition between crystals growing on nuclei on the rod surface and crystals formed in the liquid by homogeneous nucleation. It was noted that in crystals without any privileged growing direction, the crystal size obtained had a minimum for a given casting rate. This minimum was explained by the combination of two competing phenomena: the nucleation rate and the disappearance of the smaller nuclei into the larger ones.

Oak Ridge investigators[3] found that contamination during electron-beam melting may be in part due to material volatilized from the chamber walls by the radiant energy of the beam. Thorough cleaning of the furnace chamber walls between melts improved the purity of electron-beam-melted niobium. Previous contamination from the chamber walls exceeded that from the emitter.

Combustion Engineering[4] has produced a high-purity V-15Cr-5Ti* alloy ingot weighing over 100 lb. The process steps included aluminothermic reduction of V_2O_5 to provide higher purity vanadium than is commercially available. The resulting vanadium derbies were double electron-beam melted to reduce the amounts of impurities, particularly interstitial elements. The ingot was then machined into chips which were compacted with high-purity chromium and titanium to form an electrode. Double arc melting of the electrode, first in argon and then in vacuum, resulted in a vanadium-alloy ingot with a total interstitial content of less than 400 ppm.

The Russians[5] have used a 60-kw electron-beam melting unit for the industrial production of ingots of Ti, Nb, Mo, Zr, Ta, and their alloys that are up to 70 mm in diameter and 300 mm long. Electron-beam vacuum remelting increased the ductility and elongation and decreased the hardness of tantalum and niobium. For example, the hardness of niobium decreased from 85 to 65 kg/mm^2 after double remelting and to 52 kg/mm^2 after triple and quadruple remelting. The formation of very hard and brittle MoC and Mo_2C occurs in the reaction of molybdenum with oil vapor; therefore, production of ductile molybdenum requires the development of melting units with vacuum or diffusion pumps which use no oil or are equipped with special traps.

*Unless otherwise designated, all compositions are understood to be by wt.%.

Crucibles for containing molten nickel and beryllium were developed and tested by Dow.[6] Dense, fine-grained crucibles made by hot pressing a variety of refractory compounds were tested for resistance to vacuum outgassing, thermal shock, and corrosion by molten beryllium and molten nickel. Heating rates up to 900°C/min were achieved by electron-bombardment heating in vacuum of 3×10^{-5} torr. Titanium diboride was found to be a good container for molten beryllium, and a modified titanium carbide composition proved to be a satisfactory container for molten nickel.

Fabrication of Cast Products

The French[7] have patented a process for producing clad metallic fuel elements. Composite billets or blooms of zirconium-clad Zr-2 to 8 U were first diffusion bonded at 750 to 950°C and then coextruded or rolled at room temperature to 400°C to form round bars, tubes, or plates. The method eliminates the necessity for preheating at high temperatures in controlled atmospheres and the use of sealing jackets prior to fabrication.

A British patent[8] describes an extrusion apparatus which incorporates a conventional cylinder, ram, and die, with a device for applying vibratory energy at a frequency of 20,000 cps, and a special conical tubular mounting member which is designed to minimize undesirable effects such as damping and frequency shifts. The hollow mounting member has a definite frequency of vibration and an acoustical length equal to an even integral number of quarter wavelengths of sound at the frequency of operation. This technique increases the extrusion rate and permits extrusion of difficult materials.

Metal fuel-element cans with external cooling fins have been directly extruded by the British.[9] A patent describes the heated segmental dies which are used in conjunction with a stepped or tapered mandrel which applies the extruding force. A means for disengaging the die segments after extrusion and a device for ejecting the extruded can are also described.

A nomogram developed by theBritish[10] gives the expected extrusion pressure for different materials, die angles, and extrusion ratios when the compressive stress-strain curve for the alloy is known. The theory and calculations leading to the monogram are discribed, and a sample nomogram for many common materials is given. This nomogram applies only to round extrusions through a conical die.

Tantalum alloy T-111 has been deep drawn into a cup about 4 in. deep by 2 in. in diameter with a wall thickness of about 0.2 in. by Atomics International.[11] Aluminum bronze was found to be a satisfactory die material. Hardened steel was unsatisfactory because the large drawing forces necessary for the T-111 resulted in excessive contact between the T-111 and steel, thus tearing the T-111. Although multiple draws were needed, only one intermediate anneal at 2700°F (1480°C) for 1 hr was required. It was necessary to clean the die wash thoroughly from the T-111 blank between draws by caustic and acid pickles to avoid reaction with the alloy during annealing, which would cause embrittlement.

(D. E. Stellrecht)

2. Powder-Metallurgy Materials

Developments[12, 13] in powder metallurgy have been reviewed by Battelle-Columbus. Progress in fabricating superalloy parts by powder-metallurgy techniques and an atomization process for producing superalloy powders are of particular interest. Yields of minus 40-mesh Udimet 700 and B-1900 powders were greater than 70% and the oxygen content of the powders was maintained substantially below 300 ppm. Developments in the technology of slip casting superalloys are also noted.

The status of powder metallurgy[14] in Poland has been reviewed with particular consideration of metal-powder production and shaping. Progress in the manufacture of sintered structural parts, bearings, frictional materials, dispersion-strengthened materials, nuclear materials, and materials for special purposes is described. Important advances in fundamental research are cited and the directions of development in different fields of powder metallurgy are indicated.

The Russians[15] have fabricated molybdenum tubes by hot pressing tubular blanks made by powder metallurgy. Processing was accomplished in conical or spherical dies at 220 to 340°C using graphite lubrication. Prior to hot pressing, as well as after each pressing pass, the billets were annealed in either hydrogen or vacuum. Optimum deformations per pass and optimum deformation rates are described.

British investigators[16] have fabricated sheathed ceramic fuel materials by hydrostatic extrusion. The method employs a die, a container for the pressurized fluid and for the fuel element to be extruded, and a means for pressurizing the fluid to drive the element through the die. Prior to extrusion, the fuel element is coated with a tenacious deformable coating to prevent direct contact with the die and to eliminate escape of pressurized fluid past the die during extrusion.

As part of their program to develop SAP alloys, Oak Ridge investigators[17] have determined the effects of transverse extrusion on the mechanical properties of SAP 895. Specimens from SAP 895 bar extruded at Montecatini at a 20:1 ratio were further extruded in a direction perpendicular to the original extrusion direction; with the transverse extrusion ratios ranging between 1.5 and 30:1. The extrusion temperature was about 500°C, and both shear dies and 45° conical dies were used. Results of tensile testing at 450°C on this material are plotted in Fig. IV-1. The strength increased rapidly with increasing transverse extrusion ratio and surpassed the initial longitudinal stress (11,000 psi) at a reduction ratio of about 8:1. The ductility was essentially restored by this amount of transverse working. This seems to be a more effective way of improving properties than is further longitudinal extrusion.

A method of forming refractory-metal bodies containing dispersed refractory-metal carbides[18] has been developed at United Aircraft. Refractory metals such as Nb, Ta, Mo, W., Ti and their alloys in fine powder form are first coated with thin carbide shells in a fluidized bed. The powders are then warm or hot worked to fracture the shells and uniformly disperse the carbide phase throughout the structure.

(C. A. MacMillan)

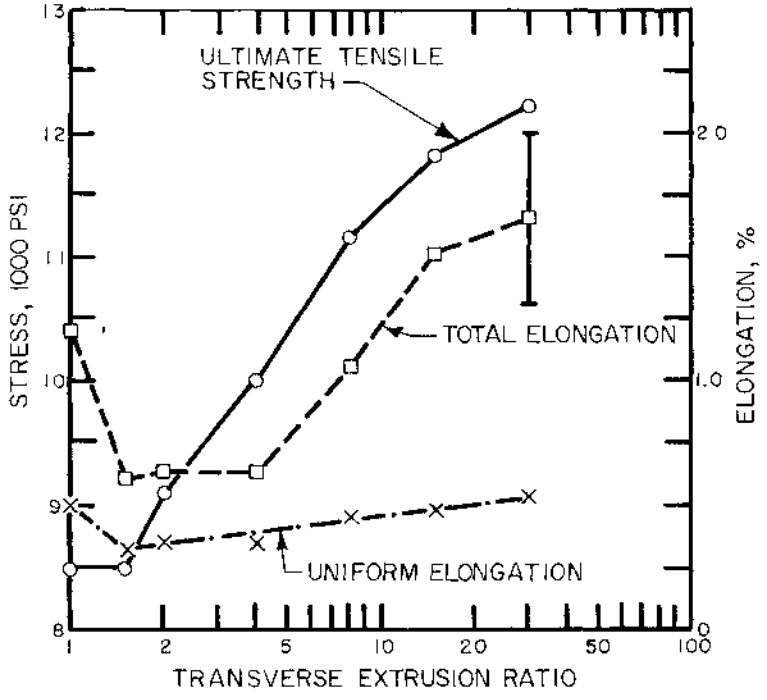

Fig. IV-1 Tensile properties of SAP 895 after transverse extrusion at about 500°C.[17]

3. Pressure Bonding

Bonding procedures and diffusion characteristics for vanadium-clad zirconium were studed by Vermani et al.[19] This materials combination was intended as a possible cladding material for use in organic-cooled reactors. The bonding surfaces were first prepared by machining and abrading and then electropolished. Zirconium surfaces were electropolished in glacial acetic acid and a perchloric acid bath, while vanadium surfaces were electropolished in a 10% sulfuric acid bath. Bonding couples of the materials were heat treated in purified helium ($\sim 0.5 \times 10^{-3}$ mm) at 400 to 1050°C for 1 hr. Metallographic examination of these couples showed very little diffusion in α-zirconium at less than 800°C. Only one diffusion band, an apparent result of volume diffusion, was observed after bonding at 900 to 1050°C. Although no tests of bond strength were conducted, a bonding temperature of 950°C appeared most satisfactory. In view of the limited diffusion observed at the lower bonding temperatures, vanadium-clad zirconium was considered satisfactory for long-term reactor operation at about 400°C.

Researchers at Los Alamos[20] have evaluated joining of nuclear-grade graphite with intermediate foils of Zr, Ta, Mo, W, and Fe. Two types of joints were produced in this investigation: a diffused joint which consisted of a carbide-carbon eutectic zone, and a continuous carbide joint. The experimental bonding conditions were achieved by

induction heating the graphite and foil assemblies in an argon atmosphere to temperatures up to 3000°C and maintaining a pressure of about 200 psi for 3 to 15 min. Diffused joints, which were formed at the higher temperatures for each system, exhibited elevated-temperature strengths superior to those of corresponding carbide joints. It was generally noted that increased bonding temperatures resulted in increased room-temperature flexure strengths of the bonds. The strongest continuous carbide joints in this study were produced with a zirconium intermediate foil.

A British patent[21] describing a method for pressure bonding ceramic-to-metal gradient seals has been issued. The sealing region in the assembly consists of a mixture of the refractory metal and ceramic, with the composition varying according to the proximity of the faying surfaces. After a series of graded powder layers are deposited at the joining surfaces of the components, the assembly is pressure bonded to consolidate the powder and bond it to both the metal and ceramic components. Joining of niobium to Al_2O_3 was cited as an example of the usefulness of this method.

Tungsten-clad W-50 vol.% UO_2 cermet fuel assemblies for thermionic applications have been fabricated by gas-pressure bonding at Battelle-Columbus.[22] Fuel forms consisting of tungsten-coated UO_2 particles and fine (0.88 μ) tungsten powder were first blended with a Parawax binder, die pressed, outgassed at 1500°C for 1/2 hr, and then hot isostatically pressed to 92 percent of theoretical density in molybdenum containers at 2900°F (1595°C) and 10,000 psi, for 3 hr. After the molybdenum was removed by acid leaching and grinding to final size, the fuel form along with arc-cast tungsten cladding components was heat treated in hydrogen at 1750 to 1800°C for 1-1/2 hr and then slow cooled (500°C/hr). All components were again assembled in a molybdenum container and pressure bonded at 3100°F (1705°C) and 15,000 psi for 3 hr. Prior to cooling, the autoclave was depressurized to permit relaxation of the bonded assembly. Clad fuel pellets produced in this manner were capable of withstanding 100 thermal cycles to 2000°K without failure.

(S. W. Porembka)

4. Plating

Nonelectrolytic Chemical Plating

Deposition of tantalum and iridium on quartz plates with previously deposited layers of carbon and SiO_2 was studied by Lainer and Kholmyanskii.[23] Thin films produced by vacuum evaporation were investigated by electron diffraction and electron microscopy. During condensation, tantalum oxidized and formed films of TaO which had a face-centered cubic lattice, while iridium films had the normal lattice of the bulk material. The crystal size as a function of the substrate temperature and the average film thickness were calculated from the broadening of the interference maxima.

The structure of tungsten films sputtered under 10^{-3} torr by argon ions at 1000 volts and condensed at a rate of 120 A/min on NaCl was investigated as a function of substrate temperature by Sella and Coppens.[24] Up to 190°C the films were amorphous; between 200 and 350°C they exhibited a body-centered cubic structure, whereas

in the range from 400 to 450°C the epitaxy structure became face-centered cubic. The effects of other parameters such as sputtering rate, pressure, and film thickness were also investigated.

Adherent metal coatings of Cd, Zn, Mg, Tl, Bi, Pb, and Ag up to 0.40 mm thick were deposited on metal substrates by means of two cathodes in a glow discharge at Mound Laboratory.[25] The samples to be coated were mounted on one of the cathodes. These samples were cleaned before and also during deposition by ion-bombardment sputtering. The other cathode contained the coating material in a tray which was thermally insulated from its support. The initial layers of the coating were deposited by bias sputtering, while the bulk of the coating was deposited at rates up to 0.015 mm/min when the coating material was evaporated. The method was defined as evaporation-abetted bias sputtering, with ion plating and bias sputtering being the physical processes involved. Coatings deposited by this method at 400°C adhered very well. Coatings deposited at 100°C adhered only moderately well, primarily because of low coating ductility at this deposition temperature.

Tungsten single crystals were prepared[26] by vapor deposition on single-crystal wires from WCl_6. The deposition temperatures were 1300, 2000 and 2700°C and deposition times were 1, 4, and 10 hr. The orientation of the rod axis in all experiments was near |110|. The exterior limiting planes were (110), (211), (100), and (111) at high supersaturation and (110) and (211) at low supersaturation. At high supersaturation the planes appeared macroscopically smooth, corresponding to the increased nucleation and reduced surface mobility. At low supersaturation the (211) and (110) planes showed a profile characterized by (110) steps. The size of the steps increased with lower supersaturation. Grain and subgrain boundaries of the substrate were continued into the deposited layer, while the number of dislocations diminished.

Experimental data and a laboratory apparatus for plating Al_2O_3 tubes with niobium were described by Fiebelmann.[27] Zinc was used for the reduction of $NbCl_5$, and the influence of pressure and temperature was examined. The main features of the deposited niobium layers were high chemical purity, good surface adherence even during sharp thermal cycles, and equal layer thickness. Brazing and diffusion bonding of niobium-plated Al_2O_3 bodies for applications in the range 800 to 1100°C was shown to be feasible.

A scaled-up apparatus for producing 1-ft lengths of 0.5-in.-diameter W-Re alloy tubing has been tested and modified at Lawrence Radiation Laboratory.[28a] Additional modification of the apparatus is required to provide greater control of mandrel temperature, feed-gas flow rate, and mandrel translation. Nevertheless, the room-temperature properties of rings taken from several sections of two of the three tubes were comparable with those previously reported for the 1-in.-long W-Re tubes. Fluorine analyses obtained on these standard 1-in.-long W-Re tubes prepared in the original apparatus indicated no apparent dependence of fluorine content on temperature, rhenium content, pressure, mole ratio of H_2/MF_6, MF_6 flow rate, or plating rate.

A study of thermionic-converter hot shells for application in a gasoline-fired thermionic power supply has been initiated.[29] Shells of SiC on tungsten indicated extensive problems as a result of thermal-shock cracking and separation of SiC from the tungsten substrate when heated at 1400°C for about 100 hr. To avoid these problems, various changes in the shell composition and deposition processes were considered and evaluated. A composite shell was developed, which consisted of a machined graphite

body 40 mils thick with tungsten deposited on the inside and SiC deposited on the outside. The graphite is completely encapsulated and provides surfaces on which to vapor-form the SiC and tungsten; it also serves as a reaction barrier between the SiC and tungsten in the area heated by the burner. These composite shells were tested at Thermo Electron and showed considerable promise. In the preparation of the shells, tungsten was deposited by hydrogen reduction of WF_6, while the SiC was deposited by pyrolysis and/or hydrogen reduction of CH_3SiCl_3.

(J. Zupan)

Electroplating

An effective method for electropolishing uranium was developed by Dow technologists.[30] Surface smoothing by 40 to 60% was accomplished in 20 to 45 min. with the removal of 20 to 46 μ (e.g., 51 to 20 μin., rms) at 13 volts in an ethanediol – sodium hypophosphite solution at 90°C. The initial cathode current density was 13 amp/sq ft.

Zirconium was electrodeposited on uranium in a pore-free condition up to a thickness of 5 mils at Battelle-Northwest[31] in a KF-LiF eutectic mixture containing 2 to 10 wt.% ZrF_4. The best cathode current density was in the range of 20 to 40 ma/cm^2. The operating temperature was 625 to 675°C. Internal voids were observed in cross sections, but acid treatments revealed no pores exposing uranium. A layer of Zr-U interdiffusion alloy appeared to be dense. Zirconium coatings thicker than 5 mils showed a structural change from fine to coarse crystals, which was attributed to degradation of the molten salt or possibly the formation of insoluble ZrF_3 particles in the bath.

Thick (10^{-3} cm) hydroxide films of U, Np, Pu, and Am are being deposited at cathode surfaces in acid solutions of the actinides with a potential of 12 volts between platinum anodes spaced 5 cm above the cathode.[32] The process is independent of the cathode material, but stainless-steel cathodes are customarily used with acid electrolytes such as: (1) 0.2M HCOOH and 0.15M $HCOONH_4$, (2) 0.125M HNO_3 and 0.02M $(COONH_4)_2$, and (3) 1.0M NH_4Cl and 0.01M $(COONH_4)_2$. Time periods of 10 to 60 min are required to deposit the films, which must then be removed from the cells before the electrical circuit is interrupted to prevent their dissolution. Hydroxyl ions generated at cathode surfaces form metallic precipitates with current densities up to 300 μa/cm^2. A small concentration of uranium or magnesium assists film formation, which must be carried out in cells with a low ratio of electrolyte volume to cathode surface area such as 3 ml/cm^2.

(W. H. Safranek)

5. High-Energy Rate Processes

[redacted][33]

The feasibility of using explosive-welded bimetal inserts for joining large sections of steel to both titanium and aluminum was studied at the University of Missouri.[34] Sections of aluminum, titanium, and steel were welded to the explosively bonded inserts by either electron-beam or Heliarc welding techniques and then evaluated with respect to the tensile strength of the explosive bond, accelerated-ambient-condition-corrosion resistance, and thermal-shock behavior. It was found that attaching segments to the insert by electron-beam welding caused very little degradation of the explosively produced bonds. For example, the bond in the aluminum and steel sample exhibited an ultimate tensile strength which was higher than the yield strength of the aluminum. However, the use of Heliarc welding reduced the bond quality in both systems considerably.

The use of gaseous detonations as a high-energy forming technique has been studied at General American Transportation.[35] A sheet metal blank and forming die were located at the end of an instrumented shock tube and then subjected to the impulse from a detonating methane/oxygen or propane/oxygen mixture. Materials formed during the test program include two high strength steels and three titanium alloys. The results showed that this forming process has considerable potential, from both a technical and an economic point of view.

(D. Laber)

6. Welding and Brazing

Electron-Beam Welding

Electron-beam welds between tubes of W-25 at.% Re-30 at.% Mo and T-111 (Ta-8 wt.% W-2 wt.% Hf) are being investigated at Lawrence Radiation Laboratory.[28b] Both direct welding and 0.018 in.-thick transition members of molybdenum and a Mo-50Re alloy have been used to join 0.5-in. OD, 0.040-in.-wall tubes. All joints cracked on cooling because the alloys formed during fusion could not sustain shrinkage strains. Cracking was most severe in the direct weld and least severe in the pure-molybdenum transition weld. Electron fractography indicated that all joints failed by cleavage with no sign of ductile behavior. It was found that hardness varied directly with the amount of tantalum in the weld and that rhenium had little apparent influence on weld hardness as shown in Table IV-1. It was believed that cracking might be prevented if a thicker molybdenum transition piece were used to dilute the tantalum or if welding conditions were developed to minimize alloying.

The quality of electron-beam-welded joints of Kovar and 321 stainless-steel tubes for an engine-cutoff sensor has been examined at Boeing.[36] The weld joint contained both a melt-through and a fillet weld. After visual and X-ray examination, hardness tests, and microscopic analysis, it was concluded that both welds were of excellent quality.

Westinghouse[37] has demonstrated the high joint efficiencies of electron-beam welds in 304 stainless steel. Welds were made on cold-rolled 304 stainless steel at 90, 60, 45, and 30° to the rolling direction, and their tensile and deformation properties were determined. Electron-beam welds of high depth-to-width ratios and reasonable scarf angles (45°) resulted in very high joint efficiencies as shown in Table IV-2.

Table IV-1 COMPOSITION AND HARDNESS OF REFRACTORY ALLOY WELDS[28b]

Alloy composition, wt. %	Composition of weld,[a] at. %	Average hardness for 200-g load,[b] DPH
W-Re-Mo base alloy	45W, 25Re, 30Mo	465
T-111:Ta-8W-2Hf welded directly to W-Re-Mo alloy	31.1W, 5.6Mo, 43.8Ta, 18.5Re	840
T-111 to W-Re-Mo with 0.018-in. transition of pure molybdenum	17.6W, 57.5Mo, 15.4Ta, 9.5Re	530
T-111 to W-Re-Mo with 0.018-in. transition of Mo-50Re	19.0W, 33.2Mo, 23.3Ta, 24.5Re	610

a At center of weld nugget, and neglecting hafnium content.
b Average hardness across weld nugget.

Table IV-2 PROPERTIES OF ELECTRON-BEAM WELDS IN 304 STAINLESS STEEL[37]

Type of specimen	Ultimate strength, 1000 psi	Uniform plastic elongation in the base metal, %	Nominal strain to fracture in 2-in. gage length, %
Annealed-welded	87.5	74	82.5
Cold rolled, unwelded	119.6	23	41.5
Cold rolled, butt welded	114	2.5	10.5
Cold rolled and welded; scarf angle = 60°	117.5	7	18.5
Cold rolled and welded; scarf angle = 45°	118.5	11.5	28.5
Cold rolled and welded; scarf angle = 30°	118.5	11.5	28.4

Experimental development of fuel-rod closure techniques using the plasma/electron-beam process has been conducted by Babcock and Wilcox.[38] Welds have been made in both 304 stainless steel and Zircaloy-4. In the first of two approaches investigated, an end cap was welded to the fuel tube in an atmosphere of 300 ppm helium. A distortion-free joint was accomplished which eliminated additional machining to remove any upset or expelled material that would interfere with rod insertion or removal. In the second approach, the end closure was formed from the tube itself.

Other Welding

A method for charging and sealing plutonium alloys into fuel elements while avoiding radioactive contamination of the container surface has been developed at Los Alamos.[39] GTA welding was used to seal the fuel elements in the special welding fixture shown in Fig. IV-2. This fixture permits welding in a high-quality inert atmosphere outside of the confines of a large glove box. The welding equipment used in this technique can accommodate a variety of container sizes and programmed welding currents from < 10 amp to >200 amp. Typical welding parameters for containers in various materials and sizes are shown in Table IV-3.

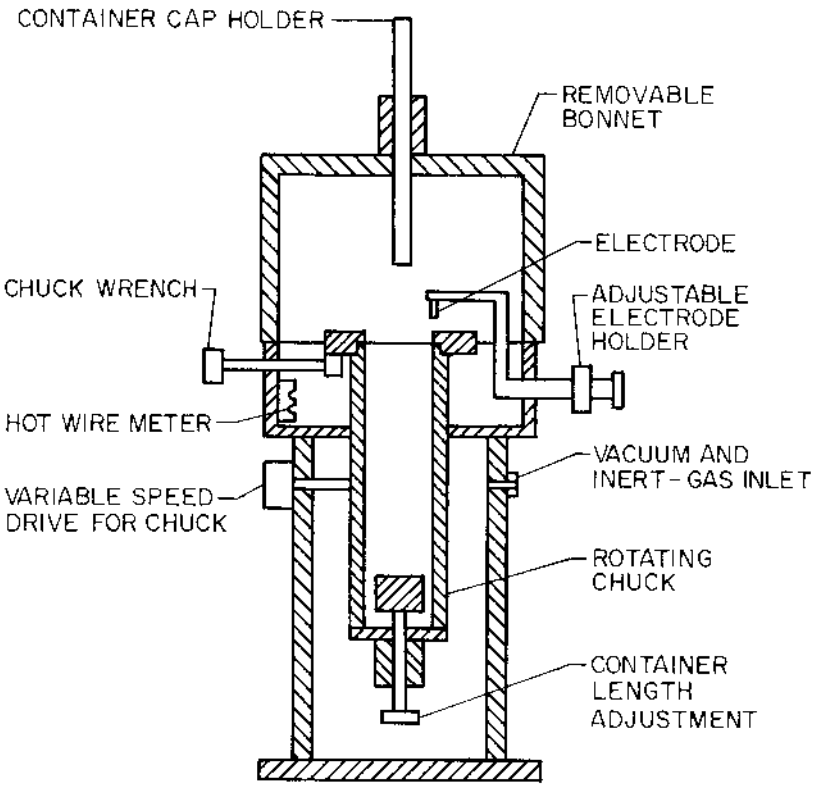

Fig. IV-2 Welding-fixture schematic.[39]

The diffusion bonding of niobium and tantalum to themselves and to each other was investigated at RAI Research Corp.[40] The temperature at which diffusion-controlled bonding occurs with an intermediate bonding aid is substantially lower than the recrystallization temperature of the parent metals in the work-hardened condition: 419°C

Table IV-3 WELDING PARAMETERS FOR VARIOUS CONTAINERS AND END CAPS[39]

Container			Types of end caps	Welding time, sec			Container rotation, sec/rev.	Electrode diameter,[a] in.	Electrode gap, in.	Fixture position from vertical, deg	Current during welding, amp
Material	Diameter, in.	Wall thickness, in.		Up slope	Weld	Down slope					
Ta	0.440	0.030	1 or 2	5	15	5	12	0.060	0.060	0	100
Ta	0.440	0.030	3, 4, or 5	5	13	5	10	0.060	0.050	0	40
S. steel	0.750	0.035	3, 4, or 5	5	20	5	16	0.020	0.050	0	15
S. steel	0.875	0.125	6	5	15	5	12	0.060	0.050	45	80
M. steel	3.000	0.060	6	5	55	5	48	0.060	0.060	0	65
Cu	0.875	0.050	3	5	10	2	8	0.093	0.090	0	120
Ni	1.500	0.005	6	5	50	5	48	0.010	0.025	80	8
Au	0.750	0.030	3 or 4	5	15	5	12	0.040	0.020	0	36
W	0.750	0.060	3	5	23	5	18	0.125	0.125	0	165
W[b]	0.750	0.060	3	5	23	5	18	0.125	0.090	0	180

a Electrodes 2% thoriated tungsten.

b Weld chamber at 6 in. absolute argon pressure.

Types of End Caps

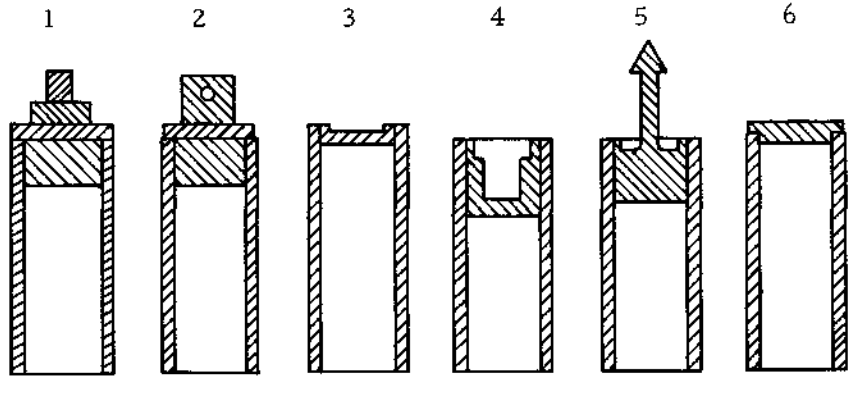

compared with 600°C for niobium and 800°C for tantalum. Using aluminum foils, good lap bonds were obtained in all three material combinations Nb-Nb, Ta-Ta, and Nb-Ta in 1/2 hr at 2000 psi and 419°C. Under the same conditions but without the foil, no bonds were obtained in 2 hr. Butt joints made using the aluminum foil had tensile strengths of 12,000 psi for niobium and 19,850 psi for tantalum. The joint efficiency was poor because only a small fraction of available contact areas (from 10 to 50%) was bonded. Oxidation was believed to be the cause of this poor efficiency and stricter atmosphere control and cleaning procedures were suggested as means of improvement.

A British patent[41] has been issued to cover the welding of a composite metal-oxide material such as SAP alloy to itself, a metal, an alloy, or another composite. One member is heated either to fusion or to a softening temperature, and the second member is gently immersed in the central area of the fused/softened zone for 5 to 6 min. The junction is then cooled in place and machined.

Brazing

Brazing procedures for Inconel 718 have been developed for use with the Phoebus-2A reactor at Los Alamos.[42] In selecting a brazing alloy, the effects of both brazing temperature and alloy composition on base-metal strength were considered. Nickel-base brazing alloys were rejected because of the tendency of carbon, boron, and silicon to diffuse along grain boundaries, thereby reducing the ductile cross section of the assembly and possibly affecting both high-temperature and cryogenic strength. After preliminary investigation, an 82Au-18Ni alloy with a flow point of 1800°F (982°C) was chosen for all structural brazes, which were made in a single brazing step. For other joints, where structural strength was not a consideration, Au-8Pd-22Ni and Au-16.5Cu-2Ni were used. These alloys have flow points of 1920 and 1720°F (1049 and 938°C), respectively.

In the final procedure, the surfaces were coated with 0.0005 in. of nickel to insure good filler-metal flow during brazing in a cam-controlled, resistance-heated furnace containing high-purity argon (less than 1 ppm H_2O and 2 ppm oxygen). Nearly 2000 assemblies have been brazed by this technique with less than 1% rejects. Tensile properties of assemblies using this and another brazing procedure are given in Table IV-4. The Group 1 assemblies were brazed at 1920°F (1050°C) using Au-8Pd-22Ni alloy for structural brazes. Group II assemblies were brazed with Au-18 Ni alloy at 1830°F (1000°C). Both groups were heat treated by holding at 1325°F (720°C) for 8 hr and then cooling at 20°F/hr (11°C/hr) to 1150°F (620°C). Elevated and cryogenic temperature properties for the Group II assemblies are shown in Tables IV-5 and IV-6.

Joining procedures were developed at Garrett Corp.[43] for three nickel-base alloys in fabricating lightweight heat exchangers designed to withstand 100 hr of operation at 1540 to 2140°F (840 to 1170°C). For 0.003-in.-wall tubes of Hastelloy X, brazing with Nicrobraz 30 alloy (Ni-19Cr-10Si-1Mo-4Fe) at 2175°F (1190°C) in either a vacuum or dry-hydrogen atmosphere was found satisfactory. Tubes of L-605 alloy having wall thicknesses of 0.006 to 0.010 in. were brazed with J8102 alloy (Ni-15.2Cr-8Si) at 2200°F (1205°C). Again, both vacuum and dry-hydrogen atmospheres were satisfactory. Several welding processes also proved satisfactory with L-605, including inert-gas tungsten-arc welding, spot welding, and laser welding. TD-nickel tubes with 0.006 to 0.008-in.-wall thicknesses were brazed in vacuum using TD-20 braze alloy (Ni-25Mo-

Table IV-4 AVERAGE ROOM-TEMPERATURE TENSILE PROPERTIES OF BRAZED AND HEAT-TREATED ALLOY 718 ASSEMBLIES[42]

Specimen type	Ultimate strength, 1000 psi	Proportional limit, 1000 psi	Yield strength (0.2% offset), 1000 psi	Elongation, %
Group I (Au-8Pd-22Ni braze)	185.9	96.7	151.5	10.1
Group II (Au-18Ni braze)	203.8	127.8	168.8	12.5

Table IV-5 AVERAGE ELEVATED-TEMPERATURE TENSILE PROPERTIES OF BRAZED AND HEAT-TREATED ALLOY 718 ASSEMBLIES[42]

Test temp., °F	Ultimate strength, 1000 psi	Yield strength (0.2% offset), 1000 psi	Initiation stress, 1000 psi
70	194.3	172.1	
1000 ± 5	150.4	134.0	131.9
1325 ± 5	128.2	126.2	

Table IV-6 AVERAGE LOW-TEMPERATURE TENSILE TEST DATA ON BRAZED AND HEAT-TREATED ASSEMBLIES[42]

Test temp., °K	Ultimate strength, 1000 psi	Yield strength (0.2% offset), 1000 psi	Elongation, %
Full-length brazed assemblies			
76	227.8	184.1	11.8[a]
Mock-up assemblies			
300	199.4	163.7	15.2[b]
20	268.6	199.2	14.9[b]

a Elongation full assembly.

b Elongation in 1-in. gage length.

16Cr-5W-4Si). However, excess quantities of the TD-20 alloy proved to be erosive to the TD-nickel. During high-temperature exposure, oxidation of the TD-Nickel was accelerated at the base of the braze fillet, creating stress risers, and limiting the service temperature of the uncoated structure to 1950°F (1065°C).

Unalloyed tantalum has been satisfactorily brazed to 316 stainless steel by NASA-Lewis.[44] Vacuum brazing was accomplished at 2150 F (1175°C) using J-8400 brazing alloy (Co-21Cr-21Ni-8Si-3.5W-0.4C-0.8B). When flat sheet and tubular specimens were tested at 1350°F (730°C) in a vacuum chamber (10^{-7} to 10^{-6} torr), all joints failed in the tantalum or stainless-steel parent metal. No unfavorable diffusion was observed between the braze alloy and the parent metals. It was also found that eliminating voids at the root of the tongue (tongue-and-groove joints) increased the ultimate strength of the joint because of increased effective cross-sectional area.

Solar[45] has developed a brazing process for attaching internal fins of Nb-1Zr foil to Nb-1Zr heat-receiver tubes. In brazing tests on T-joint and lap-joint specimens, 15 braze alloys (Cu, Au, Ti/Zr, and Zn bases) were evaluated. The three alloys that performed most satisfactorily in these tests together with the average tensile shear strengths of their respective brazed joints are:

Cu-2Ni	38,100 psi
Zr-25V-16Ti	38,500 psi
Zr-25V-16Ti-0.1Be	37,600 psi

Because of its braze fluidity and filleting characteristics, the Zr-25V-16Ti-0.1Be alloy was used to braze full-scale heat-receiver tubes. Brazing was performed satisfactorily at 2130°F (1165°C) for 5 min. in an induction furnace with a vacuum of 1×10^{-5} torr. The specimens were enclosed in cylindrical tantalum susceptors to insure uniform and rapid heating.

(J. E. Mortland and R. M. Evans)

7. Nondestructive Testing

Ultrasonic Techniques

Equipment is commercially available for measuring thicknesses down to 0.010 in. by ultrasonic means. Battelle-Northwest applied critical-angle measurements using a dual-element probe to measure thicknesses ranging from 0.001 to 0.005 in.[46] This method is believed applicable to measurement of coating thickness, if the velocity of a surface wave differs measurably between the coating and the substrate.

Battelle-Northwest has also adapted a conventional pulse-echo technique to test cylindrical isotope heat sources for weld penetration and cracks and other wall defects, and to measure wall thickness.[47] It was initially designed for inspection of end-cap welds on the heat sources.

The nonlinear interaction between high- and low-frequency ultrasonic waves has been used by Lawrie[48] to enhance detection of imperfect bonds. The low-frequency wave perturbs the interface and produces modulation of the high-frequency transmitted wave.

It has been known for a long time that stress affects the velocity of sound in materials, but the effect is so small that it is difficult to measure. Benson[49] has developed techniques by which relationships between the ultrasonic velocity and stress have been established for a number of aluminum alloys. These techniques were applied to aluminum plates containing weldments. It was necessary to determine the orientation of the principal axes of stress and the effect of material properties such as grain orientation. The accuracy of measurements obtained ultrasonically compared favorably with those obtained by destructive tests.

(D. Ensminger)

NDT Methods Other Than Ultrasonics

A series of NASA classroom instruction manuals and tests on commonly used methods of nondestructive testing has been completed by General Dynamics and is available on microfiche. The titles and respective accession and report numbers are listed as follows.

Title	Accession No.	NASA No.
Liquid Penetrant Testing	N68-28777	CR-61205
Magnetic Particle Testing	N68-28778	CR-61206
Eddy Current, Vol 1: Basic Principles	N68-28779	CR-61207
Eddy Current, Vol 2: Equipment, Methods, and Applications	N68-28780	CR-61208
Ultrasonics, Vol 1: Basic Principles	N68-28781	CR-61209
Ultrasonics, Vol 2: Equipment	N68-28782	CR-61210
Ultrasonics, Vol 3: Applications	N68-28783	CR-61211
Radiography, Vol 1: Origin and Nature of Radiation	N68-28784	CR-61212
Radiography, Vol 2: Radiation Safety	N68-28785	CR-61213
Radiography, Vol 3: Radiographic Equipment	N68-28786	CR-61214

Title	Accession No.	NASA No.
Radiography, Vol 4: Making a Radiograph	N68-28787	CR-61215
Radiography, Vol 5: Film Handling & Processing	N68-28788	CR-61216
Magnetic Particle Testing: Classroom Training Manual	N68-28789	CR-61227
Liquid Penetrant Testing: Classroom Training Handbook	N68-28791	CR-61229
Eddy Current Testing: Classroom Training Handbook	N68-28792	CR-61230
Radiographic Testing: Classroom Training Handbook	N68-28793	CR-61231

An eddy-current tubing tester using the multiple-parameter separation and suppression techniques previously developed at Hanford has been described by Battelle-Northwest investigators.[50] This two-channel, two-frequency instrument reduces the undesirable effect of test-probe wobble signals on both channels. A new analyzer circuit or signal transformation section is used for the successive elimination of parameters. The tester can be operated using either of its two test frequencies, 100 and 300 kHz, singly or simultaneously. When the tester is operated in its single frequency mode, two test parameters such as probe wobble and defects giving signals having components in quadrature with probe-wobble signals may be separated.

When the tester is operated in a two-frequency mode, the effect of one test parameter can be minimized and the effects of two other test parameters may be determined. Results are given for the two-frequency mode of operation in which probe-wobble signals were minimized on both of the two output channels, while at the same time, signals due to defects opening on the inner wall of the tubular test specimen appeared on one channel, and signals due to defects opening on the outer wall of the specimen appeared on the other channel.

Acoustic emission has been studied at Battelle-Northwest[51] as an in situ nondestructive test for welds in stainless-steel plate. The method is aimed at detection of defects as they initially occur. A direct correlation was established between acoustic emission rate and radiographic analysis of single-pass machine welds in 1/8-in. 304L stainless-steel plate containing induced defects at specific locations. It was found that the onset of acoustic emission is delayed 20 to 45 sec as the defect region begins to cool and that during cooling the acoustic emission rate from induced defect regions increases to a peak at about 400°C. The acoustic-emission rate from multipass welds in 1/2-in. 304L and 316 plate was greater than that from the single-pass welds by about an order of magnitude, and the same defect correlation between radiographic analysis and acoustic-emission rate was observed.

The apparent propagation velocity of the acoustic pulses from the induced defect regions varied as much as a factor of 2, which suggests that the acoustic-emission signals reach the receivers by indirect routes. The characteristic emission-pulse shape and spectral distribution vary with distance or direction from the acoustic-emission

source. Since pulse lengths are sufficient to set up complex reflection patterns in the plate, the received signal characteristics are determined by source location, receiver location, and plate geometry.

It was believed that this work established that it was possible to detect certain types of weld defects by acoustic-emission monitoring. The primary advantage noted for this technique is that defects can be detected during the welding process. Acoustic-emission techniques appear to be sensitive to microfissures beyond the resolution limits of presently applied ultrasonic and radiographic methods. On that basis, this technique, used in conjunction with other weld-inspection methods, could reduce significantly the rejection rate in final inspection of welds.

(A. F. Leatherman)

[redacted]

[redacted]

IV. SPECIAL FABRICATION TECHNIQUES

REFERENCES

1. P. Blum and J. Devillard, Apparatus for Continuous Casting of Refractory Metallic Compounds, British Patent 1,108,930, Apr. 10, 1968.

2. J. Trouve and A. Accary, Characteristics of Solidification in the Continuous Casting of Uranium Carbide, Rev. Int. Hautes Temp. Refract., 4: 225-230 (July – September 1967).

3. R. E. Reed, C. W. Dean, R. E. McDonald, and J. F. Emery, Sources of Contamination During Electron-Beam Melting, USAEC Report ORNL-TM-2208, Oak Ridge National Laboratory, July 1968.

4. C. T. Wang, E. F. Barock, J. C. La Vake, and S. Christopher, Vanadium Purification – Sixth Quarterly Progress Report, January 1 – March 31, 1968, USAEC Report CEND-3742-336, Combustion Engineering Inc., April 1968.

5. V. Papov and E. Demin, Electron-Beam Unit for Metal Melting, Elektron. Obrab. Mater., No. 2: 77-84 (1966).

6. M. C. Lunde and W. P. Meier, Forming of Containers for Molten Nickel and Beryllium at High Temperatures and Vacuum, USAEC Report RFP-882, Dow Chemical Co., Rocky Flats Division, Apr. 15, 1968.

7. J. Stohr, Process for Producing Cladded Fuel Elements, U.S. Patent 3,344,508, Oct. 3, 1968.

8. J. Jones and W. Tarpley, Mounting Member for Vibratory Device and Extrusion Apparatus Incorporating Same, British Patent 1,105,566, Mar. 6, 1968.

9. J. Richards and H. George, Improvements in or Relating to Radial Extrusion Dies, British Patent 1,106,992, Mar. 20, 1968.

10. P. J. Thompson and P.R.C. Daniels, A Nomogram for the Prediction of Extrusion Pressures in the Simple Hydrostatic Extrusion of Round Bar through Conical Dies, British Report TRG-Report-1523(S), Nov. 14, 1967.

11. Atomics International, Large Radioisotope Heat Source Capsule (LRHSC), Third Quarterly Progress Report, January-March, 1968, USAEC Report AI-AEC-12676, pp. 25-37, Apr. 22, 1968.

12. J. F. Joyce, Powder Metallurgy, DMIC Review, Battelle-Columbus, Defense Metals Information Center, Oct. 20, 1967.

13. J. F. Joyce, Powder Metallurgy, DMIC Review, Battelle-Columbus, Defense Metals Information Center, Feb. 21, 1968.

14. W. Missol and W. Cegielski, Trends in the Development of Powder Metallurgy, Rudy Metale Niezelaz., pp. 77-81 (February 1968).

15. V. N. Korolev and A. I. Galakhov, Pressing of Molybdenum Tubes, Kuznecho-Shlampovochnoe Proizvod., No. 7: 22-26 (July 1967).

16. D. Green, Hydrostatic Extrusion of Sheathed Ceramic Nuclear Fuel Material, U.S. Patent 3,344,507, to UKAEA, Oct. 3, 1967.

17. P. Patriarca (Comp.), Fuels and Materials Development Program Quarterly Progress Report for Period Ending December 31, 1967, USAEC Report ORNL-TM-2090, Oak Ridge National Laboratory, April 1968.

18. E. J. Delgrosso and L. A. Friedrich, Method of Forming a Refractory Metal Body Containing Dispersed Refractory Metal Carbides, U.S. Patent 3,343,952, Sept. 26, 1967.

19. S. K. Vermani, S. P. Murarka, and R. P. Agarwala, Diffusion Bonding in Vanadium and Zirconium, Indian Report BARC-303, 1967.

20. D. J. Sandstrom, Joining Graphite to Graphite With Transition Metal Foils, USAEC Report LA-3960, Los Alamos Scientific Laboratory, June 1968.

21. Pressure Bonded Ceramic-to-Metal Gradient Seals, British Patent 1,110,706, to USAEC, Apr. 24, 1968.

22. P. J. Gripshover and J. H. Peterson, Development of Uranium Dioxide:Tungsten Cermet Fuel Specimens for Thermionic Applications, Report NASA-CR-1059, Battelle-Columbus, July 1968. (Classified)

23. D. I. Lainer and V. A. Kholmyanskii, Structure of Ultrathin Films Produced by Vacuum Evaporation of Tantalum and Iridium, Kristallografiya, 12(6): 1051-1057 (November-December 1967).

24. C. Sella and R. Coppens, Structure of Tungsten Films Prepared by Triode Sputtering at Low Pressure and Energy, Compt. Rend., Ser. B, 265: 410-413 (Aug. 16, 1967).

25. T. W. Wood, Thick Adherent Metal Coatings by Means of Two Cathodes in a Glow Discharge, USAEC Report MLM-1453, Mound Laboratory, August 1966.

26. G. Weise, J. Kunze, B. Pegel, K. Schlaubitz, and D. Schulze (Eds.), Characterization of Tungsten Single Crystals Grown from the Gas Phase in Realstruktur und Eigenschaften von Reinststoffen, Part 3, pp. 305-312, Institute fuer Metallphysik und Reinstmetalle, Dresden, Germany, 1967.

27. P. Fiebelmann, Fabrication and Properties of Chemical Vapor Deposited Niobium Layers on Al_2O_3 Bodies for Thermionic Application, EAEC Report EUR-3743.e, Nov. 13, 1967.

28. University of California, Lawrence Radiation Laboratory, Advanced Space Nuclear Power Program, Quarterly Report, January-March 1968, USAEC Report UCRL-50004-68-1, (a) pp. 1-3, (b) 3-8.

29. L. J. Lazaridis and P. G. Pantazelos, Development of a Gasoline-Fired Thermionic Power Supply, Report ECOM-87341-1, Thermo Electron Corp., January 1968.

30. E. L. Childs and F. E. Evans, Nonaqueous Electropolishing Path for Uranium, Plating, 55: 164-167 (February 1968).

31. D. A. Nissen and R. W. Stromatt, Zirconium Electroplating on Uranium from Molten Alkali Fluoride Salts, USAEC Report BNWL-825, Battelle–Northwest, June 1, 1968.

32. G. A. Barnett, Hydroxide Electrodeposition Techniques for Some Actinides from Aqueous Media, British Report AEEW-M-772, October 1967.

33. S. H. Carpenter and H. E. Otto, Explosive Welding of Lead to Steel, Trans. Met. Soc. AIME, 239: 1866-1867 (November 1967).

34. D. L. Gibson and K. E. Yager, Joining Dissimilar Metals by Utilizing Explosive Welded Inserts, Report NP-16491, Missouri University, July 1965.

35. D. W. Fedderson, L. E. Fugelo, F. E. Ostrem, and E. B. Watt, Investigation of Gas Detonation Forming on Aerospace Materials, Report AFML-TR-68-3, General American Transportation Corp., February 1968.

36. T. Ceasar, Investigation of Electron Beam Welds in a Sensor Tube, Report NASA-CR-61812 (N68-25523), The Boeing Co., Mar. 1, 1968.

37. A. Arbel, Tensile Properties of Electron-Beam Welded 304 Stainless Steel, Trans. Amer. Nucl. Soc., 11: 139-140 (June 1968).

38. S. P. Grant, Experimental Welding Developments for Power Reactors, Trans. Amer. Nucl. Soc., 11: 139 (June 1968).

39. J. W. Anderson and J. R. Nichols, Encapsulation of Plutonium and Other Radioactive Materials in Welded Containers, USAEC Report LA-3937, Los Alamos Scientific Laboratory, April 1968.

40. S. Korman, P. Keusch, and C. Gonzalez, Research Study of Diffusion Bonding of Refractory Materials, Columbium and Tantalum, Report AMMRC-CR-67-15(F), RAI Research Corp., Nov. 10, 1967.

41. G. Beghi and G Musso, A Process for Welding Composite Metal-Oxide Materials Such as Sintered Aluminum Powder (SAP), British Patent 1,108,018, to European Atomic Energy Community, Mar. 27, 1968.

42. R. S. Kirby and G. S. Hanks, Brazing of Nickel-Chromium Alloy 718, Welding J., 47(3): 97s-105s (March 1968).

43. O. A. Buckman, Development of Manufacturing Processes for a Lightweight Heat Transfer System, Report AFML TR-67-300 (Part 1), The Garrett Corp., December 1967.

44. A. C. Spagnuolo, Evaluation of Tantalum-to-Stainless-Steel Transition Joints, NASA-TM-X-1540 (N68-21898), National Aeronautics and Space Administration, Lewis Research Center, April 1968.

45. C. E. Smeltzer and W. A. Compton, Development of a Brazing Process for Cb-1Zr Heat Receiver Tubes, Report RDR-1611, Solar, Division of International Harvester Co., Jan. 31, 1968.

46. C. E. Fitch, Jr., Prototype Ultrasonic Thickness Test for NbC Coating on NbC-Graphite Composite, USAEC Report BNWL-839, Battelle–Northwest, May 1968. (Classified)

47. B. E. Dozer, Ultrasonic System for Testing Isotope Heat Capsules, USAEC Report BNWL-649, Battelle–Northwest, March 1968.

48. W. E. Lawrie, Ultrasonic Nondestructive Coating Evaluation, in Symposium on Physics and Nondestructive Testing, pp. 343-371, Illinois Institute of Technology Research Institute, 1967.

49. R. W. Benson and Associates, Inc., Development of Nondestructive Methods for Determining Residual Stress and Fatigue Damage in Metals, Report NASA-CR-61584 (N68-21875), Mar. 8, 1968.

50. H. L. Libby and C. R. Wandling, Multichannel Eddy Current Tubing Tester, USAEC Report BNWL-765, Battelle–Northwest, May 28, 1968.

51. W. D. Jolly, An In Situ Weld Defect Detector – Acoustic Emission, USAEC Report BNWL-817, Battelle–Northwest, September 1968.